COMPLEMENTARY USE OF AIRBORNE LiDAR AND TERRESTRIAL LASER SCANNER TO ASSESS ABOVE GROUND BIOMASS/CARBON IN AYER HITAM TROPICAL RAIN FOREST RESERVE

Cora Jane C. Lawas

March 2016

SUPERVISORS:
Drs. E. H. Kloosterman
Dr. Y. A. Hussin

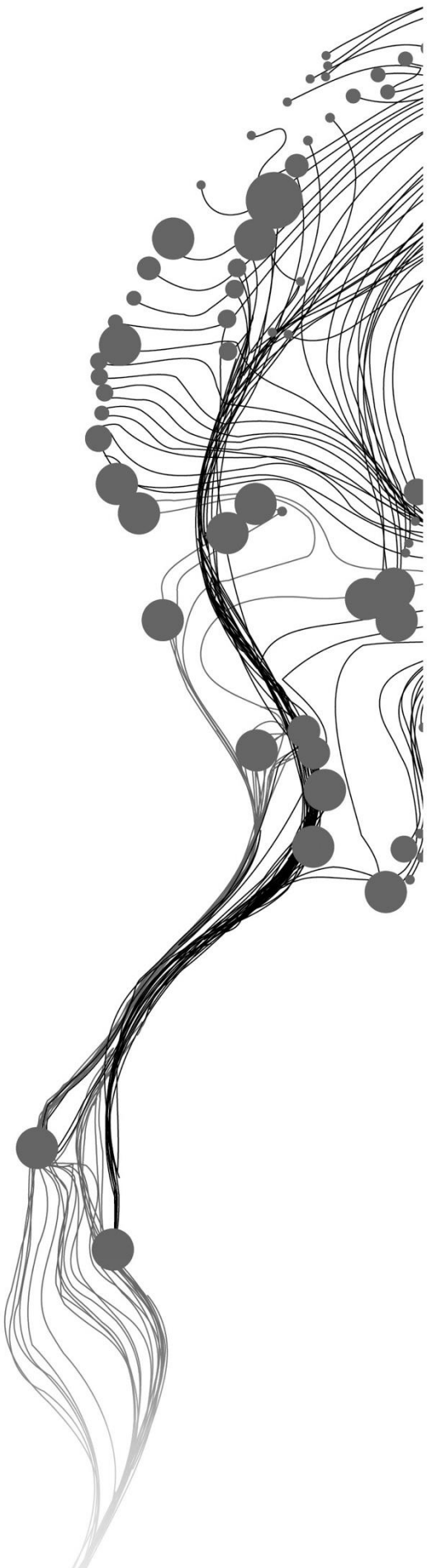

COMPLEMENTARY USE OF AIRBORNE LiDAR AND TERRESTRIAL LASER SCANNER TO ASSESS ABOVE GROUND BIOMASS/CARBON IN AYER HITAM TROPICAL RAIN FOREST RESERVE

CORA JANE C. LAWAS
Enschede, The Netherlands, 2016

Thesis submitted to the Faculty of Geo-Information Science and Earth Observation of the University of Twente in partial fulfilment of the requirements for the degree of Master of Science in Geo-information Science and Earth Observation.
Specialization: Natural Resource Management

SUPERVISORS:
Drs. E. H. Kloosterman
Dr. Y. A. Hussin

THESIS ASSESSMENT BOARD:
Prof. Dr. A.D. Nelson (Chairman)
Dr. Mohd Hasmadi Ismail (External Examiner, University of Putra Malaysia)

ABSTRACT

The mitigating instrument to address global deforestation under the UNFCCC and Kyoto Protocol is the implementation of the reducing emission from deforestation and forest degradation (REDD+), plus (conserving and enhancing forest stocks and sustainable management of forests) program. To achieve the objectives of this program functional and sustainable monitoring, reporting and verification (MRV) system needs to be implemented. In tropical countries where there is widespread forest degradation and deforestation, the implementation of the REDD+ program needs an updated inventories of the carbon stock in their forests. Moreover, there is a great need for accurate method for assessment of complex multi-layered tropical rain forests.

This study aimed to develop a novel method of accurately assessing the AGB/carbon stock of a tropical lowland rainforest with a vertically complex structure. The complementary strengths of airborne LiDAR and terrestrial laser scanning system to assess the upper and lower canopies of the forest achieved reasonable and robust results.

The upper canopy layer was assessed by generating tree parameters using airborne LiDAR to obtain height from CHM and segmenting the Orthophoto to obtain CPA. DBH was modelled through multiple regression using the derived parameters as independent variables and the field DBH as the dependent variable. The modelled DBH achieved an R^2 value of 0.90 and RMSE of 0.02 cm for the 16 plots. To estimate the AGB an allometric equation was applied to the modelled DBH together with LIDAR derived height. The modelled AGB was validated using the field DBH and LiDAR derived height. A robust model with an R^2 of 0.98 and RMSE of 69.44 Kg was achieved for the 16 plots.

The lower canopy layer was assessed using the registered scene from the TLS. This is to complement the trees that were not identified from the upper canopy layer. Scanned trees in the plot were extracted. Then DBH and height parameters were measured using RiSCAN Pro software interface. These parameters were then used for the allometric equation to estimate the AGB for the lower canopy. The correlation of the TLS measured DBH and field measured DBH was established and achieved an R^2 value of 0.99 and RMSE of 1.03 cm. The modelled AGB was estimated using the TLS measured height and DBH by applying the allometric equation. The model was validated using the field measured DBH and TLS derived height. The result was a robust model with an R^2 value of 0.99 and RMSE of 19.23 Kg for the 16 plots.

The derived AGB from the upper and lower canopies were combined. The accuracy of the complementary method of deriving the estimated AGB from the two sensors was assessed by obtaining the R^2 and RMSE of the two sensors. The achieved R^2 and RMSE is 0.98 and 188.35 kg respectively for the 16 plots.

Based on the robust results this study presented a novel method to address the need of the REDD+ program to provide accurate AGB/carbon assessment for a complex multi-layered tropical rain forest.

Keywords: Complementary, Airborne LiDAR, Terrestrial laser scanner (TLS), Segment, AGB, allometric equation.

ACKNOWLEDGEMENTS

Looking back, this journey would have not been fulfilled without God. My gratefulness to you Lord is beyond words for the opportunities that you gave me.

I would like to thank the University of Twente Excellence Scholarship Program and the University of the Philippines System Master's Fellowship Program for the fellowship grant. My home institution University of the Philippines Cebu for the privilege to study on leave.

I would like to express my heartfelt gratitude to the AMAZING people that I have worked with to achieve this goal.

Let me start with my two supervisors Drs. Henk Kloosterman and Dr. Yousif Hussin. Henk your mentorship and dedication in the field is simply amazing. Thank you for redirecting the focus of my study. Yousif, your perseverance to mentor, empathy and guidance to do my best is simply remarkable. Both your valuable advice and support gave value and direction to this work.

To Ir. Louise van Leeuwen-deLeeuw for the extra time and effort to advise, your help is very much appreciated.

To Ms. Anahita Khosravipour, for generously sharing her time and expertise in processing the LiDAR data. I am very grateful for your help.

To the University of Putra Malaysia (UPM) for accommodating us to conduct the study in the AHFR. To Dr. Mohd Hasmadi Ismail for facilitating our entry to Malaysia and helping us in the field. To the management and staff of the forest, Mr. Farhan, Mohd Naeem Abdul Hafiz Bin Mohd Hafiz, Siti Zurina Binti Zakaria, Fazli Bin Shariff, Jelani Bin Alias, Noor Azlina Binti Azizdim, Mohd Fakhrullah Bin Mohd Noh, Fazrul Azree Bin Mohd Arif, may Almighty Allah bless all of you.

To my fellow Ayer Hitamers, who are not only colleagues, but friends who give empathy and encouragement AGGIE, TASI, PHAN, SADADI AND ZEM all of you are the BEST.

To my NRM-GEMM family thank you for the support and making academic life bearable and the wonderful times that we shared as family.

To all my friends and colleagues back home and abroad thank you for the constant encouragement.

To my family, Mama Gliz, Tiya Lita, sister Florence, brothers Ryan and Lester, brother and sister-in law Wayne and Nona, nieces Justine and Jade thank you for the love and prayers.

In memory of my Papa Walter.

Cora Jane C. Lawas
Enschede, The Netherlands
February, 2016

TABLE OF CONTENTS

LIST OF FIGURES

LIST OF TABLES

LIST OF ACRONYMS

AGB	Aboveground Biomass
AHFR	Ayer Hitam Forest Reserve
CHM	Canopy height model
CPA	Crown projected area
DBH	Diameter at breast height
DSM	Digital Surface Model
DTM	Digital Terrain Model
FAO	Food and Agricultural Organization
FRA	Forest Resource Assessment
GPS	Global Positioning System
IMU	Inertial Measurement Unit
IPCC	Intergovernmental Panel on Climate Change
LiDAR	Light Detection and Ranging
MRV	Monitoring Reporting, Verification
OBIA	Object Based Image Analysis
QQ plots	Quantile Quantile plots
REDD+	Reducing Emission from Deforestation and forest Degradation
	Plus (conserving and enhancing forest stocks and sustainable management of forests)
RMSE	Root Mean Square Error
TLS	Terrestrial Laser Scanner
UNFCC	United Nations Framework Convention on Climate Change

LIST OF APPENDIXES

1. INTRODUCTION

1.1. Background

The ecosystem function of forests to store carbon has an important role in the global agenda of climate change. Carbon stored in above ground biomass, litter and soils in the world's forests is around 652 tons with an average carbon content of 161.8 tons per hectare as estimated by Global Forest Resource Assessment (FRA) (FAO, 2006). The function of forests to store more carbon than any other terrestrial ecosystem serve as an important natural brake on climate change (Gibbs, et al., 2007). The disruption of this ecosystem function through anthropogenic activities such as deforestation and forest degradation have an adverse impact on the ecosystem. Deforested and degraded forests will serve as carbon sources instead of sinks due to the release of carbon dioxide (CO2) in the atmosphere. Increased levels of carbon dioxide in the atmosphere is one of the main drivers of climate change. It is estimated that approximately 20% of global CO2 emission comes from tropical deforestation and degradation which ranked as the second largest source of emission from fossil fuels (Hirata et al., 2012). Further the Intergovernmental Panel on Climate Change (IPCC) reported on their Third Assessment Report (2001) that CO^2 emissions due to deforestation and forest degradation in developing countries have a large impact on the global climate change (Houghton et al., 2001).

The mitigating instrument to be implemented to address the land use related emissions from developing countries is reducing emissions from deforestation and forest degradation (REDD+), conserving and enhancing forest stocks and sustainable management of forests (Corbera & Schroeder, 2011; Pistorius, 2012). The REDD+ mitigation framework started as one of the agenda concerning the climate change mitigation under the United Nations Framework for Climate Change (UNFCC). It was further modified to include bilateral and multilateral activities by Parties of Convention and private activities (UNFCC, 2010). Recent forest conservation activities to mitigate climate change in developing countries come under the REDD+ framework. It is the acknowledged framework that provide incentives (credits, funds, etc.) for reducing CO2 removals by enhancing forest carbon stocks (Hirata et al., 2012).

Achieving the objectives of the REDD+ framework which is the sustainable and time bound reductions in forest related greenhouse gas emissions require a functional and sustainable national monitoring, reporting and verification (MRV) systems. The challenge however is the reliability to account for the amount of forest carbon stock that includes changes over time as defined according to the greenhouse gas (GHG) reporting standards (2000) and IPCC guidelines (2006) (UN-REDD Programme, 2015). The UNFCC methodological guidance calls countries to use the most recent IPCC guidelines as basis for estimating forest related GHG emissions and to use a combination of remote sensing and ground based forest carbon inventory for obtaining the estimates. Further, remote sensing must be used for the clarification of forest cover types and the area occupied by each type (Hirata et al., 2012).

Estimating carbon stocks on REDD+ recommends the application of remote sensing methods due to constrained access to forest areas and the difficulty of extracting the area to be sampled (Bhattarai1, et al., 2015). The application of remote sensing would also provide retrieval of forest attributes at varying levels of accuracy with due cost effectiveness (Tokola & Hou, 2012). Indeed remote sensing is an alternative method in the retrieval of forest structural parameters. However, the applicability of the method of assessment is dependent on the specific type of forest, the complexity of the geographical location and

conditions of the forest (Ediriweera et al., 2014; Tonolli et al., 2011). These situations poses the primary challenge in the assessment of a lowland tropical rainforest like Ayer Hitam Forest Reserve (AHFR) in Malaysia. A typical structure of this type of forest is shown in Figure 1. Due to its geographical location with high rainfall and constant warm temperatures, it provides the best condition for rapid plant growth and reproduction that consequently produces a highly diverse types of plants and animals. Moreover this condition of rapid plant growth and competition promotes the distinct stratification of trees contained in this type of forest. According to Walter, (1974) the structure of this type of forest are classified in different layers (Figure 1). Namely as an emergent layer that occupied the highest stratum, of heights ranging from 40-50m. Followed by a canopy layer of heights that range from 30-40m, the understory that range from 20-30m and the forest floor of 10m.

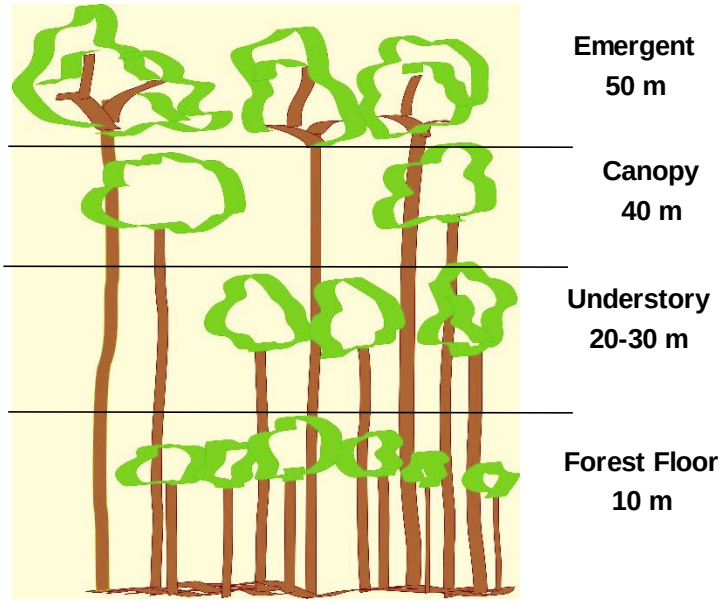

Figure 1. Structure of a tropical lowland rain forest

Under the REDD+ framework monetary incentives can only be provided for carbon reduction initiatives if above ground biomass (AGB) of forests with these characteristics will be accurately accounted through remote sensing methods. This poses the greater challenge because current studies on remote sensing application to assess AGB as per review is for a reforested tropical forest such as the work of (Baral, 2011; Karna et al., 2015; Mbaabu, et al., 2014). The remote sensing methods employed are to assess a reforested upland forest which is different in terms of geographical location and structure. Moreover, recent studies done by Sium, (2015) and Prasad, (2015) was done in a tropical rainforest however on a highland location that implements the application of remote sensing methods specific for that forest condition. A comprehensive review done by Koch, (2010) on the application of remote sensing for forest biomass mapping pointed out there is a very limited information on LiDAR derived data for forest biomass mapping in the tropics. Moreover, Hirata et al., (2012) cited that there is a need for separate biomass assessment methods to appropriately assess multi-layered tropical forests. As emphasized by Chambers et al., (2007) the most effective use of remote sensing data towards developing a novel understanding of tropical forest structure and dynamics is to combine the most appropriate ecological field investigations and an effective balance with remote sensing to overcome spatial, temporal and logistical challenges. For this reason a novel approach of accurately assessing the AGB of a vertically complex tropical rainforest has to be developed in answer to the REDD+ requirement. The overall concept of this study is the synergistic use of airborne LiDAR with an Orthophoto for the assessment of the emergent and canopy layers of the forest.

Complementary to this, is the use of a terrestrial laser scanner for the assessment of the understory layer of the forest. Due to the distinct vertical structure of this type of forest its assessment would require both airborne and terrestrial remote sensors that can detect tree structural parameters across different layers. As reviewed by Van Leeuwen et al., (2011) these laser sensors have their inherent strength and weakness when applied to temperate forests. Airborne laser sensors have limitations to characterize vegetation structure in the lower canopy. Whereas terrestrial laser sensors are biased towards lower parts of the canopy (Hilker et al., 2010). Studies on the integration of these technologies in temperate forests by Chasmer et al., (2006) and Hilker et al., (2010) enhances the detail of structural information. The complementary application of these remote sensing technologies in a lowland tropical rainforest as of this writing has yet to be tested. This innovative concept will be studied if this have potential to provide a robust information on the accurate assessment of AGB for a vertically complex tropical rain forest for the application of REDD+ program.

1.2. Problem Statement

The implementation of the REDD+ program to address global tropical deforestation and degradation initiates the need for the development of robust and transparent national forest monitoring systems (Goetz & Dubayah, 2011). Assessment of AHFR having a complex vertical structure of trees would make an important research case on the complementary applicability of using both airborne and terrestrial laser sensors to obtain forestry metrics to assess its overall AGB. This complementary method of using two laser sensors have the potential to fully account the AGB contributed by the trees from the different canopy layers. A portion of the forest canopy height model (CHM) generated in 3D is shown in Figure 2. This graphical representation would confirm to the description by Nurul Shida et al., (2014) that the forest have distinct emergent and canopy layers as well as a thick lower canopy layers.

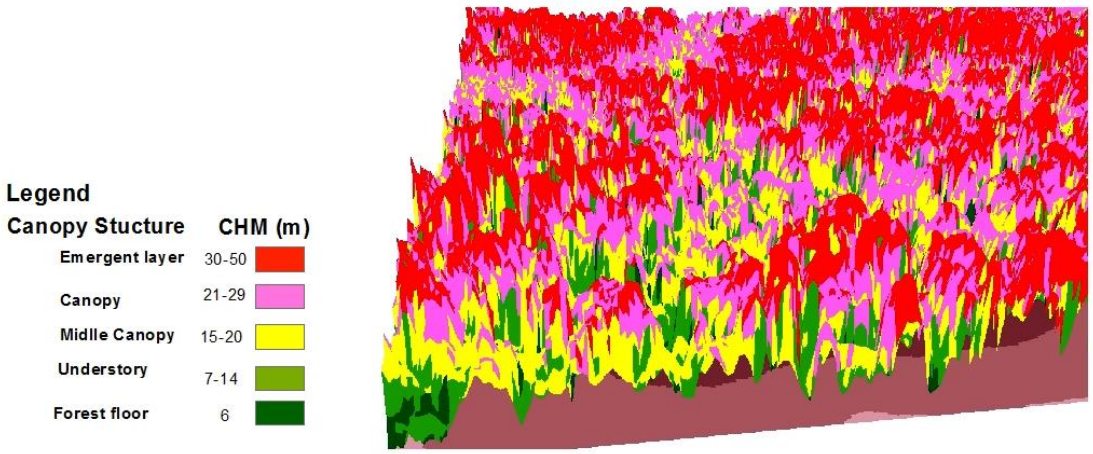

Figure 2. Canopy structure of AHFR.

Accurate assessment of the carbon stock would therefore take into account the trees in all the canopy layers of this vertically complex forest. Remotely sensed data according to the REDD+ framework can be applied using the indirect method of estimating carbon stocks per unit area. This can be done through use of the over story height model and crown diameter model Hirata et al., (2012). Forest structural height can be accurately measured using airborne LiDAR (Gibbs, et al., 2007). Using canopy height models (CHM) from LiDAR derived heights to estimate carbon stocks in temperate forests provided accurate results (Patenaude et al., 2004; Koch et al., 2006; Popescu, 2007) as well as in subtropical forest (Bautista, 2012; Karna et al., 2015; Mbaabu et al., 2014). On the other hand research on tree crown delineation using aerial imagery like

Orthophoto has been studied by (Gougeon, 1995; Culvenor, 2002; Wang et al., 2004) to estimate forest and tree parameters. Further, Holopainen & Talvitie, (2012) pointed out that these are two promising remote sensing technologies that would increase accuracy and efficiency of forest inventory on tree and stand wise measurements. Thus, these methods have greater applicability to assess the AGB of the trees that belong to the emergent and canopy layers of AHFR. Moreover, recent advances in terrestrial laser scanning technology utilizes tree data acquisition to determine accurate information on tree structural metrics (Kankare et al., 2013). The use of this method have the potential for the accurate assessment of AGB of trees that belong to the understory layer of the forest. To rationalize, assessment of AHFR a vertically complex tropical rain forest system would entail the acquisition of complementary tree metrics that can be derived from airborne LiDAR which is the height and crown projected area from Orthophoto in quantifying AGB for higher tree canopies. Based on the findings of Chasmer, et al., (2006) laser pulse return from airborne LiDAR system is biased towards the top of the tree canopy thus making this suitable to estimate the height from the upper layers. Complementary to this, to derive tree metrics for lower tree canopies diameter at breast height (DBH) and height can be acquired through the use of the terrestrial laser scanner (TLS). Based on the revealed results by Kankare et al., (2013)they pointed out that the system could be used to measure DBH and height and even stem volume accurately in estimating individual tree biomass.

Researches on the complementary use of the airborne and terrestrial laser systems has been done in temperate forests. As described by Hilker et al., (2010) the fundamental difference between these two systems in the measurement of the foliage elements is according to random media model (Poisson distribution). Objects closer to the instrument have a greater of chance of measurable return. As a consequence airborne laser system can provide detailed information on the upper canopy. On the other hand terrestrial laser system can provide a detailed assessment of the lower canopy. As pointed out by (Van Leeuwen et al., 2011) there are intrinsic strengths and weaknesses of these two systems and that they must be treated in a complementary manner to overcome the challenges in obtaining forest metrics. To illustrate Figure 3 show the complementary use of the two sensors.

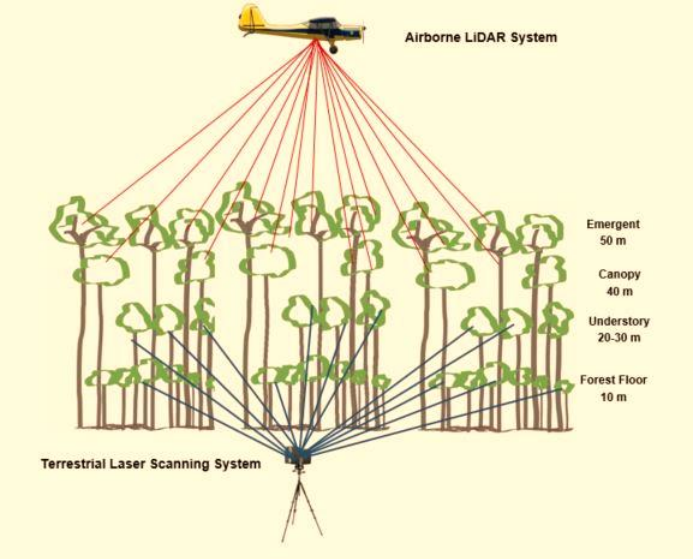

Figure 3. Complementary use of airborne LiDAR and terrestrial laser scanning system.

The application of this complementary approach to assess a vertically complex tropical rain forest like AHFR has not been tested. Acquiring a primary data like this poses greater challenges due to the logistical and geographical limitations of the forest. An innovative way to quantify all the AGB that can be derived from the different layers of the forest has to be developed. The robust information that can be derived from

this study have a greater potential to provide better evidence in the assessment of AGB for the application of REDD+ program.

1.3. Research Objective, Research questions and Hypothesis

General objective

AHFR in Malaysia is a tropical lowland rain forest with a complex vertical structure of trees. To accurately assess the AGB of this forest this would entail measurement of trees from the emergent and canopy layer as well as the understory layer of trees. The primary objective of this research is therefore to develop an accurate assessment of the carbon stock through the use of Airborne LiDAR and Orthophoto to assess the trees from the higher canopy and Terrestrial Laser Scanner to assess the trees from the lower canopy.

Specific Objectives

1. To assess relationship between CHM from Airborne LiDAR and CPA from the segmented Orthophoto and field measured DBH to model the DBH of trees from the higher canopy structure.
2. To assess the relationship between the modelled DBH and field DBH to estimate the AGB of the trees from the higher canopy structure.
3. To assess the relationship between the modelled AGB measured using the TLS measured DBH and height and field measured DBH and TLS height to estimate AGB of trees from the lower canopy structure.
4. To quantify the AGB of the whole area from the measured AGB both from trees from higher and lower canopies of the forest.

Research Question

1. How accurate is the modelled DBH from CHM derived from airborne LiDAR derived CHM and segmented CPA from Orthophoto and field measured DBH?
2. How accurate is the modelled AGB compared to the estimated AGB from field measured DBH and airborne LiDAR derived height of trees from higher canopy?
3. How accurate is the TLS modelled AGB compared to the field estimated AGB of trees from lower canopy?
4. How accurate is the estimated AGB combined from both TLS and airborne LiDAR based models to assess the biomass/carbon stock of the study area?

Research Hypothesis

1. Ho: The accuracy for the modelled DBH derived from airborne LiDAR and CPA from Orthophoto and field measured DBH is ≥70% at 95% level of significance.
Ha: Accuracy for the modelled DBH from airborne LiDAR and CPA from Orthophoto and field measured DBH <70%.
2. Ho: Accuracy of the modelled DBH and airborne LiDAR height to measure AGB of trees from the higher canopy is ≥70% at 95% level of significance.
Ha: Accuracy of the modelled DBH and airborne LiDAR height to measure AGB of trees from the higher canopy is <70% at 95% level of significance.
3. Ho: At 95% level of significance the modelled AGB from TLS compared to field measured AGB is 90 >%.
Ha: At 95% level of significance the modelled AGB from TLS compared to the field measured AGB is 90<%.
4. Ho: At 95% level of significance the combined models to estimate the AGB/carbon stock of the study area compared to the field measured AGB is 80 >%.

Ha: At 95% level of significance the combined models to estimate the AGB/carbon stock of the study area compared to the field measured AGB is 80<%.

1.4. Theoretical Framework of the Research

Relevant related literature of the study was conducted and the research problem was identified. The identification of the research problem served as the basis for defining the research objectives and research questions. The pertinent secondary data needed was requested and acquired for this served as basis to conduct the fieldwork. The acquired primary data were analysed and research results were discussed and concluded based on the results. The graphical presentation is presented in Figure 4.

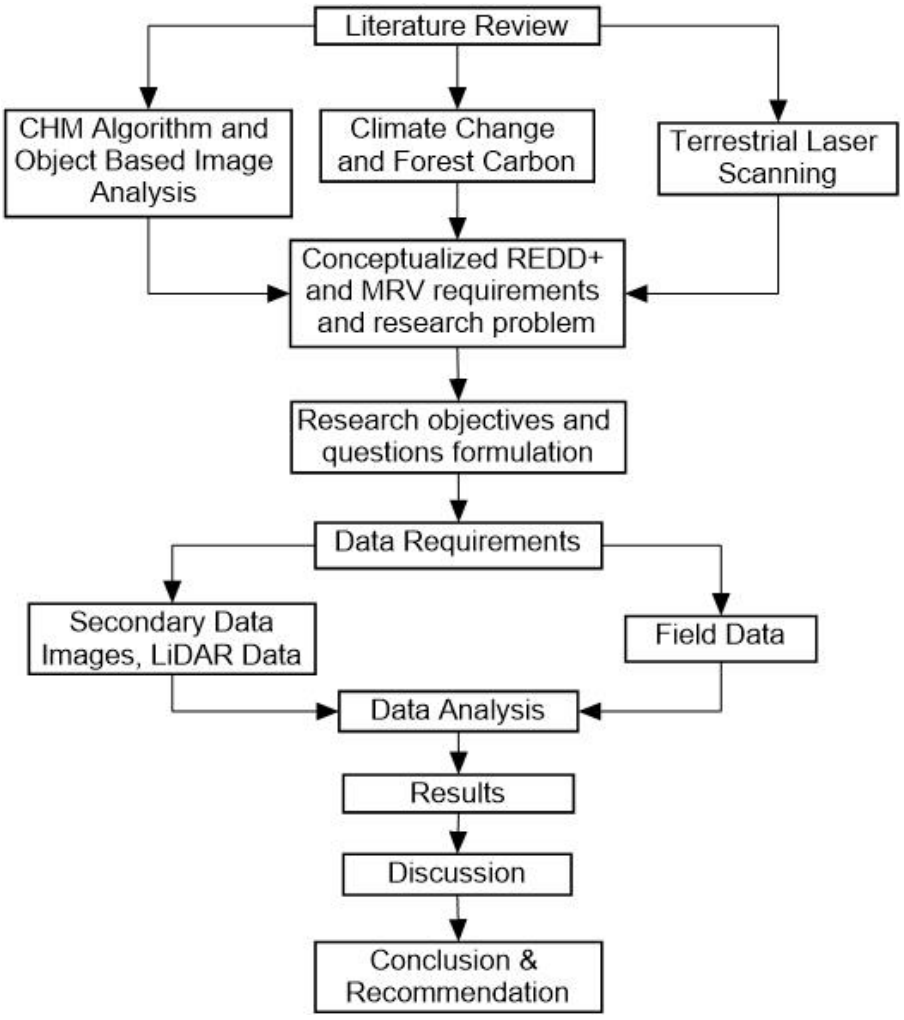

Figure 4. Theoretical framework of the research.

2. LITERATURE REVIEW

2.1. Concepts and Definitions

2.1.1. Structure of a lowland tropical rainforest

Lowland tropical rainforests generally are composed of broadleaved trees found in wet lowlands around the Equator (Smith, 2015). The high rainfall and constant warm temperature provides the optimal condition for animal and plant growth that in turn promotes high biological diversity in the forest and define its vertical structure. A particular striking feature of this forest is the complex pattern of distribution between the ground and canopy (Bourgeron, 1983). Hogan, (2011) described the vertical structure of a typical tropical rainforest to have the following tiers: emergent canopy, base canopy, middle tier and forest understory. The emergent may attain heights of 35 to 50 meters. Followed by the canopy whose heights typically about 25-30 meters. Then followed by the midtier plants that have heights between 20-25 meters and the forest floor of about 10 meters. According to Walter, et al., (1973) in spite of the species richness of tropical rainforest, the physiognomy of this type of forest in the different parts of the world are similar. To illustrate the vertical structure of a typical lowland tropical rainforest is presented in Figure 5.

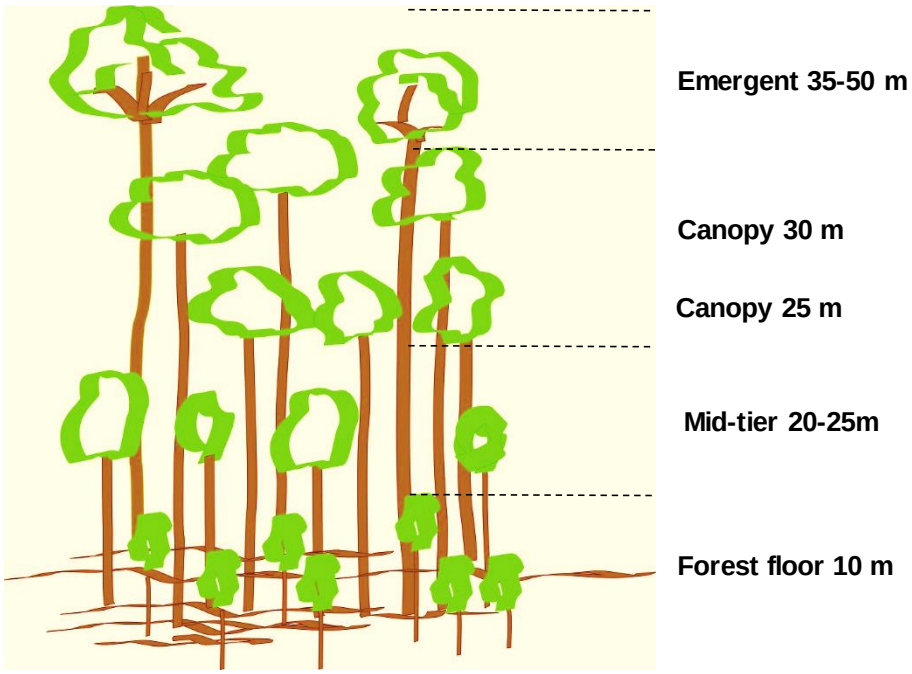

Figure 5. Illustration of the vertical structure of a lowland tropical rainforest.

2.1.2. Biomass

As defined by Condit, (2008) biomass is the mass of the living organisms in the forest which are the trees. Quantifying biomass of a forest involves an efficient method of measuring the size of the tree and from its dimensions to estimate the weight. Biomass estimation mainly focuses on the above ground biomass (AGB) because it is where the largest pool of carbon is stored and also the most vulnerable to deforestation and degradation (Gibbs et al., 2007). Moreover in a forest ecosystem it is an important measure of forest productivity and sustainability Vashum, (2012). Figure 6 is an illustration by Gschwantner et al., (2009) showing how the tree is partitioned to demarcate the above and below ground biomass. Through the

estimation of AGB forest carbon can then be estimated by multiplying a 50% factor of dry woody biomass (Drake et al., 2003).

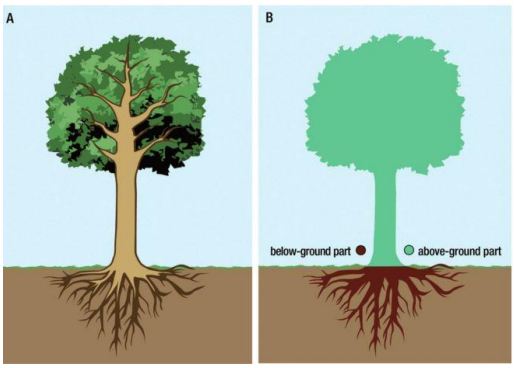

Figure 6. Above and below biomass of a tree Source: (Gschwantner et al., (2009)

2.1.3. Allometric Equation

The use of allometric equation is a common method of estimating forest biomass that relate individual tree biomass to obtain non-destructive tree parameters such as diameter (Ketterings et al., 2001). It is an equation that relates to tree structural parameters that can be repeatedly measured in the field. One of the key consideration in the selection of allometric equation is the suitability of the type of forest and the geographical location (Hoover, 2008). Further selecting the appropriate allometric equation is essential in AGB/carbon estimation to ascertain the quantitative contribution of carbon stored in tropical forests (Chave et al., 2005). The allometric equation developed by Chave et al., (2014) has been adapted for this study.

2.1.4. Crown Projected Area (CPA)

Crown projected area is the proportional area covered on the ground by a vertical projection of the canopy (Jennings, et al.,1999). The relationship between tree crown size and stem size is useful in deriving volume from aerial photographs. This is useful to define the relationship between diameter at breast height (DBH) and crown (Wile, 1964). The calculation of CPA assumes a circular crown projection from the maximum crown diameter (Kuuluvainen, 1991). The graphical illustration of CPA is shown in Figure 7.

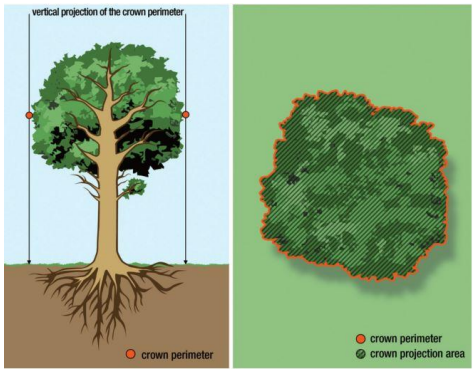

Figure 7. Crown projection area, Source: (Gschwantner et al., (2009).

2.1.5. Object Based Image Analysis

The development of acquiring quality georeferenced high spatial resolution aerial multispectral digital images is one of the ways that lead to the development of obtaining automatic forest management inventories (Gougeon, 1995). Remote sensing has evolved from what was predominantly per-pixel multispectral based

approaches to a multiscale object-based methods (Hay, et al.,2005). This development became a necessity as availability of higher and higher resolution images became available and the need for improved methods of analysis also arises. This technique differ from the traditional pixel based classification methods because it entails the grouping of neighbouring pixels into distinct image objects within designated parameters (Riggan & Weih, 2009). In order to obtain image objects, object based classification starts by segmenting the image. Segmenting will subdivide the image into homogenous groups of pixel to form image objects. The next step is the classification of the object based on spectral, textural, shape and contextual information (Hay et al., 2005; Li & Zhang, 2009)

2.1.6. Airborne LiDAR or Airborne Laser Scanning

Laser altimetry or Light Detection and Ranging (LiDAR) is an active remote sensing technology the determines distances by using the speed of light and the time required for the emitted laser to travel to a target object (Lim, et al., 2003). Measurement of the time elapsed when a laser is emitted from a sensor and intercepts an object can be used either by 1) pulsed ranging where travel time of a laser pulse from a sensor to a target object is recorded or 2) continuous wave ranging where phase change is transmitted via a sinusoidal signal produced via a continuously emitted laser converted to travel time (Wehr & Lohr, 1999). An airborne LiDAR system operates from an airborne platform that carries a set of instruments: laser device, an inertial navigational measurement unit (IMU), which continuously records the aircraft's attitude vectors (orientation); a high-precision airborne global positioning system (GPS) unit, which records the three-dimensional position of the aircraft; and a computer interface that manages communication among devices and data storage (Gatziolis & Andersen, 2008). Further this requires a GPS base station installed at a known location on the ground and in the vicinity (within 50 km) of the aircraft, to operate simultaneously in order to differentially correct, and thus improve the precision of, the airborne GPS data (Gatziolis & Andersen, 2008). Figure 8 is an illustration of a typical airborne LiDAR survey.

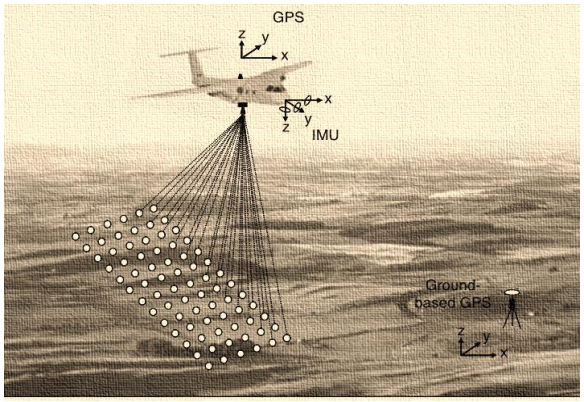

Figure 8. Typical airborne LiDAR survey Source (Heritage & Large, 2009)

2.1.7. Airborne LiDAR in Forestry Application

The Airborne LiDAR technology is an alternative remote sensing technology that have the potential to increase the accuracy of biophysical measurements and extend spatial analysis into the third (z) dimension (Lefsky et al., 2002). Further, it measures directly the three dimensional distribution of plant canopies as well as subcanopy topography that will produce high resolution topographic maps and vegetation heights, cover and canopy structure of high accuracy (Lefsky et al., 2002). The application of this technology in topographic mapping and forestry applications, have wavelength pulses in the near-infrared part of the spectrum typically between 1040 and 1065 nm (Gatziolis & Andersen, 2008). For forestry applications the two types of LiDAR data acquisition is differentiated based on the backscattered laser energy that is recorded by the system's receiver. The energy reflected back to the sensor as a continuous signal is called waveform

LiDAR. Whereas the reflected energy quantized at amplitude intervals is recorded at precisely referenced points in time and space is called discrete-return, small-footprint LiDAR or point cloud (Gatziolis & Andersen, 2008). For this study discrete-return LiDAR data is used. A conceptual illustration from Lefsky et al., (2002) of the difference between how the two types of LiDAR data acquired is shown in Figure 9.

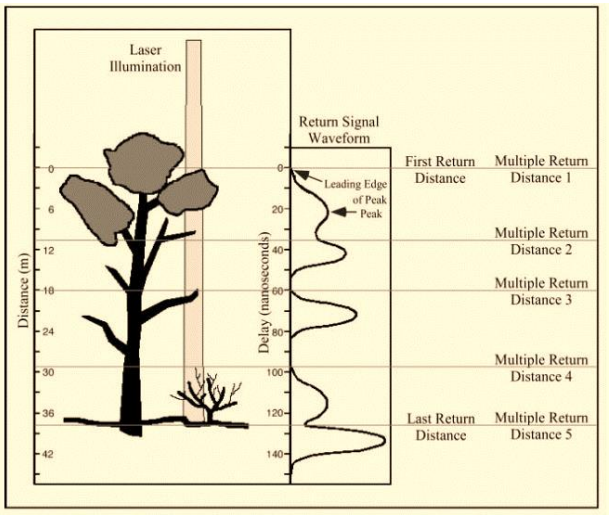

Figure 9. Conceptual illustration of the difference between discrete and waveform LiDAR Source (Lefsky et al., 2002).

2.1.8. Terrestrial Laser Scanning (TLS)

Terrestrial laser scanning uses a terrestrial laser scanner instrument that enable the non- destructive, rapid and precise digitisation of physical scenes into three-dimensional (3D) point clouds (Dassot, et al., 2011). The principle behind TLS as described by (Kankare et al., 2013) is the high assemblage of laser beam scans over a predefined solid angle in a regular scanning pattern and measures the time of flight of the laser signal. Further, the distance that can be measured of the scanning range of midrange terrestrial system is between 2 to 800 meters. The principle of distance measurement can be categorised based on how the system correlates to both range and resulting accuracy. Frohlich & Mettenleiter, (2004) summarises the three technologies for range measurement for laser scanners. The most popular measurement system is the flight principle. The technique is a clear cut measurement of distances up to several hundred meters. The long range measurement has the advantage for reasonable accuracy. The phase measurement is limited to one hundred meters and the accuracy of measured distances within millimeters are possible. Close range laser scanners used for industrial applications uses optical triangulation having accuracies to some micro meters. Laser scanners are classified according this measurement principle. This study uses RIEGL VZ 400 which falls under the time of flight classification. Pfeifer & Briese, (2007) described pulse time of flight ranging scanners as suited better for outdoor operation where longer ranges have to be measured and are typically panoramic scanners, with a field of view of 360°. Figure 9 is RIEGL VZ 400 used to implement this study and the specification of the instrument.

Sensor	specifications
Field of view	100 X 360 degrees
Pulse rate	up to 122,000Hz
Range	up to 600 m
Accuracy	5mm
Beam divergence	0.3 mrad
Spot size	3cm at 100m distance
Minimum range	1.5m
Laser wavelength	Near infrared (1550 nm)
Camera	High precision digital NIKON D610

Figure 10 RIEGL VZ 400 and the specifications of the instrument (RIEGL, 2013).

2.1.9. Terrestrial Laser Scanning (TLS) for Forestry Applications

Terrestrial laser scanning technology is used in forestry applications to bridge the gap between conventional inventory methods and airborne laser scanning data processing to facilitate three dimensional tree geometry parameters in large plots (Maas, et al., 2008). Detailed discussion on the application of this technology to forest inventory measurements such as plot cartography, species recognition, DBH, tree height stem density, basal area and plot level wood volume estimates as well as canopy characterisation such as virtual projections, gap fraction and three-dimensional foliage distribution is done by Dassot et al., (2011). The review revealed that there is a significant improvement of the technology however the use for measurements purpose is dependent on the device specification and objective of the study. Further automation and reliable programs are still needed for forestry applications to fill the gap between manual methods and the wide scale airborne LiDAR scanning. It is interesting to note that applications using this technology in forestry is mainly done in temperate zone.

2.1.11. Complementary Applications of Airborne LiDAR and TLS Forestry

The review done by Dassot et al., (2011) foresees that the future development of TLS is on its complementary application with airborne LiDAR. The system can provide different information but it can complement the airborne LiDAR data. The synergistic use of these two technologies will have a complementary effect on its strengths and weakness for forestry applications (Van Leeuwen et al., 2011). The strength of airborne LiDAR is to estimate structural parameters such as stand height, gap probability and canopy volume however it has limitations to characterize lower canopy vegetation structure (Hopkinson, et al., 2004; Lovell et. al., 2003). This is because the capability of airborne LiDAR to characterize forest canopy height profiles is dependent on point density of laser returns (Lovell et al., 2003) As a consequence the vegetation understorey is often under-represented by airborne LiDAR due to the top-down perspective and resultant bias towards the upper part of the canopy (Van Leeuwen et al., 2011). Moreover for forests with extremely dense over storey canopies infrequency of laser returns is obvious from the mid and understorey layers (Van Leeuwen et al., 2011). Another limitation of airborne LiDAR is the restricted view angles to near-nadir ($\pm 20^{o}$), which are less suitable for the estimation of canopy clumping and leaf angle distribution (Chen, et al., 2003; Ni-Meister et al., 2008). Lastly, airborne LiDAR has limitations on its ability to characterize woody component of vegetation, because the vertical projection of the stem contains very limited information on bole size (diameter) and shape (Van Leeuwen et al., 2011).

On the other hand the primary limitations of TLS is the limited range to obtain tree and stand structural characteristics. This is dependent on stand density wherein a typical range of TLS acquisitions is less than 100m from the sensor position. The decline in point densities with distance will limit the processing of TLS data to range distances not exceeding 10-30m (Maas et al., 2008). Since static TLS features a radial field of view, the point cloud densities will decline markedly with distance from the sensor due to near field obstruction. This bias has to be taken into account when trying to derive stand-level estimates from TLS data (Hilker et al., 2010) Since TLS returns are typically biased towards lower parts of the canopy, and as a

result the upper crown structure and tree heights are often difficult to assess (Hilker et al., 2010; Chasmer et al., 2006). In comparison to airborne LiDAR most TLS systems are able to describe vegetation structure from a broad range of view angles (Côté, et al., 2009; Jupp et al., 2008)

Integrating these two technologies to a common coordinate frame enhances the detail of structural information obtained and overcomes the above mentioned challenges with respect to either technique (Chasmer et al., 2006; Lindberg et al., 2012; Hilker et al., 2010). The method of co-registering the two techniques successfully enables the study of tree-level structure by combining the complementary values of airborne LiDAR and TLS in one dataset. This facilitated the study of tree allometry using LiDAR remote sensing or enhances leaf area estimates at various canopy strata done by (Huang & Pretzsch, 2010). Lastly, the study of Lindberg et al., (2012) revealed the important advantage of integrating airborne LiDAR and TLS is that TLS allows calibration and validation of airborne data in an accurate and rapid manner. It is important to note that these studies are mostly done and applied in temperate forests which have different environmental characteristics compared to tropical forests. There is therefore a big potential for the application of these complementary techniques in tropical rainforests.

3. STUDY AREA, MATERIALS AND METHODS

3.1. Study Area

3.1.1. Criteria for Study Area Selection

Study area selection was based was based on the following criteria.

Logistics

Logistical requirement is the primary reason for the study area selection. Implementing this complex study, requires the collaborative partnership of the University of Putra Malaysia who is managing the study area, which is Ayer Hitam tropical rain Forest Reserve. Local knowledge to navigate where to establish the plots and species identification was very important. Further, local help was needed to clear the thick undergrowth to establish the TLS plots otherwise scan output will render poor results and more difficulty in tree extraction would be experienced.

Availability of data

WorldView3 of the area was purchased and served as base map source for field work plan. After fieldwork additional data from UPM was acquired which are the Airborne LiDAR Data and Orthophoto.

3.1.2. Geographic Location of Ayer Hitam Forest Reserve

Ayer Hitam tropical rain Forest Reserve (AHFR) is a logged over lowland mixed-dipterocarp forest in the State of Selangor, Malaysia which covers an area of 1,248 hectares (Ibrahim, 1999). The forest is one of the three remaining lowland dipterocarp forests in the Klang Valley. It has been isolated from the neighbouring forests due to the residential and other economic development that surrounds the whole forested area (Nurul Shida et al., 2014). AHFR's location is 3° 01' N and 101° 39' E is shown in Figure 11. This forest reserve has been leased to the University of Putra in Malaysia (UPM) for 80 years for education, research and extension purposes (Ibrahim, 1999).

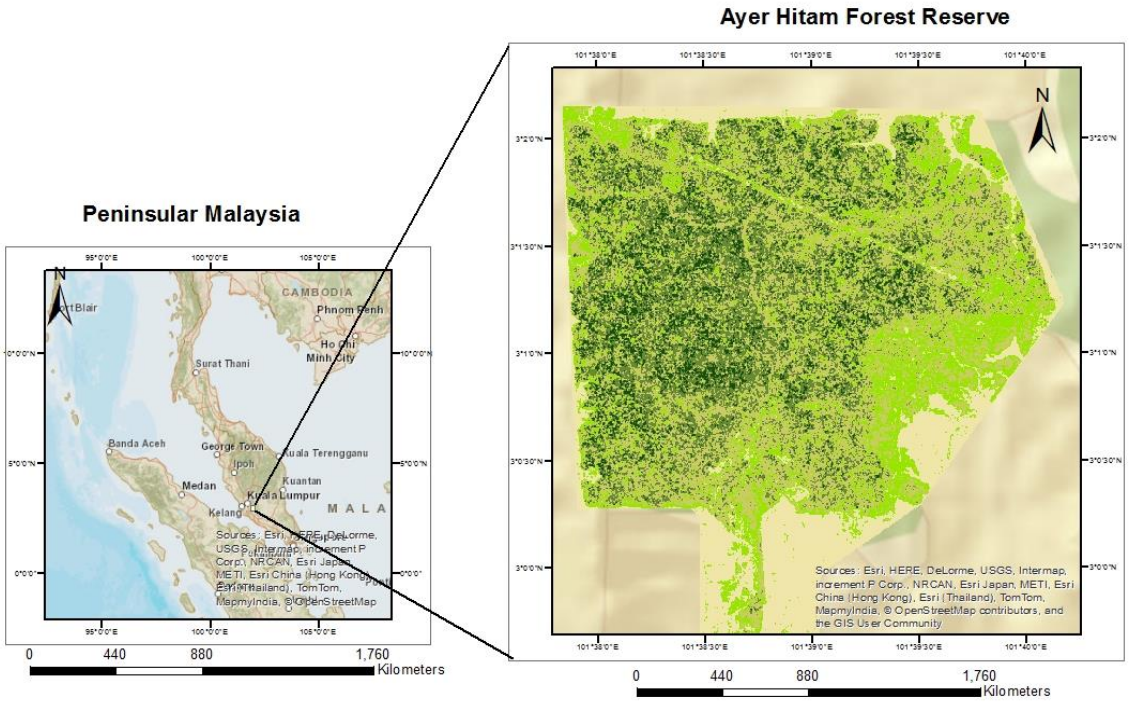

Figure 11. Location map of Ayer Hitam Forest Reserve.

3.1.3. Topography and Meteorology

The topographical and meteorological description of the study area is adapted from the description of (Nurul Shida et al., 2014) because the original document is in Malay language. AHFR have distinct topographical characteristics namely ridge, hillside and valley. The elevation ranges from 15m to 233m. The slope of the terrain is 34°. Figure 12 shows the 3D digital terrain of the area. The temperature would range from 22 to 32 °C, the average relative humidity is 83% and the annual rainfall is 2,178 mm. There are two rivers that flow in this forest namely Rasau and Bohol. The soil type is derived from metamorphic and sedimentary rocks.

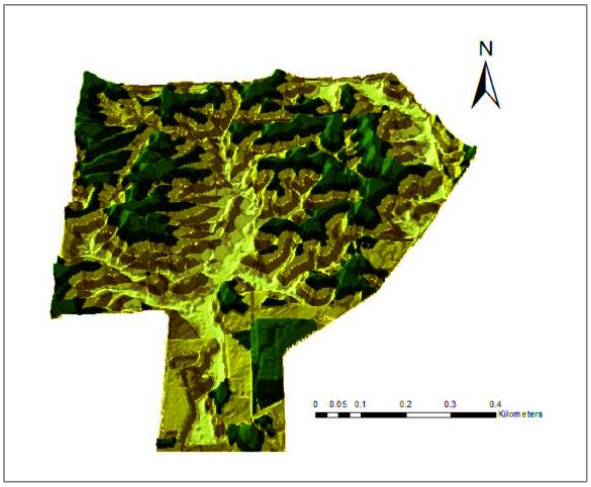

Figure 12. Digital terrain of Ayer Hitam Forest Reserve.

3.1.4. Vegetation Diversity and Structure

The preliminary assessment done by Ibrahim, (1999) on the plant diversity of the forest has identified 430 species of seed plants in 203 genera and 73 families. There are 33 species of ferns and fern allies. Of the trees assessed 127 are timber species, 29 are fruit tree species and 98 have medicinal values. As described by Ibrahim, (1999) the forest it is at the late stage of regeneration in terms of forest recovery. Nurul Shida et al., (2014) described the forest with distinct emergent and canopy layers as well as a thick lower canopy layers. Figure 13 is the 3D graphical representation of the canopy structure of the forest.

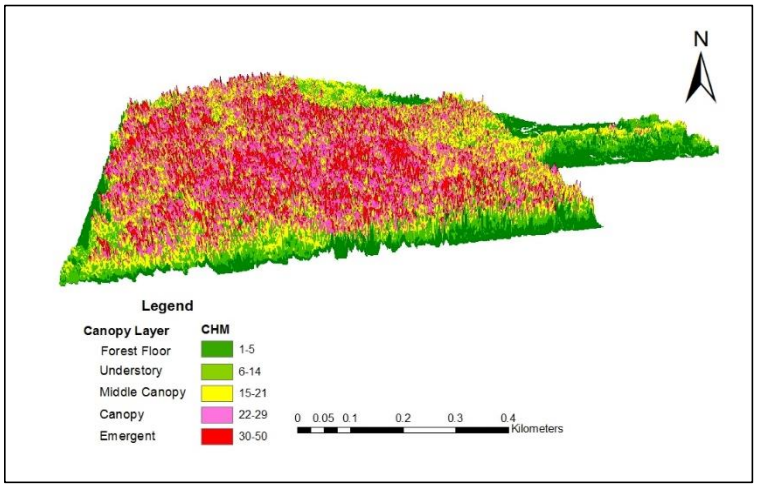

Figure 13. Three dimensional graphical representation of the canopy structure of the forest.

3.2. Materials

3.2.1. Remote Sensing Data

Airborne LiDAR

The raw airborne LiDAR data was provided by the University of Putra Malaysia. The point cloud density of the data is 5-6 points per square meter. The data was collected by the vendor using LiteMapper 5600 a waveform-digitizing LiDAR for terrain and vegetation mapping system. Based on the description of the data supplier, the study site was flown over with 80–100 knot speed at 600m–1000 m above the ground. This manoeuvre would provide data with sufficient point densities and footprint sizes to achieve at least 3 points/m². The laser footprint covered targeted areas with an average overlapping of 50% between adjacent flight lines. The maximum scan was set at 11°; pulses transmitted at scan angles that exceeded 8° were excluded from the final data in order to avoid low-quality data at the edge of strips (Hug et al., 2004). The technical parameters for Lite Mapper 5600 system provided by the data supplier is presented in Table 1.

Table 1. Technical parameters of Lite Mapper 5600 system.

Pulse rate Scan	Range between 70 kHz and 240 kHz (normal 70 kHz)
Scan angle	60°
Scan pattern	Regular
Effective rate	46,667 Hz
Beam divergence	0.5 mrad
Line/sec	Max 160
A/c ground speed	90 kts
Target reflectivity	Min 20% max 60% (vegetation 30%, cliff 60%)
Flying height	700 m–1000 m
Laser points/m2	0.9 to 1.2 points with swath width 808 m to 1155 m
Spot diameter (laser)	0.35 to 0.50 m 1040
Max (above ground level)	1040 m (3411ft)

3.2.2. Orthophoto Image

The Orthophoto was taken simultaneously with the acquisition of the airborne LiDAR data. The spatial resolution of the image is 13 cm. The Lite Mapper-5600 system is equipped with an IGI DigiCAM to complement the LiDAR data. The coverage of the camera is the same swath as what the LiDAR system sees. This provided a high resolution imagery of the surface in true color to aid surface classification and to provide extra planimetric resolution (Hug et al., 2004). Further, the calibrated lenses of the DigiCAM is tightly integrated with the LiteMapper-5600 and the IGI CCNS-4 flight management systems to facilitate reliable and easy operation. The camera is mounted together and boresighted with the laser scanner and the IMU to enable direct georeferencing of its images and automated orthoimage generation using the DSM output of the LIDAR system (Hug et al., 2004).The technical specification of the digital camera is presented in Table 2.

Table 2. Specification of DigiCAM-H (Hasselblad camera).

DigiCAM-H (Hasselblad camera)	Modified imacon 39 m pixel CCD backplane with 4080 x 5440 pixels at 6 μm. Digi-control computer with resolution of 8 mm at an altitude of 600 m at mean sea level
DigiCam total pixel 39mp	Total pixels that can be projected on the internal sensor
Pixel size	6.8um (micron): each pixel has a size of 6.8um.
Sensor size	36.8mm x 49.07mm: true size of the internal sensor
Image size	7216 x 5412 pixels: size of the image produced in terms of width x length in pixel unit (7216x5412=39052992 = 39mp)
Lens: Focal length	50 mm
Max aperture	3.5 mm
Forward cross track Forward	52°
Forward along track	40°

3.2.3. Field Instruments

The field instruments that worked during field work and their corresponding application in the field is presented in Table 3. During pre-field work preparation 5 types of navigating instruments were prepared namely iPAQ, Magellan GPS, Etrex GPS, Google Nexus Tablet, and Experia Smart phone. This was to ensure that alternative instruments are available for navigation since it was already pre-empted that this is a thick forest with occlusions. Further, for height measurements Leica laser distance meter as well as Nikon laser range finder was prepared. TLS was used to scan the trees in the plot.

Table 3. . Field Instruments.

Item No.	Instrument	Application
1	RIEGL VZ 400 TLS	Tree scanning within plots
2	Leica DISTO D510 Laser Ranger	Tree height measurement
3	Diameter tape	Tree girth measurement
4	Measuring tape (30 and 50 m)	Plot diameter measurement
5	Suunto Clinometer	Bearing measurement
6	Suunto compass	Slope measurement
7	Spherical densiometer	Measure canopy density
8	Fieldwork datasheet	Field Data recording
9	Magellan GPS	Navigation and plot location
10	Google Nexus Tablet	Navigation and plot location
11	Sony Experia Smart Phone	Navigation and plot location

3.2.4. Software

The research uses various software needed for data analysis and their respective application is presented Table in Table 4. Statistical data analysis was mostly done in MS Excel 2013 and SPSS 23. For laser data

analysis, LP 360 (trial version) LAS tools was used to process airborne LiDAR data. Whereas for the terrestrial laser data was processed using RiScanPro software. For the segmentation of the Orthophoto eCognition 9.1.2 was used. For image data analysis ERDAS, LPS 2015.1, and for GIS analysis ArcGIS 10.3.1 were used respectively. Carry Map Observer (trial version) extension tool for ArcGIS for map file conversion. For three dimensional visualization of images ArcScene 10.3.1 was used. For the construction of charts Click Chart Diagram (Trial version) was used. To compile and synthesize the research output into formal document MS Word 2013 was used. To present the output of the research MS Power point 2013 was used.

Table 4. List of software used in the study

Software	Application
MS Excel and SPSS 23	Statistical Analysis
LP 360	LiDAR data format conversion
LAS tools	LiDAR data analysis
RiScanPro	TLS data processing
eCognition 9.1.2	Image segmentation
ERDAS, LPS 2015.1	Image processing
CarryMap Observer (trial version)	ArcGIS extension tool
ArcGIS 10.3.1	GIS analysis
ArcScene 10.3.1	3D visualization
Click Chart Diagram	Construction of Charts
MS Word 2013	Word processing
MS Power point 2013	Presentation

3.3. Research Methods

The activities conducted to carry out this study are the following: remote sensing, field data collection, statistical analysis and biomass and carbon estimation. Using the remotely sensed data upper canopy tree parameters were obtained namely height from the CHM which was derived from the airborne LiDAR and CPA from the Orthophoto were used as independent variables to model the DBH parameters. The height from CHM and modelled DBH parameters consequently were used to derive the modelled AGB for the upper canopy using the allometric equation. Whereas for the lower canopy tree height and DBH were obtained from TLS point cloud data. Using these two parameters lower tree canopy AGB was modelled using the allometric equation. Field data collection involved biometrics data collection by measuring the DBH and height as ground truth data. Using the field DBH, the accuracy of the modelled DBH was validated. Further using the same field DBH and the height from CHM the field AGB for the upper canopy was estimated to validate the modelled upper canopy AGB. Whereas the TLS height and field DBH was used to estimate field lower tree canopy AGB to validate the accuracy of the modelled lower tree canopy AGB. Statistical analysis were done to establish the relationship between the dependent and independent variables as well as model accuracy. The process in detail is presented in Figure 14.

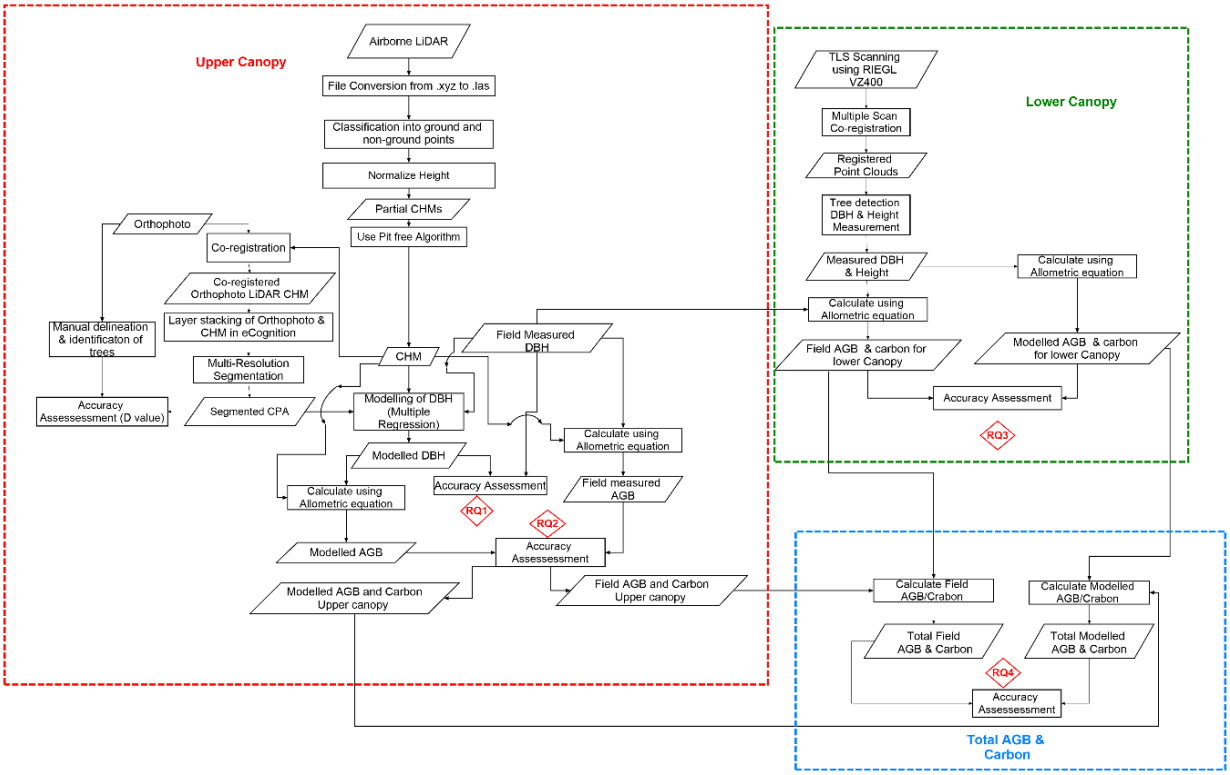

Figure 14. Flowchart of the research method.

3.3.1. Pre-fieldwork

- Preparing the equipment for navigation. Worldview3 image was converted into .cmf (Carry Map File) a file format. This is the compatible format for the Google Nexus tablet and the Sony Experia Smart phone. This tool is an Arcmap extension from Dataeast. Accordingly the stratified grid was converted into this format to overlay the Worldview 3 image. Likewise the same dataset were converted to ECW format and uploaded to iPAQ.

- In the field during the topography shape file of the area was acquired and accessibility inside the forest reserve was derived based on how the forest is managed. These two additional information was converted to shapefiles because these are essential information for navigating through the forest. Accordingly these were converted into a .cmf file format and overlayed on the Worldview 3 image and uploaded into the Google Nexus Tablet.

3.3.2. Sampling Design

The sampling strategy done for this research is purposive. This is a non-probability method of sample selection based on the strategic choices of the researcher. The way the sampling is done is based on the objectives of the researcher that will be achieved. This method was implemented because in the field navigating and carrying a 23 kg TLS system into the forest is a very challenging task. The primary consideration was then the accessibility to establish the plot based on the slope and terrain of the area. Moreover, the thickness of the undergrowth was another factor considered because clearing the area must be done to prevent occlusions from the small stems during scanning. Plot distribution and distances between plots was based on the prepared grids and was confirmed in the field through the use of the tablet. This was

to ensure that the distance from one plot to another is more than 50 m. The established 26 plots had a total area of 500 m^2 per plot. In each plot, central location was established that provides the most suitable viewing position of the TLS. Layout of the sampled plots is shown in Appendix 5.

3.3.3. Field data collection

3.3.3.1. Biometrics Data

The actual field work was done from Sept. 29 to Oct. 12, 2015. This is to collect the ground truth primary data of the study area. Circular plots of 12.62 m was demarcated. The plots was established based on the layout of the area to be sampled. Using a circular plot has its advantage. The geometric shape represents the smallest perimeter that allows the production of the lowest number of borderline tree than other plots shape of the same size (Asmare, 2013). Slope correction was done for plots established with elevation. For each established plot the central coordinates were taken. The DBH of trees within the plot having a 10 cm or greater DBH were measured. To obtain uniform DBH from the ground a 1.3 m measured stick was used as standard measuring guide above the buttress of each tree (Maas et al., 2008). Trees with less than 10 cm girth were not considered because they do not contribute much to the carbon of the forest (Brown, 1999). Moreover the height of these measured trees were measured using Leica DISTO D510 Laser Ranger. The purpose of which was to establish primary ground height data.

3.3.3.2. TLS Data Acquisition

The following sub sections will discuss the methods of acquiring the TLS data. Prior to the actual tree scanning appropriate steps must be done to ensure the quality of the TLS point cloud data.

Plot preparation

The central part of the plot was located by taking into consideration minimal occlusion, blind spot in the case of the sloping terrain, as well as trees very near the centre during scanning. Once the central location was identified clearing of the thick undergrowth was essential. Otherwise quality of the gathered point cloud will be compromised. Moreover, this forest has a very thick undergrowth that was a hindrance in demarcating the area where to establish the outer scan positions. To determine the 3 outer scan positions, 3 suitable locations were identified from the centre location and accordingly 15 m radius was measured. This is also done to identify where to establish the retro reflectors as shown in Figure 15.

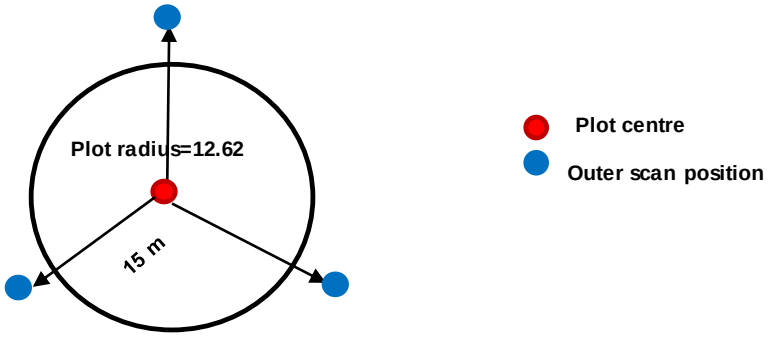

Figure 15. TLS Plot preparation.

Tree Tagging

The trees inside the plot (Figure 16) with measured biometrics and species identified were tagged with plastic laminated numbers so that during the scanning process, they will be identified. This is to ensure that the tree metrics from the actual field measurement will correspond from the tree metrics derived from TLS.

Figure 16. Tagged trees in the plot.

Setting up the scan position

There are two approaches in obtaining terrestrial laser point cloud data namely single and multiple scan mode. Single scan mode allows fast and easy recording however the level of detail for multiple scan mode is higher (Maas et al., 2008). To illustrate, Figure 17 shows the comparison between the two techniques. This study employed the multiple scan technique to ensure that there is sufficient overlap of the scanned data, better canopy height, quality of the point cloud data will not be compromised and consequently better three dimensional representation of the scanned object (Watt & Donoghue, 2005). Moreover, employing multiple scans will improve DBH measurement accuracy compared to single scans (Kankare et al., 2013). Multiple scanning generally took four scans around the object. Accordingly the point clouds from these different scans were merged into a single point cloud. At the minimum, three retro reflectors were placed for the purpose of registration and to ensure complete 3D point targets.

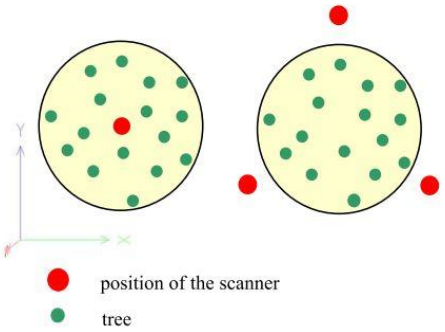

Figure 17. Depiction on how multiple scan positions is set up source (Bienert et al., 2006).

Establishment of retro-reflective objects or tie points

Retro-reflective objects (tie points) were established which serve as reference points for co-registration of the multiple scans. Establishment of these object is to be done because this study implemented a tie point based registration since the potential of misdetection by the sensor or obstruction by trees is considered. There were 15 tie points established for each plot, these were cylindrical (3 dimensional) and circular (2 dimensional) retro-reflectors. The circular tie points were pinned into the tree stem near the central location of the scanner whereas the cylindrical tie points were positioned on approximately 1 m height sticks to establish elevation from the ground (Figure 18). To ensure that these tie points were recognized during scanning, the position of these tie points were based on the following conditions: levelling on the tripod, even distribution with a linear pattern, they are within the scanning range, stability of their position and visibility from all scanning positions.

Figure 18. Set up of cylindrical and circular reflectors in the plot.

Setting the TLS and scanning

The TLS instrument RIEGL-VZ-400 was set on the tripod with the NIKON D610 camera mounted on top. Levelling was done by adjusting the legs of the tripod to align the instrument vertically and horizontally. The scan position for each plot was set as a new project with the specified scanner settings as shown in Table 5. To fix the scan position, each plot was saved as new scan position prior to setting the instrument for pulse ranging. Then after fixing the scan position, fine scanning of reflectors was done for automatic registration of multiple scans. This is done for reflector identification and marking them manually. For fine scanning of the reflectors fine scanning mode of the scanner was set automatically.

Table 5. RIEGL-VZ-400 scanner settings for data acquisition.

Sensor	settings
Image acquisition	Accurate
Reflector threshold	0.05db
Scan mode	Panorama-60
Range	50m
Scan form	Range
Reflector size	>10 cm

3.3.3.3. Field Data Analysis

Generating Pit free CHM

The airborne LiDAR data was provided by the University of Putra Malaysia. The data provided had two file folders that contain raw and processed format. The processed folder contains a point cloud data in .xyz format. For further processing in LAS tools this file format was converted to .las file format using the LP 360 (trial version). The CHM was then generated by adapting the method of Khosravipour, et al., (2014) using the algorithm to create a pit free raster CHM. This method employ the direct processing of point cloud data in into raster format unlike another method of subtracting the DTM from DSM. Using LAS tool lasground the converted files were classified into ground and non-ground points. Then using the las height tool height was normalized by replacing the elevation of each point with its height above the ground. Using the las2dem partial CHMs were generated then the pit free algorithm was used to convert the partial CHMs into a pit free raster CHM. It is important to note that pit free CHM is a new method of creating CHMs as pointed out by Khosravipour, et al., (2014) and detailed comparison of the method had proven that it can provide better height metrics. Moreover, in this study adapting the method of generating better height metrics was essential because of the reliability of the primary ground data that was acquired.

Manual Identification and Delineation of Trees

One of the many challenges encountered in this study is the identification of trees. This is because, the handheld GPS system used could not function properly under thick tree canopy conditions. Moreover, for the terrestrial laser scanner, converting the scanner's local coordinate system into a global coordinate system also had conversion problems even though this was referred to the instrument supplier. A reasonable

solution to this challenge was to reconstruct the plot in the generated CHM and Orthophoto. Based on the acquired centre plot location, and geotagged tree points near the centre plot, individual trees were identified first using the images derived from the TLS. Its relative location was identified in RiSCAN software. Based on that information location of the tree was identified into the reconstructed plots in the Orthophoto using plot bearing as a guide to locate the tree. Using the height information of the tree from the TLS its location was further verified using the generated CHM. Tree crown delineation per plot was subsequently done using manually identified trees in the Orthophoto.

Layer stacking of CHM and Orthophoto in eCognition

The generated CHM and Orthophoto was co-registered into the same coordinate system before creating a project in eCognition. This is a prerequisite step in eCognition prior to combining two datasets with different resolutions. Layer stacking of the two images was done to combine the two datasets for subsequent segmentation. This is a data fusion method in eCognition to establish the same rulesets prior to the segmentation process (http://www.americaview.org/event/data-fusion-ecognition-webinar-2-pm-edt Retrieved 12/15/2015). Moreover the technique is applied to identify features using the scale and homogeneity parameters obtained from the spectral reflectance values from the Orthophoto and the elevation from the CHM (Suárez, et al., 2005).

3.3.3.4. Segmentation

Dividing an image into spatially continuous, disjoint and homogeneous regions is the principle behind image segmentation (Cheng, et al., 2001). The process of segmentation is one of the primary steps in object based classification with the assumption that the segmentation results will directly affect the performance of the subsequent classification (Gao, et al., 2001). Defining an object is a basic step in the segmentation process (Kim, et al., 2008) because image objects with defined homogeneity, size and shape are the building blocks for further image operations (Definiens, 2009). There are two basic segmentation approaches namely the top- down and the bottom-up approach. Top down approach splits the larger object into smaller objects. A typical example is the chessboard or quad tree based segmentation (Definiens, 2012). On the other hand bottom up approach or region based merges smaller objects into larger objects based on the homogeneity criteria. The procedure starts with a single image object and repeatedly merges them on a pairwise loops to larger units as long as it does not exceed the upper threshold of local homogeneity. Multi-resolution segmentation is one example of this approach (Definiens, 2012).

Multi-resolution Segmentation

Multi-resolution segmentation is a region based algorithm used for successfully implementing image segmentation applications. The algorithm locally minimizes the average heterogeneity of image objects for a given resolution of image objects. The process can be done at the object or pixel level for creating new image object (Definiens, 2012). The method consecutively merges the best fitting neighbouring pixel in the creation of the image object within a defined minimum heterogeneity (Benz, et al., 2004). The initial step of the procedure is with a single image object of one pixel and repeatedly combines them in several loops in pairs to form larger objects on the condition that the upper threshold of homogeneity is not locally exceeded. The homogeneity criterion is the combination of the spectral and shape homogeneity that can be influenced by the user (Definiens, 2012). An illustration of the process is shown in Figure 19. The method has been implemented as an approach to forest biomass estimation (Van Aardt, et al., 2004). Subsequently, this study applied this method using eCognition 9.1.2.

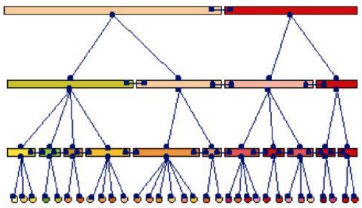

Figure 19. Illustration of multi-resolution segmentation (Benz et al., 2004)

Scale parameter

Scale parameter determines the upper limit for the permitted change of the heterogeneity throughout the segmentation process. This also determines the average size of the object thus, higher scale parameter will allow more merging that would result to bigger objects and vice versa (Rahman and Saha, 2008). This parameter is dependent on the judgment of the user because it is a subjective measure of real world to generate image objects. Therefore obtaining the appropriate scale entails an iterative process of trial and error to determine the appropriate scale. The Composition of homogeneity criterion is the object homogeneity which the scale parameter refers to. The three criteria for homogeneity, that are internally computed, are color (spectral response), smoothness and compactness (shape) (Definiens, 2012). The concept of Multiresolution is presented in a flow diagram in Figure 20.

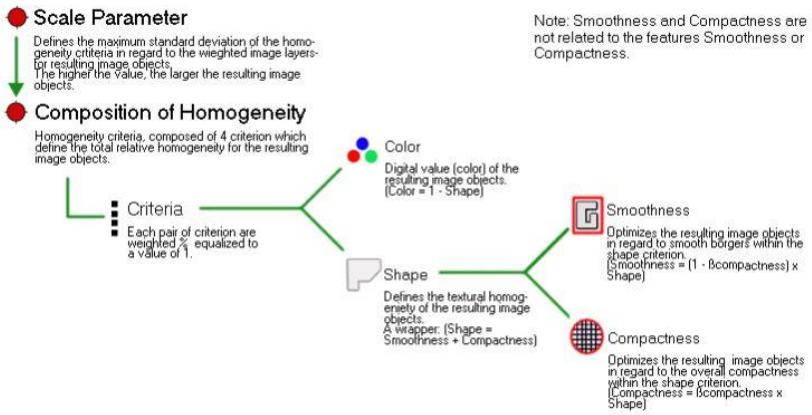

Figure 20. Conceptual flow diagram of Multiresolution.

ESP tool for Estimation of Scale Parameter

The application of multi scale image segmentation as a fundamental step to object based image analysis needs a tool to objectively guide in the selection of the appropriate scale for segmentation. (Drăgut et al., 2010) developed an estimation parameter tool (ESP) a technique for estimating the scale parameter in image segmentation of remotely sensed data with Definiens Developer. This is based on the local variance (LV) of object heterogeneity within the scene. The tool generates image objects at an iterative process at multiscale levels in a bottom up approach and calculates the LV for each scale. The ROC-LV values are plotted against a scale value where it shows peaks of multi scales. This indicates the suitable level which the image can be segmented. The ESP tool is shown in (Figure 21).

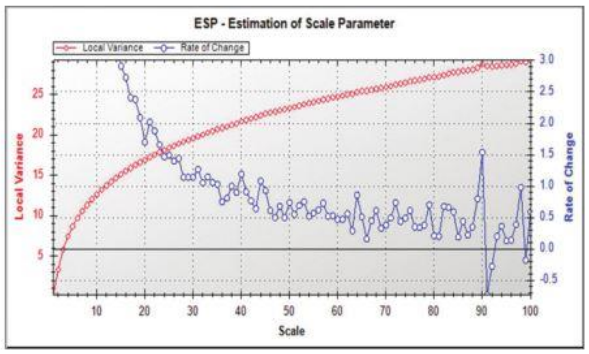

Figure 21. ESP tool for determining scale parameter (Definiens, 2012).

Masking out of Shadow, Urban Area and Water Bodies

Due to the viewing angle on the acquisition of the Orthophoto shadow areas were observed. Moreover there are parts of the forest that have concrete and asphalted roads as well as some water bodies. These areas were masked out based on the brightness values of the objects. The reflectance values of these objects were checked and determined using the image object information. These reflectance values were used to develop the ruleset to masked out these objects. The obtained reflectance values for water bodies and shadow areas is below 30 and above 90 for urban areas.

Watershed transformation

The application of watershed algorithm was used to separate image objects. For tropical forests this is an important technique for separating overlapping tree crowns. The tree crown is separated based on a splitting threshold based on the crown diameter of the tree. In this case the basis for tree crown diameter is based on the measured tree crowns of the extracted trees from the TLS. Due to time constraints and difficulty of measuring tree crowns in the field this method was implemented.

This algorithm considers the image to be processed as topographic surface. This considers three basic principles: minima, catchment basins and watershed lines (Chen, et al., 2004)) as illustrated in Figure 22. In an inverted grayscale object where the local maxima becomes the local minima and holes are punctured at the local minima. In between the local minima and maxima are catchment basins that would resemble tree crown. The watershed lines are the local maxima of the inverted image and the image would look like a watershed catchment basins. If these water catchment basins are flooded with water each valley would collect water from the local minimum and create a spill over effect into the adjacent valley (Wang et al., 2004). Since each valley is surrounded by watershed lines that separate the whole surface into different catchment basins a desired image boundary is formed. For forestry applications this will treat clumping of tree canopies as the catchment basin and when flooded the trees which are considered as valleys will touch each other separating them as individual trees.

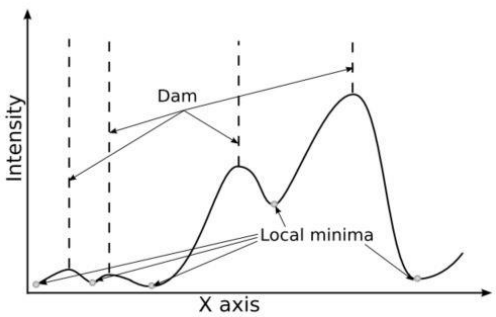

Figure 22. Illustration of watershed transformation (Derivaux, et al., 2010)

Morphology

The algorithm refers to the image processing technique to smoothen the border of the image objects based on mathematical morphology. There are two basic operations namely opening and closing. Open image object removes pixels from an image and is defined as the area that will completely contain the mask. Whereas close image object adds surrounding area of an image object that can completely contain the mask. Further, to define the shape and size the circular mask is used. It is a mathematical morphology operation used to define structuring element of the image objects. Circular masks is applied for this study since tree crowns are circular and more appropriate to represent shape for tree crowns (Definiens, 2012).

Removal of undesirable objects

When the segmentation procedure was completed, removal of tiny objects was performed to exclude smaller elongated segments because they do not represent trees. In this study segments with less than 6 pixels (calculated as the length factor) were removed for they are unlikely to be tree crowns.

Segmentation Validation

The degree of fitness of the segmented objects must be validated relative to the known object. The validation is based on the optimal customization of parameter settings as well as data quality such as noise, spatial and spectral resolution (Möller, et al., 2007) that determines how the segmented object match to the target object. Accuracy of the segmentation can be based on visual and geometric techniques. The visual assessment developed by Möller, et al., (2007)assess the accuracy of the segmentation based on the relative area in reference to the manually digitized polygons. The best score is given if the referenced polygons is completely covered by the segmented objects. According to (Zhan, et al., 2005) at least a 50% overlap of the reference and segmented objects is acceptable. Moreover, the completeness and correctness of the matched objects considers size, shape and position. A visual illustration by Zhan, et al., (2005) is shown in Figure 23. This explains four matched cases wherein the matched region is in orange. The green region is extracted but not explained by the referenced data. Blue is a region in a referenced data that is not extracted. Illustration ***a*** showed a 50% match, ***b*** showed a match with the same shape and size but in different position, ***c*** and ***d*** a match in the same position but differ in spatial context.

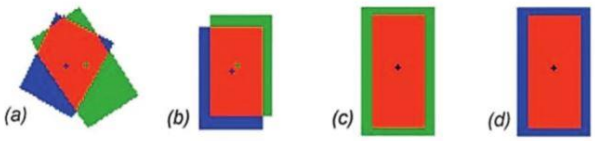

Figure 23. Illustration on matching of segmented and referenced polygons (Zhan et al., 2005).

Another method of assessing the accuracy of segmented polygons developed by (Clinton, et al., 2010) is based on the geometric extent of the segmented output with reference to a defined training set. The quality of the segmented output is defined in terms of over and under segmentation. Over segmentation and under segmentation is explained by Clinton, et al., (2010) based on Equations 1 and 2.

$$OverSegmentation_{ij} = 1 - \frac{area(x_i \cap y_j)}{Area(X_i)}, y_i \epsilon Y_i^* \quad \text{..... Equation 1}$$

$$UnderSegmentation_{ij} = 1 - \frac{area(x_i \cap y_j)}{Area(Y_i)}, y_i \epsilon Y_i^* \quad \text{..... Equation 2}$$

Where: xi is reference object and yj is its corresponding segmented object

The goodness of fit is explained in terms of the distance index (D) which is the combination of over and under segmentation. The D value range is from 0 to 1, where 0 is a perfect match between the reference polygon and the segmented object and 1 is the minimum mismatch. The goodness of fit is calculated using Equation 3.

$$D_{ij} = \sqrt{\frac{Oversegmentation_{ij}^2 + Undersegmentation_{ij}^2}{2}} \quad \text{..... Equation 3}$$

3.3.3.5 Point Cloud Data Analysis

The acquired point cloud data from the field was processed using RiSCANPRO software provided by RIEGL. RiSCANPRO is companion software for 3-D terrestrial laser scanner systems. The system has a built in project data structure where the acquired data is organized and stored. The acquired data set includes scans, digital images, tie point coordinates and the transformed matrices used in the transformation of multiple scans into a defined coordinate system. Additional functionality of the software is also provided for the subsequent processing of the point cloud data. The subsequent sections will discuss the steps implemented to further process the TLS acquired point cloud data.

Registration

This study implement coarse registration of point cloud data. The concept of this method is rough estimation of the rigid motion between two point clouds (Xie, et al., 2010). This was done by defining the tie points from the acquired scan position dataset in 2D mode. In this case the reference data set is the first scan position which was centrally located and the dataset to be registered are the outer scan positions. The corresponding tie points for each scanned datasets were located and tie points were defined as it was registered. The co registered scans were added to the view and were visually assessed and the standard deviation was calculated to assess the quality of the registration. To improve the quality of the registration Multistation Adjustment was implemented. This algorithm iteratively adjust the position and orientation of the scan position until the error is below the user defined threshold.

Plot Extraction

Since the scanned point cloud data covers a large area the circular plots were filtered. The plot measurement was based on the recorded field data that considers the slope correction of each plot. To define the area of interest points that were within the plot distance were selected using the range function of RiSCAN PRO.

Individual tree detection

To extract the individual trees, the point clouds that were related to tree shapes were selected using the viewer mode of RiSCAN PRO. Through visual inspection noise (creepers and visible undergrowth) were manually removed. The recognized trees were then sliced and saved as poly data for further tree parameter assessment.

Tree Height Measurement

The extracted tree that was saved as poly data was retrieved in the RiSCAN PRO view menu. Each individual tree was manually measured using the measuring tool of the software. The lowest (ground) and highest (tree top) points of each tree were located. The measurement tool read the x, y, & z values of measured points and the height was measured along the vertical axis between the lowest and highest points (Figure 24). The obtained height measurement was stored in a database format using Excel.

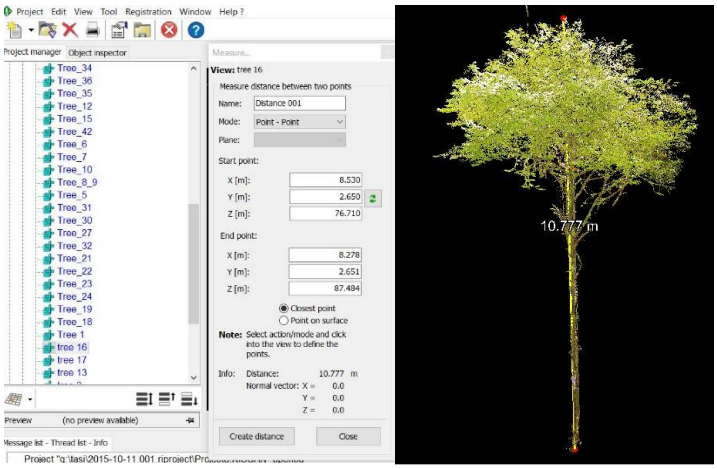

Figure 24. Tree height measurement of extracted trees.

DBH Measurement

DBH measurement was also done for each individual tree using the measuring tool in RiSCAN PRO. This was determined at 1.3 m from the lowest point of the tree and the width of the stem of the tree of this height was measured on a point to point basis. The measurement tool then reads the x, y, & z values of the measured points and the width measurement is taken along the horizontal distance of the stem (Figure 25).

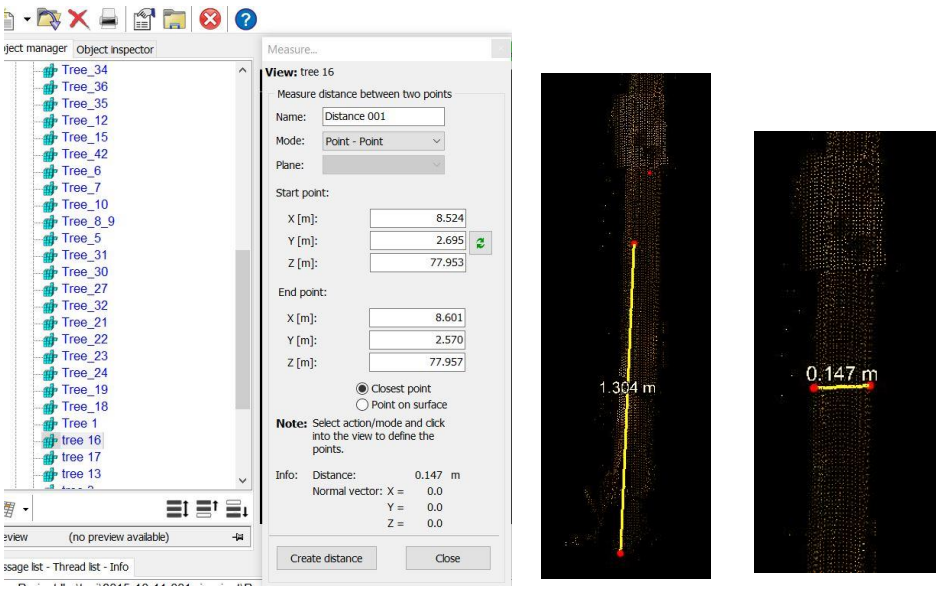

Figure 25. DBH measurement of extracted trees.

3.3.4. AGB and Carbon Stock Estimation

Using allometric equation is a common method of estimating forest biomass that can be used in large forest areas through non-destructive methods (Ketterings, et. al, 2001). The equation relates to tree structural parameters that can be repeatedly measured on the ground and can be used to estimate AGB. However for a tropical forest like AHFR which stores a highly diverse species of trees, local or geographical allometric equations are not appropriate (Gibbs et al., 2007). Thus, in this case the generic equation (Equation 4) developed by Chave et al., (2014) is adapted. Adapting generic allometric equations have the potential to increase the precision of the AGB estimates because the equation is established based on a larger number

of trees (Gibbs et al., 2007; Chave et al., 2005)). Consequently, the precise estimation of the AGB will also provide precise carbon stock be estimation by multiplying the 50% factor (Drake et al., 2003).

$$AGB_{est} = 0.0673 \times (\rho D^2 H)^{0.976}$$ ..... Equation 4

Where,
AGB: Above ground biomass (Kg)
ρ: specific wood density
D: diameter at breast height
H: Height

3.4.5. Regression Analysis and Model Validation

Regression analysis is an established method for modelling the relationship between remotely sensed data and field measurements (Popescu, 2007; Lim et al., 2003). The objective of the method is to quantify the relationship between the response variable and the explanatory variable. It also assess the relationship between the dependent and independent variable and the causal effect of the relationship. Moreover the change in the independent variable will also result in the change in the dependent variable (Husch et al., 2003). Since the objective of this study is to account for the total AGB/Carbon a regression analysis was heavily used in establishing relationships among the derived forestry parameters. To assess the upper canopy layer of the forest multiple linear regression was used to model the relationship between the field measured DBH and the airborne LiDAR derived height and CPA derived from the Orthophoto to obtain a modelled DBH. While to assess the relationship between the modelled AGB and field measured AGB a linear regression was implemented. In assessing the AGB of the lower canopy layer of the forest, linear regression was used to establish the relationship between the modelled AGB using the TLS measured DBH and height and the field measured AGB using the field measured DBH and TLS height. Then to assess the relationship between the modelled total AGB and the total field AGB linear regression was used. To assess the performance of all modelled parameters the RMSE was calculated using the general equation (Equation 5).

$$RMSE = \sqrt{1/n \sum_{1}^{n} (P - O)^2}$$ ..... Equation 5

Where,
P: Predicted
O: Observed
n: number of observations

4. RESULTS

4.1. Descriptive analysis of field data

The trees measured in the16 field plots were identified by species name and family name as shown in Table 6. The complete list of identified and count per species is tabulated in Table 7. Tree parameters (DBH and crown diameter) of the individual sampled trees were measured. The total number of trees used for the comparative analysis with measured DBH and crown diameter is 428 and 232 respectively. Descriptive statistics of these parameters are shown in Table 8 and the normal distribution and QQ plots of the measured parameters are shown in Figure 26. Table 9 show the normality test of the two parameters.

Table 6. Summary of trees measured in the field.

		No. of Trees
Average No. of tree species per plot	17	
Total No. of Trees Identified by species name	107	391
Total No. of Trees Identified by family name	5	37
Total No. of Trees		428

Table 7. Identified trees and count per species from the field plots.

Species No.	Species	Count per Species	Species No.	Species	Count per Species
1	*Acacia auriculiformis*	5	21	*Caelostegia griffitii*	1
2	*Adenanthera spp*	1	22	*Calophyllum rubiginosum*	1
3	*Aglaia spp*	2	23	*Calophyllum sp*	1
4	*Albizia splendens*	1	24	*Calophyllum spp*	3
5	*Anisoptera costata*	1	25	*Campnosperma spp*	1
6	Annacardiaceae	1	26	*Carallia brachiata*	2
7	Annonaceae	4	27	*Carallia spp*	2
8	*Antidesma caspidatum*	1	28	*Castanopsis spp*	1
9	*Ardisia densiflora*	1	29	*Cinnamomum iners*	12
10	*Arthocarpus scortechinii*	1	30	*Cinnamomum porrectum*	1
11	*Arthrophyllum diversifolium*	1	31	*Citrea spp*	1
12	*Artocarpos rigidus*	3	32	*Cratoxylum spp*	1
13	*Artocarpos scontechinil*	1	33	*Cryptomeria japonica*	2
14	*Artocarpus rigidus*	2	34	*Cyathocalyx spp*	1
15	*Artocarpus scortechiunii*	8	35	*Delek*	1
16	*Artocarpus spp*	6	36	*Dialium spp*	1
17	*Blumeodendron tokbrai*	1	37	*Diospyros argentea*	1
18	*Bridelia tomentosa*	1	38	*Diospyros spp*	9
19	Burseraceae	12	39	*Diplospora malaccensis*	1
20	*Byera costulata*	2	40	*Dipterocapus crinitus*	3

Table 7. Continued.

Species No.	Species	Count per Species	Species No.	Species	Count per Species
41	*Dipterocarpus costulatus*	13	77	*Palaquim gutta*	9
42	*Dipterocarpus crinitus*	1	78	*Palaquim maingayi*	3
43	*Dipterocarpus verrucosus*	2	79	*Palaquim spp*	2
44	*Dyera costulata*	1	80	*Parkia singularis*	1
45	*Elaeocarpus spp*	5	81	*Pela calyxyia*	1
46	*Eleocarpus spp*	1	82	*Pellacalyx axillaris*	3
47	*Endospermum diadenum*	19	83	*Pellacalyx spp*	2
48	*Fagraea spp*	1	84	*Pentace spp*	2
49	*Ficus spp*	1	85	*Pentaspadon spp*	1
50	*Garcinia spp*	1	86	*Porterandia anisophylla*	2
51	*Gilba sp.*	1	87	*Pouteria malaccensis*	7
52	*Gironniera nervosa*	7	88	*Ptenandra spp*	4
53	*Gironniera spp*	1	89	*Rambutan hutan*	1
54	*Gluta spp*	2	90	*Rhodamnia cinerea*	1
55	*Gynotroches axillaris*	4	91	*Rotoxylum spp*	1
56	*Gynotroches axillaris*	4	92	*Sandoricum koetjape*	3
57	*Herittiera spp*	2	93	*Santiria spp.*	1
58	*Hopea odorata*	2	94	*Scaphium macropodum*	4
59	*Hopea sulcata*	14	95	*Scaphium spp*	1
60	*Ixonanthes icosandra*	4	96	*Shorea accuminata*	6
61	*Knema spp*	4	97	*Shorea hypocra*	2
62	*Koompassia malaccensis*	1	98	*Shorea leprosula*	3
63	Lauraceae	6	99	*Shorea macroptera*	11
64	*Lithocarpus spp*	7	100	*Shorea parvifolia*	9
65	*Litsea costata*	7	101	*Shorea sumatranum*	1
66	*Litsea spp*	6	102	*Sterculia spp*	5
67	*Macaranga gigantea*	3	103	*Streblus elongatus*	32
68	*Macaranga spp*	5	104	*Strombosia javanica*	1
69	*Maclurodendron porterii*	5	105	*Swintonia spp*	2
70	*Mallottus spp*	1	106	*Syzygium polyanthum*	12
71	*Memecylon spp*	4	107	*Syzygium spp*	20
72	*Mesua spp*	1	108	*Timonius wallichianus*	2
73	*Metadina trichotoma*	7	109	Unidentified	1
74	Myrysticaceae	13	110	*Xantophyllum spp.*	2
75	*Naphelium spp*	5	111	*Xerospermum spp*	3
76	*Ochanostchys amentaceae*	3	112	*Xylopia ferruginea*	2
				Total No. of Trees	**428**

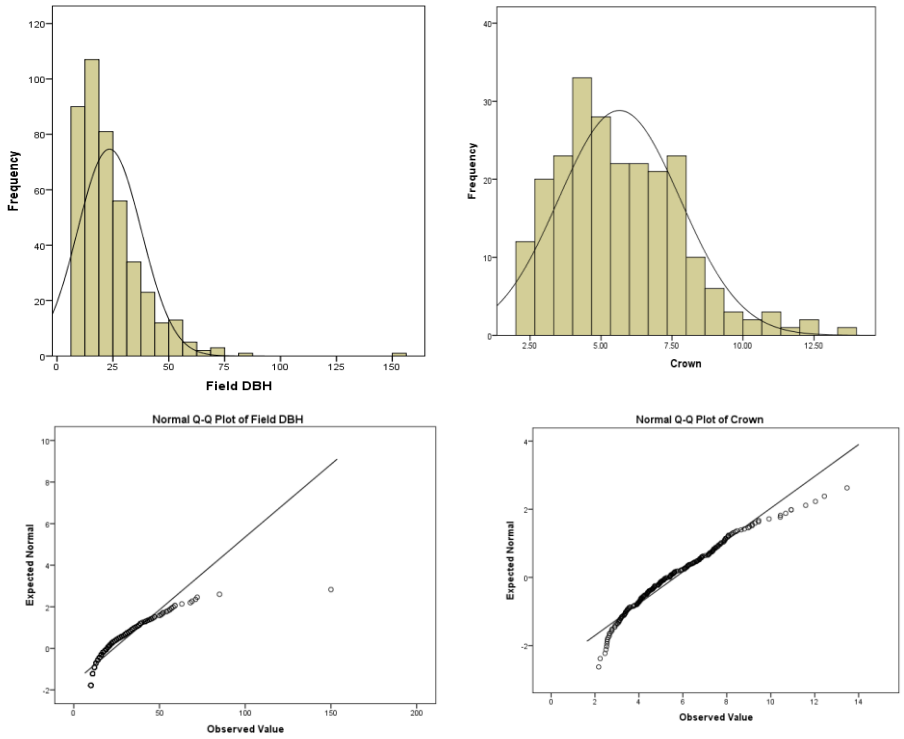

Figure 26. Distribution and QQ plots of field DBH and tree crowns

Table 8. Descriptive statistics of the sampled trees.

Statistic	DBH (cm)	Crown Diameter (m)
Mean	23.47	5.65
Minimum	10	2.17
Maximum	150	13.47
Standard Deviation	14.29	2.14
Number of trees	**428**	**232**

Table 9. Normality test of field measure DBH and crown.

	Kolmogorov-Smirnova			Shapiro-Wilk		
	Statistic	df	Sig.	Statistic	df	Sig.
DBH	0.173	0.428	0.000	0.789	0.428	0.000
Crown	0.076	232	0.002	0.956	232	0.000

4.2. Pit-Free CHM generation from Airborne LiDAR Data

The airborne LiDAR data was processed to generate the CHM for the upper canopy layer of the forest. The point cloud data was classified into ground and non-ground points (Figure 27). The height was then normalized and partial CHMs were created (Figure 28). The presence of pits in the partial CHMs would have significant effect to subsequent height estimation. As a final step to the process the pit-free algorithm developed by Khosravipour, et al., (2014) was applied. The final pit-free CHM is shown in Figure 29.

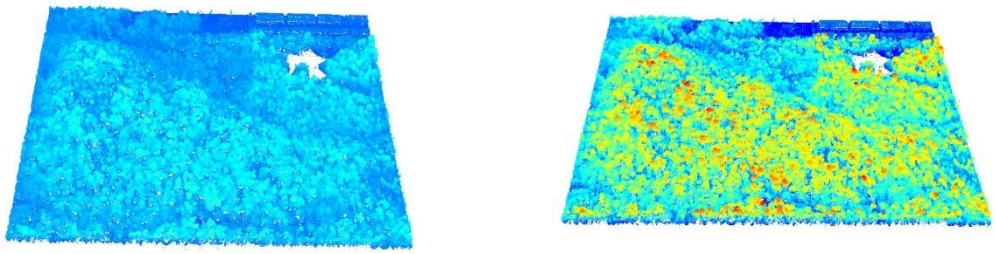

Ground Height

Figure 27. Classification of point cloud data into ground and non-ground points.

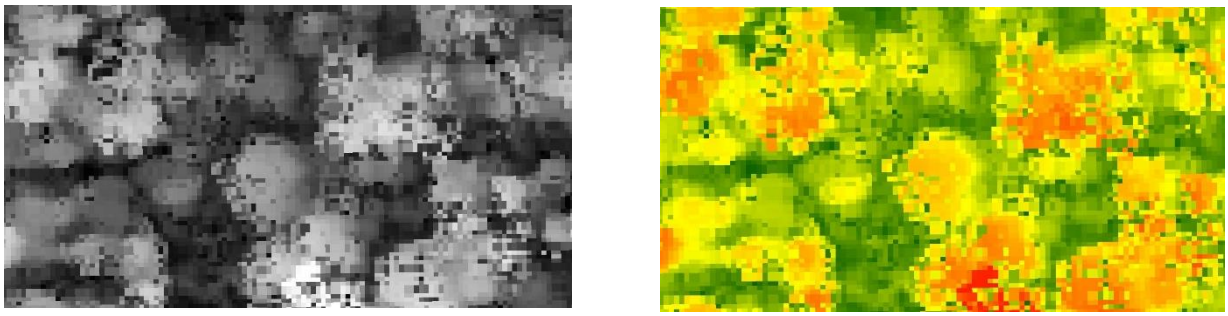

Figure 28. Partial CHM

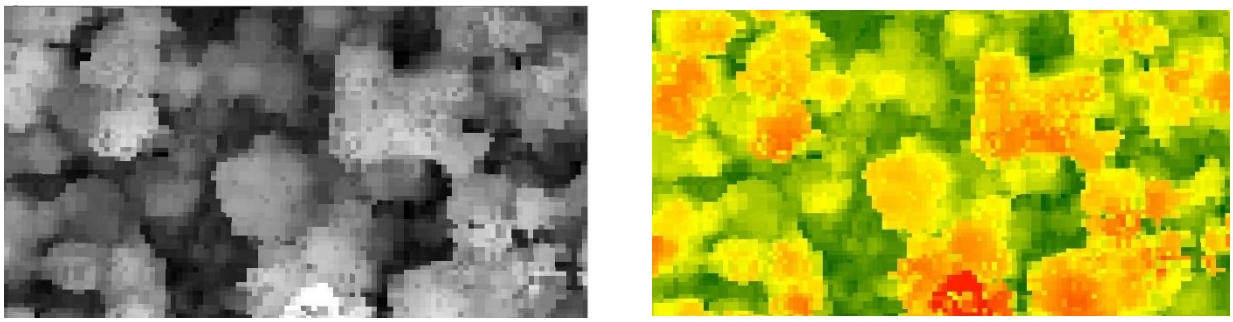

Figure 29. Pit-free CHM.

4.3. Image segmentation

To derive the CPA of the upper canopy layer image segmentation of the Orthophoto layered with the CHM was implemented using multi-resolution segmentation. The process involves the execution of the following sequential steps to obtain image objects that would represent tree crowns.

4.3.1. Estimation of Scale Parameter (ESP)

The eCognition Developer 9.1.2 software, has the ESP tool to assess the most suitable scale parameter in creating image objects. The application of the tool indicates that high peaks in rate of change (ROC) and local variance (LV) will determine the appropriated scales by which the image can be segmented. Figure 30 show the scale parameter of the Orthophoto layered with the CHM by which the scale of 10 is the suitable one.

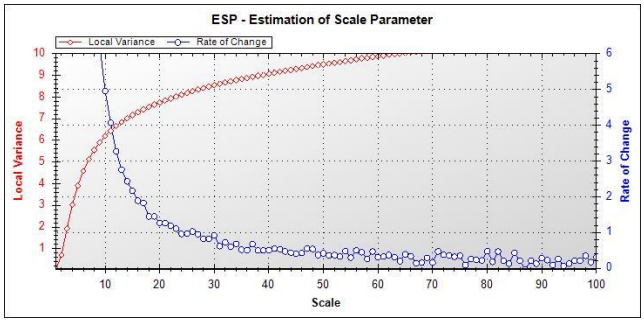

Figure 30. Scale parameter for Orthophoto and CHM layer using ESP tool.

4.3.2. Multi-resolution Segmentation

Using the scale parameter as estimated from the ESP tool multi-resolution segmentation was applied. The scale of 10 was adapted to set this parameter as based on the highest value calculated by the tool. Moreover, based on visual assessment and matching with the manually delineated crowns this gave a good match and accuracy which will be shown in the next section. A portion of the segmented section is presented in Figure 31.

Figure 31. Segmented portion of the Orthophoto layered with CHM.

4.3.3. Assessment of segmentation accuracy

Accuracy assessment of the segmented objects were based on the identified trees per plot that matched with the automatically segmented objects. Of the total 208 trees identified and manually delineated 160 trees had a 1:1 match which is 77% match. Figure 32 shows the overlay between the manually delineated referenced polygons (purple outline) over the corresponding segment (outlined in black line). The over and under segmentation at the scale of 10 is 0.09 and 0.03 respectively and the D value of 0.25 (75%). This indicates that overestimation of the tree crowns is greater than underestimation. Table 10 show the segmentation accuracy assessment.

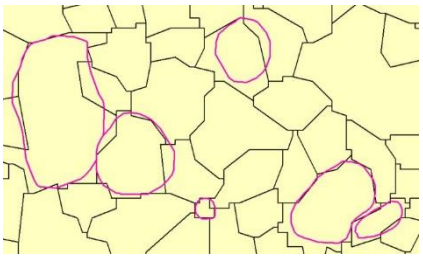

Figure 32. Overlay between referenced and segmented polygons.

Table 10. Segmentation accuracy assessment.

	Total reference polygons	Total 1:1 match	Over segmentation	Under segmentation	D-value
1:1	208	160			
Goodness of fit			0.09	0.03	0.25
Total Accuracy		77%			75%

4.4. Registered Scans

Registration of 4 TLS scans using the point cloud data which aligned the scanned positions to obtain a three dimensional perspective of the scanned scene Figure 33. Creating the three dimensional scene would then allow the subsequent steps of identifying individual trees, tree extraction and tree parameter measurements (DBH and Height). Applying the method and the subsequent multistation adjustment (MSA) obtained a standard deviation of 0.01- 0.0234 cm of the point cloud data.

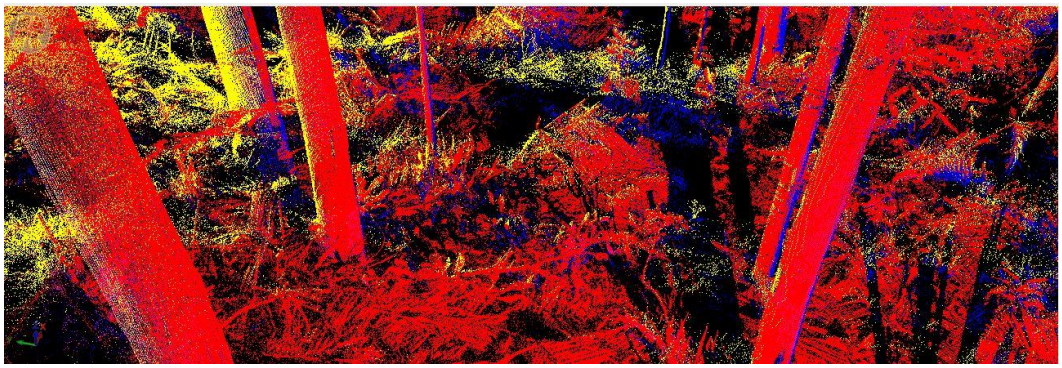

Figure 33. Three dimensional scene after registering the point cloud data.

4.5. Individual Tree Detection

Detecting individual trees was done by identifying point clouds that fit the shape of an individual tree. Identification was done through the tagged numbers to the individual trees in the plot. The process is based on the assumption that point clouds tend to aggregate near the circular points that is distributed through the vertical axis of some height which is separated from the adjacent stem. Tagged individual trees that were visibly identified were recognized as trees.

4.6. Individual Tree Extraction

Trees that were individually detected were extracted manually in RiSCAN PRO and stored as individual polydata. Figure 34 shows sample of individual trees extracted trees from RiSCAN PRO. From the extracted trees individual tree parameters such as DBH and height were measured using the measure interface of RiSCAN PRO. The obtained parameters were subsequently used for AGB modelling and estimation.

Figure 34. Sample of extracted trees.

4.8. Plot selection for DBH and AGB analysis

The total number of plots measured, recorded and scanned in the field was 26. However, for the analysis used for the study only 16 plots were viable for the subsequent model analysis and AGB estimation. This is because for the rest of the 10 plots not all trees were detected from the CHM from airborne LiDAR and CPA from the Orthophoto. On the other hand not all trees scanned were detected and extracted from TLS. Estimating the AGB on a plot basis must have the complete number of trees per plot for precise AGB accounting. Therefore, plots that contained trees that would complement from both sensors were identified and selected for the analysis. Table 11 show the number of trees per plot identified and extracted by the respective sensors.

Table 11. Trees identified and extracted by the respective sensor.

Plot no.	No. Trees Detected by Airborne LiDAR & Orthophoto	Extracted trees obtained from TLS	Total No. of Trees
1	12	3	15
2	13	10	23
3	20	7	27
4	13	11	24
5	18	3	21
6	16	8	24
7	11	15	26
8	11	14	25
9	12	16	28
18	10	25	35
20	10	14	24
21	13	30	43
22	13	24	37
24	11	15	26
25	13	10	23
26	12	15	27
Total	**208**	**220**	**428**

4.9. Upper Canopy AGB calculation

4.9.1 CHM and CPA parameters

To calculate for AGB of the upper canopy, height parameter from the generated CHM and CPA from the segmented Orthophoto was obtained. These are the main parameters required to model the DBH. The mean height and CPA per plot is presented in Table 12. The descriptive statistics of the two parameters are shown in Table 13. The normality of the data distribution of these two parameters were tested using SPSS 23. Figure 35 show the distribution curve and QQ plots of the two parameters. Table 14 show the normality test output indicating that height is normally distributed with a p-value greater than .05 (shown as sig on Shapiro-Wilk of the table). Whereas for the CPA the distribution is slightly skewed to the right which is indicated in the p-value lower than 0.05. Since DBH cannot be measured directly from the images, subsequent modelling through multiple regression analysis was applied using these two parameters.

Table 12. Average CPA and height per plot.

Plot No.	CPA	Height	Plot No.	CPA	Height
1	5.83	20.53	9	7.38	17.68
2	8.37	19.42	18	6.32	20.86
3	5.83	20.53	20	7.17	23.28
4	5.85	22.04	21	5.62	20.79
5	6.45	21.79	22	7.29	24.06
6	7.03	19.32	24	6.08	21.79
7	7.62	17.34	25	5.98	23.07
8	6.35	11.59	26	6.55	21.24

Table 13. Descriptive statistics of CPA and height.

Statistic	CPA (cm)	Height (m)
Mean	6.68	20.06
Minimum	1.89	6.32
Maximum	16.14	38.06
Standard Deviation	2.98	5.29
Number of trees	**208**	**208**

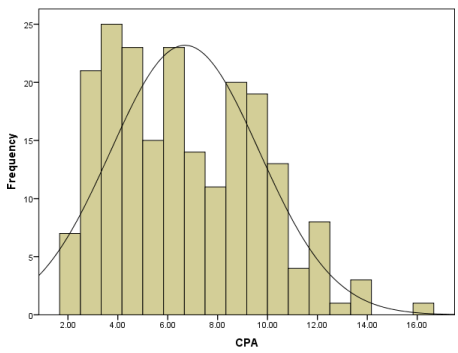

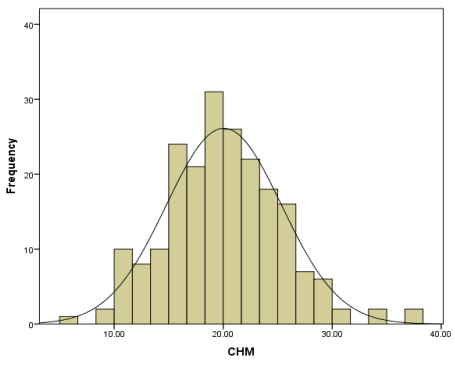

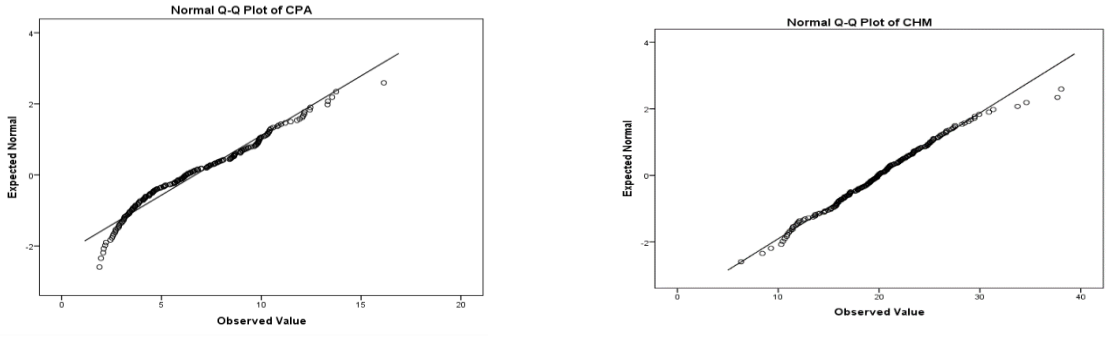

Figure 35. Distribution and QQ plots of CPA and height.

Table 14. Normality test of height and CPA.

	Kolmogorov-Smirnova			Shapiro-Wilk		
	Statistic	df	Sig.	Statistic	df	Sig.
CHM	0.0426	208	0.2000	0.9884	208	0.0907
CPA	0.0898	208	0.0003	0.9613	208	1.871E-05

4.9.2 DBH modelling using multiple regression analysis

Modelling the DBH for the upper canopy layer employed multiple regression analysis. This was done using the above mentioned parameters. Height from CHM and segmented CPA were used as independent variable and the field measured DBH as the dependent variable. Table 15 show the average modelled DBH and the average field measured DBH. The descriptive statistics of these average values of the two parameters are shown in Table 16. The normal distribution and QQ plots of the modelled and field DBH was then tested (Figure 36). The normality output is shown in Table 17 and the p-value indicated that the distribution of both modelled and field are skewed to the right. Figure 37 show the overall relationship between the modelled and field measured DBH for the 16 plots. The regression statistics, probability and reliability of the 16 plots is in Table 18. The regression statistics per plot is shown in Table 19. The regression probability and reliability summary per plot is shown in Table 20. Further, Figure 38 show the relationship at the plot level.

Table 15. Average modelled and field DBH per plot.

Plot No.	Modelled DBH	Field DBH	Plot No.	Modelled DBH	Field DBH
1	23.91	23.92	9	29.70	29.92
2	38.63	38.62	18	34.30	34.33
3	29.28	29.30	20	38.00	38.00
4	30.68	30.69	21	27.35	27.54
5	30.67	30.67	22	27.77	27.77
6	24.54	24.56	24	36.72	36.73
7	20.18	20.18	25	27.70	27.85
8	20.28	20.09	26	24.88	24.33

Table 16. Descriptive statistics of averaged modelled and field DBH.

Statistic	Modelled DBH	Field DBH
Mean	29.03	29.03
Minimum	20.17	20.09
Maximum	38.62	38.61
Standard Deviation	5.72	5.76
Number of plots	**16**	**16**

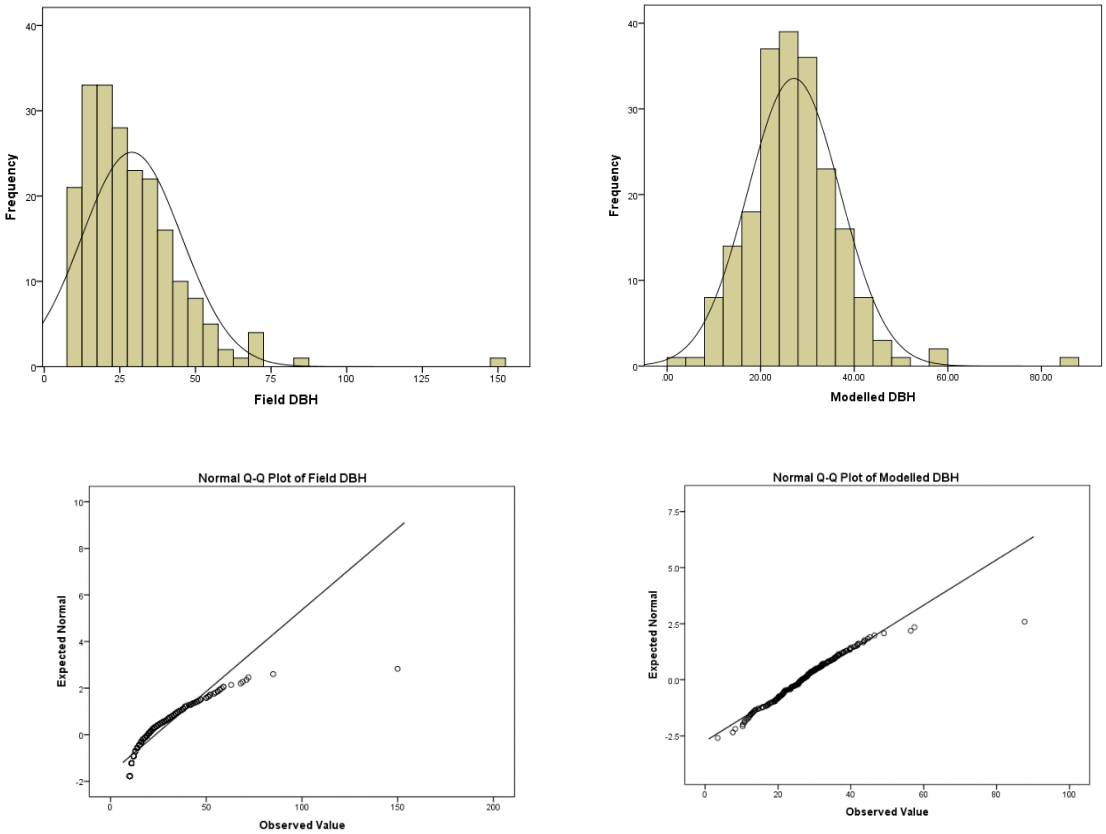

Figure 36. Distribution and QQ plots of field and modelled DBH

Table 17. Normality test of the modelled and field DBH.

	Kolmogorov-Smirnova			Shapiro-Wilk		
	Statistic	**df**	**Sig.**	**Statistic**	df	Sig.
Modelled DBH	0.0656	208	0.029683	0.933315	208	3.82E-08
Field DBH	0.1255	208	1.82E-08	0.820594	208	9.53E-15

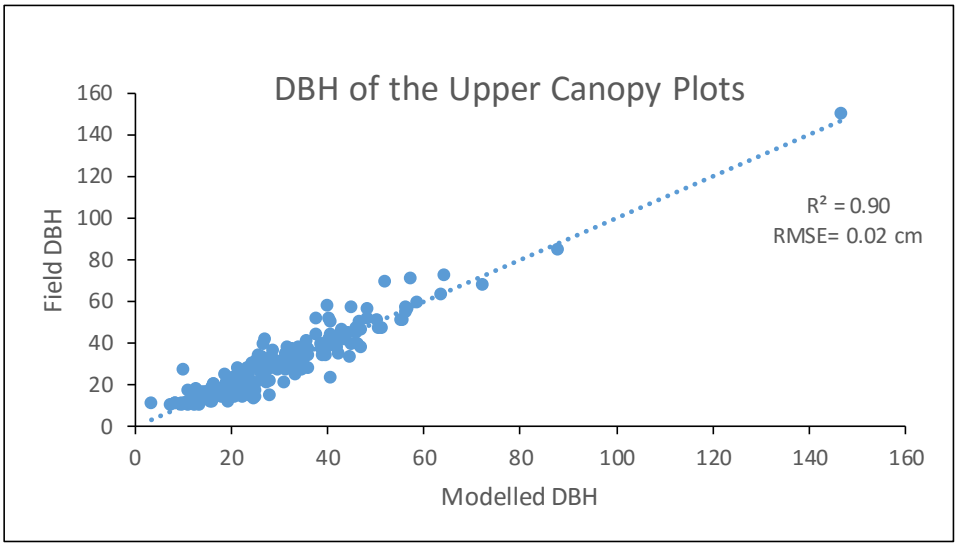

Figure 37. Overall relationship between modelled and field DBH for the 16 plots.

Table 18. Regression statistics, probability and reliability of the modelled and field measured DBH for the 16 plots.

Regression Statistics				
R Square	**Adjusted R Square**		**RMSE**	
0.90	0.89		0.02 cm	
Regression probability and reliability				
	Coefficients		P-value	
Significance F	**Intercept**	**Modelled DBH**	**Intercept**	**Modelled DBH**
5.8E-105	-0.047	1.001	0.95	5.8E-105

Table 19. Regression statistics of modelled DBH per plot.

Plot No.	**R Square**	**Adjusted R Square**	**RMSE (cm)**	**Plot No.**	**R Square**	**Adjusted R Square**	**RMSE (cm)**
1	0.93	0.91	3.13	9	0.91	0.89	4.52
2	0.97	0.96	6.82	18	0.95	0.94	4.76
3	0.89	0.87	5.56	20	0.88	0.84	8.61
4	0.78	0.74	5.97	21	0.86	0.83	4.80
5	0.85	0.84	6.97	22	0.89	0.87	4.28
6	0.75	0.71	5.08	24	0.76	0.70	8.31
7	0.89	0.86	2.48	25	0.80	0.75	8.50
8	0.79	0.74	4.76	26	0.81	0.77	6.22

Table 20. Regression probability and reliability of modelled DBH per plot.

		Coefficients			P-value		
Plot Number	**Significance F**	**Intercept**	**CPA**	**Airborne LiDAR**	**Intercept**	**CPA**	**Airborne LiDAR**
1	0.00054	-23.8318	3.44213	1.20555	0.02522	0.00045	0.00712
2	0.00000	-35.1645	-4.33123	5.66599	0.00057	0.00003	0.00000
3	0.00000	6.4450	-3.84735	2.20564	0.34477	0.00000	0.00000
4	0.00052	-36.2943	2.11197	2.47879	0.01150	0.00249	0.00042
5	0.00000	-70.6549	3.25972	3.68582	0.00001	0.00052	0.00000
6	0.00012	8.6789	-1.84090	1.49180	0.23153	0.00119	0.00039
7	0.00015	-3.2429	-0.93731	1.76242	0.43788	0.00322	0.00006
8	0.00194	5.3558	-2.04895	2.39355	0.42917	0.00452	0.00179
9	0.00002	9.3777	-2.53780	2.22004	0.15895	0.00041	0.00002
18	0.00002	-57.2368	3.46529	3.33836	0.00036	0.00030	0.00012
20	0.00069	-33.2824	-2.29377	3.76809	0.05461	0.01997	0.00033
21	0.00006	-32.9637	2.55242	2.21920	0.00197	0.00901	0.00008
22	0.00002	-53.4245	1.62452	2.88215	0.00016	0.00144	0.00001
24	0.00343	-35.7297	5.83201	1.69921	0.06259	0.00198	0.02333
25	0.00036	-28.6656	0.20537	2.39613	0.01390	0.85124	0.00021
26	0.00054	-23.8318	3.44213	1.20555	0.02522	0.00045	0.00712

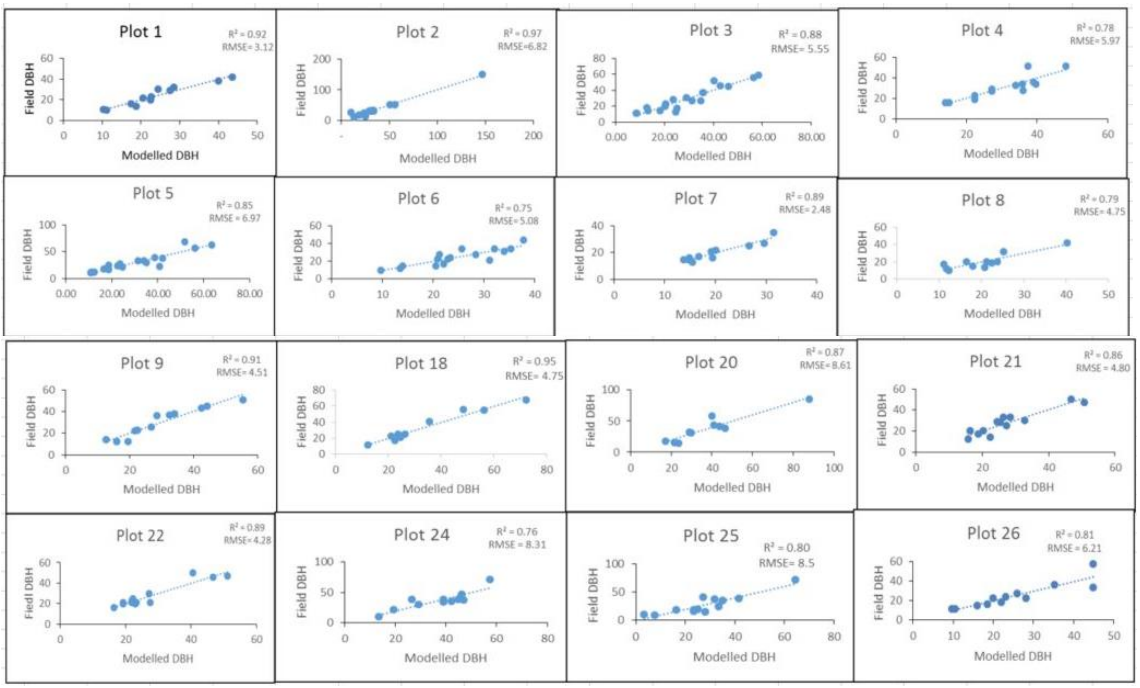

Figure 38. Plot level comparison between the modelled and field DBH of the upper canopy.

4.9.3. AGB model calculation and validation

The modelled AGB for the upper canopy layer was calculated by applying the allometric equation by Chave et al., (2014) using the modelled DBH and the height from the generated CHM. To validate the model, field measured AGB was calculated. The allometric equation was applied to the field measured DBH and height

from CHM. Regression analysis between the modelled and field AGB was then conducted. Figure 39 show the relationship between the modelled and the field AGB for the 16 plots. Table 21 show the average AGB for the 16 plots. Table 22 show the regression statistics, probability and reliability of the relationship of all the 16 plots. The descriptive statistics is shown Table 23. The regression statistics of the calculated AGB for each plot is shown in Table 24. The QQ plot of the modelled and field AGB is shown in Figure 40. The summary of the regression probability and reliability per plot is shown in Table 25. Figure 41 show the scatterplot of the modelled and the field measured AGB.

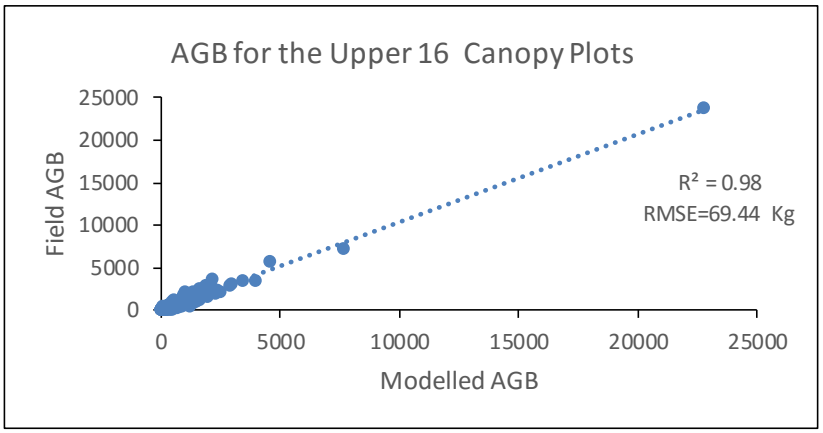

Figure 39. Overall relationship between the modelled and field measured AGB of the 16 upper canopy layer plots.

Table 21. Average AGB for the 16 upper canopy plots.

Plot Number	Modelled AGB (kg/ plot)	Field AGB (kg/plot)	Plot Number	Modelled AGB (kg/plot)	Field AGB (kg/plot)
1	401	333	9	647	647
2	2324	2371	18	1055	1061
3	752	767	20	1495	1513
4	741	758	21	611	795
5	879	911	22	710	720
6	430	430	24	1027	1054
7	262	262	25	853	922
8	196	199	26	531	533

Table 22. Regression statistics, probability and reliability of the modelled and field measured AGB for the 16 plots.

Regression Statistics				
R^2	Adjusted R^2		RMSE	
0.98	0.98		69.44 Kg	
Regression probability and reliability				
Coefficients			P-value	
Significance F	Intercept	Modelled AGB	Intercept	Modelled AGB
1.8E-170	-3.88	1.03	0.86	1.8E-170

Table 23. Descriptive statistics of modelled and field AGB.

Statistic	Modelled AGB	Field AGB
Mean	807.13	829.84
Minimum	195.70	199.24
Maximum	2324.17	2371.29
Standard Deviation	518.19	531.19
Number of plots	**16**	**16**

Table 24. Regression statistics of modelled and field AGB per plot.

Plot No.	Modelled AGB (kg/plot)	Field AGB (kg/ plot)	R^2	RMSE kg
1	4808	3991	0.95	68.67
2	30214	20827	0.99	171.90
3	15045	15348	0.95	200.20
4	9627	9855	0.75	309.73
5	15822	16396	0.84	451.30
6	6876	7075	0.77	175.49
7	2883	2920	0.91	68.95
8	2153	2192	0.94	65.21
9	7767	7928	0.95	147.07
18	10553	10609	0.95	249.05
20	14955	15131	0.96	425.53
21	7944	10332	0.93	221.29
22	9235	9365	0.88	250.34
24	11295	11597	0.72	454.81
25	11084	11987	0.95	334.71
26	6372	6401	0.74	366.95

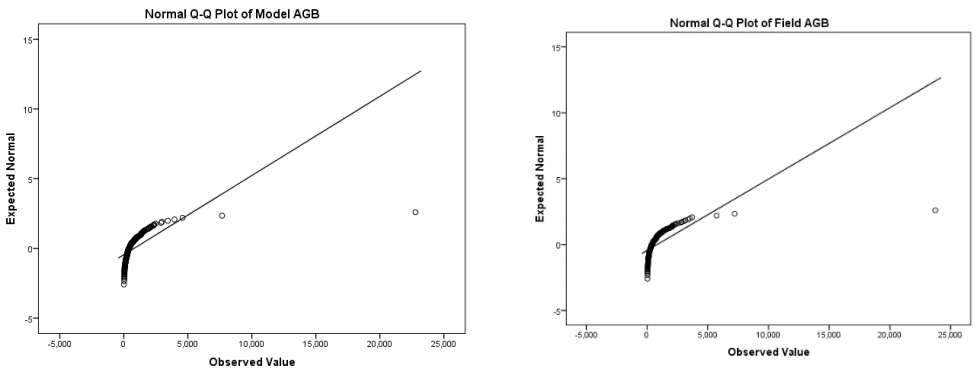

Figure 40. QQ plots of modelled and field AGB.

Table 25. Regression probability and reliability of modelled AGB per plot.

		Coefficients		P-value	
Plot No.	**Significance F**	**Intercept**	**Modelled AGB**	**Intercept**	**Modelled AGB**
1	0.00000	30.91941	0.75296	0.31536	0.00000
2	0.00000	-55.00008	1.04394	0.30578	0.00000
3	0.00000	7.64259	1.00996	0.90065	0.00000
4	0.00012	-14.63952	1.04337	0.92789	0.00012
5	0.00000	-48.57211	1.09156	0.74684	0.00000
6	0.00001	4.95256	1.01741	0.94946	0.00001
7	0.00000	-14.23454	1.06701	0.69263	0.00000
8	0.00000	-12.80616	1.08357	0.64020	0.00000
9	0.00000	85.98751	0.88797	0.17574	0.00000
18	0.00000	87.24263	0.92265	0.43312	0.00000
20	0.00000	124.03345	0.92885	0.47356	0.00000
21	0.00000	23.82234	1.26157	0.78844	0.00000
22	0.00000	32.66846	0.96814	0.75245	0.00000
24	0.00081	-84.96709	1.10942	0.75905	0.00081
25	0.00000	-135.65397	1.24053	0.26571	0.00000
26	0.00032	-78.75753	1.15282	0.62391	0.00032

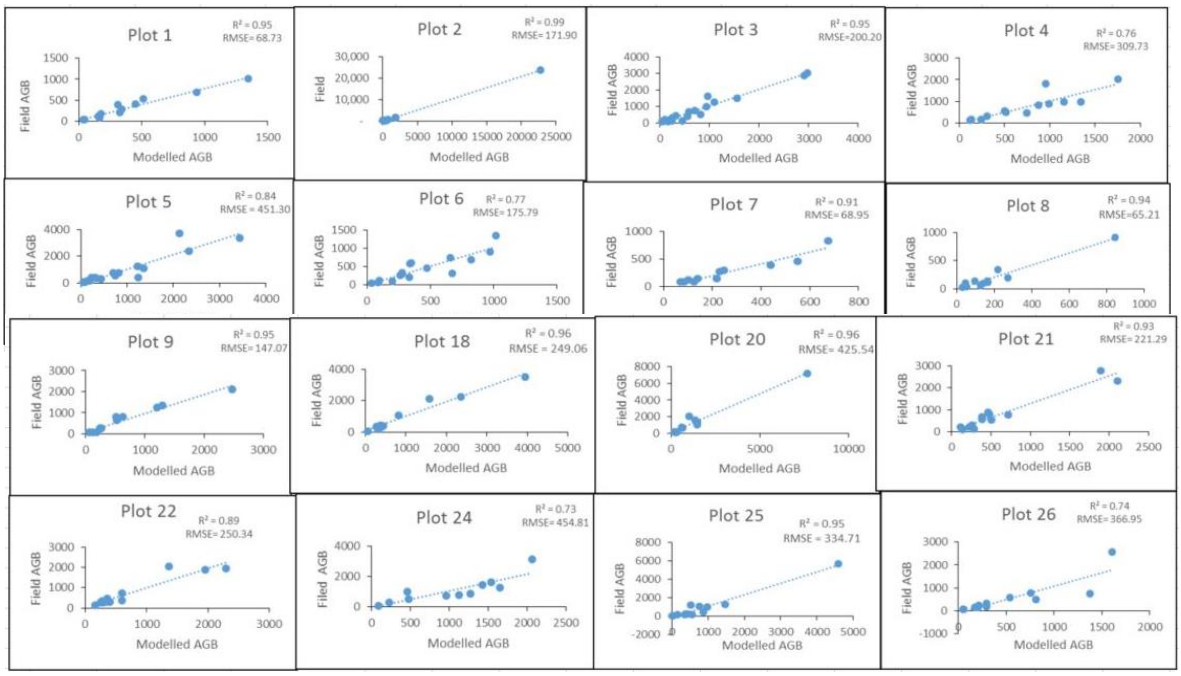

Figure 41. Plot comparison between the modelled and field upper canopy AGB.

4.10. Lower canopy AGB calculation

4.10.1. TLS Height and DBH and field measured DBH

Height and DBH are parameters measured directly from the extracted trees from the TLS. These measured parameters are needed to model the AGB of the lower canopy of trees. The mean height and DBH from the extracted trees per plot as well as the field measured DBH are shown in Table 26. The descriptive statistics of these parameters are shown in Table 27. Figure 42 show the normal distribution and QQ plots of the three parameters. The normality test output is shown in Table 28. The p-values indicate that the three parameters are not normally distributed. As shown in Figure 42 the TLS height is little skewed whereas both TLS and field DBH are positively skewed. The relationship between the TLS and field DBH was established by correlating the two parameters. Figure 43 show the graphical relationship. Table 29 show the regression statistics probability and reliability.

Table 26. Mean height and DBH from trees extracted from TLS and mean field measured DBH.

Plot No.	TLS Height(m)	TLS DBH(cm)	Field DBH(cm)	Plot No.	TLS Height(m)	TLS DBH(cm)	Field DBH(cm)
1	9.87	16.53	16.70	18	14.69	18.84	19.00
2	13.75	13.26	14.00	20	14.65	19.43	19.43
3	14.60	19.39	22.00	21	15.55	17.87	17.80
4	15.36	20.15	20.18	22	15.58	16.79	16.79
5	14.33	22.47	23.67	24	15.53	18.52	19.20
6	14.80	12.64	12.75	25	16.26	16.85	17.00
7	15.15	22.35	22.33	26	13.86	17.37	17.40
8	8.64	19.89	20.00	18	14.69	18.84	19.00
9	12.95	16.79	16.81	20	14.65	19.43	19.43

Table 27. Descriptive statistics of the TLS measured height and DBH and field measured DBH.

Statistic	TLS Height(m)	TLS DBH(cm)	Field DBH(cm)
Mean	14.41	18.08	18.30
Minimum	4.07	9.4	10
Maximum	28	58.3	59
Standard Deviation	4.17	9.88	9.23
Number of trees	**220**	**220**	**220**

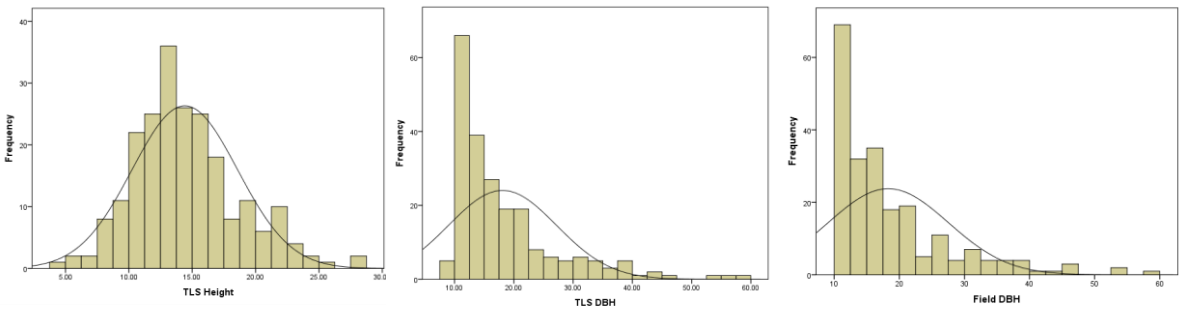

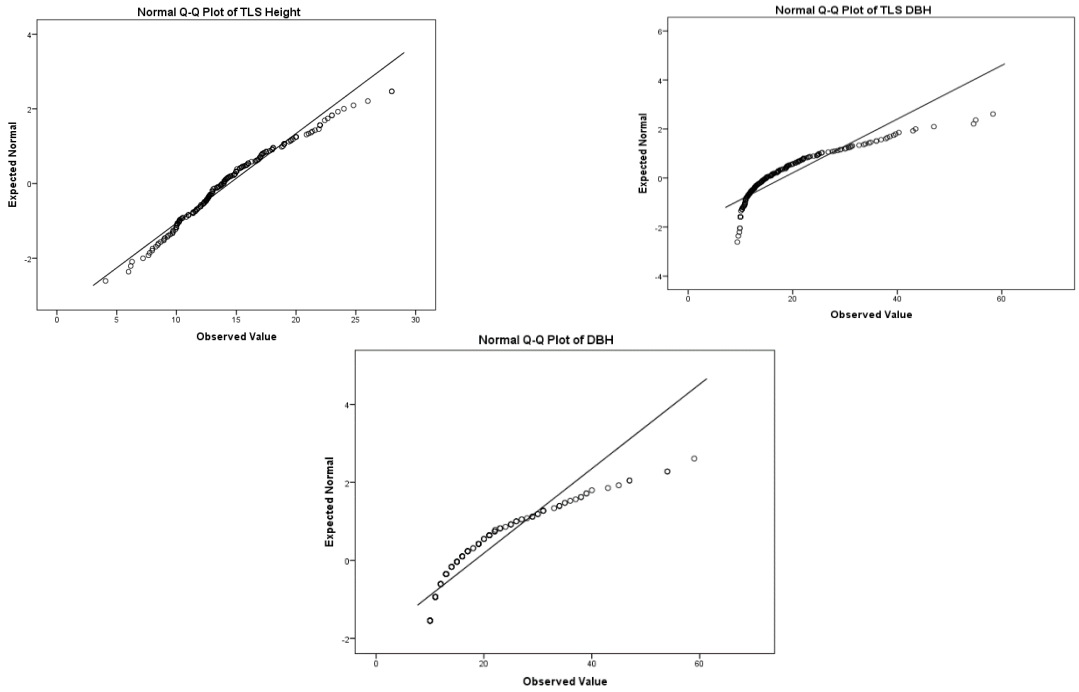

Figure 42. Distribution and QQ plot of TLS measured height and DBH and field DBH.

Table 28. Normality test of TLS measured height and DBH and field DBH.

	Kolmogorov-Smirnova			Shapiro-Wilk		
	Statistic	**df**	**Sig.**	**Statistic**	df	Sig.
TLS DBH	0.173	220	0.000	0.798	220	0.000
TLS Height	0.094	220	0.000	0.973	220	0.000
Field DBH	0.184	220	0.000	0.802	220	0.000

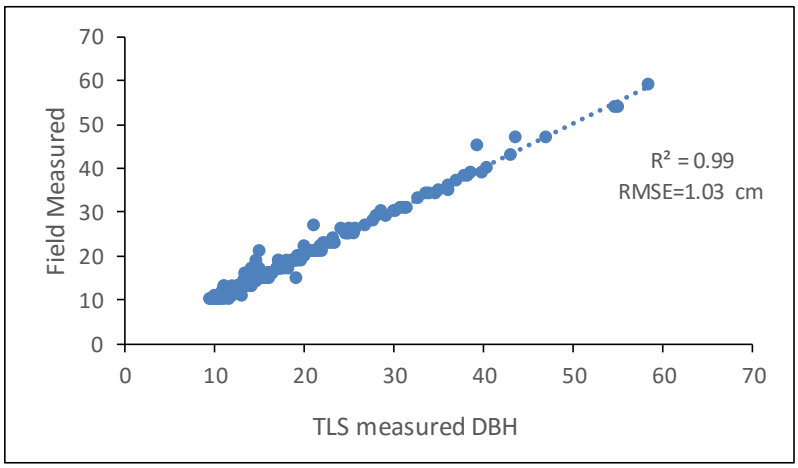

Figure 43. Scatterplot of the TLS and field measured DBH.

Table 29. Regression statistics, probability and reliability of the modelled and field measured DBH.

Regression Statistics				
R ²	**Adjusted R ²**		**RMSE**	
0.99	0.99		1.03 cm	
Regression probability and reliability				
Coefficients			**P-value**	
Significance F	**Intercept**	**TLS DBH**	**Intercept**	**TLS DBH**
3.9E-209	0.111	1.07	0.472	3.9E-209

4.10.2. AGB calculation and validation

Using the same allometric equation AGB for the lower canopy was modelled using the TLS measured DBH and height parameters. To validate the model field measured AGB was also calculated by applying the allometric equation using the field measured DBH and TLS height. Regression analysis between the TLS modelled and field measured AGB was then conducted. Figure 44 show the overall relationship of the modelled and field AGB. Table 30 show the average AGB for the lower canopy plots. Table 31 show the regression statistics of the average calculated AGB for the lower canopy per plot. The descriptive statistics is shown in Table 32. Table 33 show the regression statistics per plot of the modelled and field AGB. Figure 45 show the point distribution of the modelled and field AGB shown in the respective QQ plots.

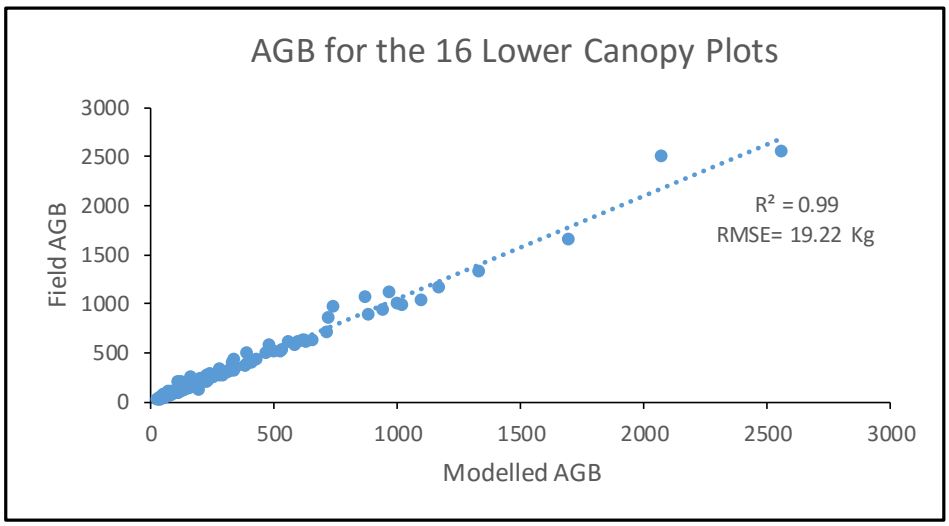

Figure 44. Overall relationship between the modelled and field AGB of the 16 lower canopy plots.

Table 30. Average AGB for the 16 lower canopy plots.

Plot. No.	Modelled AGB (KG/plot)	Field AGB (KG/plot)	Plot. No.	Modelled AGB (KG/plot)	Field AGB (KG/plot)
1	96.04	97.84	9	148.48	149.28
2	83.11	96.59	18	242.40	243.10
3	209.85	273.94	20	251.31	251.31
4	242.40	243.87	21	242.22	291.59
5	364.46	417.11	22	195.13	193.31
6	100.01	102.26	24	307.36	307.36
7	346.11	345.89	25	208.14	206.91
8	135.30	136.25	26	171.90	173.03

Table 31. Regression statistics, probability and reliability of the modelled and field measured AGB for the 16 lower canopy plots.

Regression Statistics				
R^2	Adjusted R^2		RMSE	
0.99	0.99		19.23 Kg	
Regression probability and reliability				
Coefficients			P-value	
Significance F	Intercept	Modelled AGB	Intercept	Modelled AGB
1.5E-205	-0.55	1.05	0.86	1.5E-205

Table 32. Descriptive statistics of modelled and field AGB for the 16 lower canopy plots.

Statistic	Modelled AGB	Field AGB
Mean	209.01	220.60
Minimum	83.11	96.59
Maximum	364.46	417.10
Standard Deviation	85.21	93.65
Number of plots	**16**	**16**

Table 33. Regression statistics of the modelled and field AGB.

Plot No.	AGB TLS (kg /plot)	AGB Field (kg /plot)	R^2	RMSE (Kg)
1	288	294	1	2
2	831	966	0.77	33.21
3	1469	1918	0.99	33.27
4	2666	2683	0.99	3.45
5	1093	1251	0.99	7.29
6	800	818	0.99	1.59
7	5192	5188	0.99	7.15
8	1894	1907	0.99	2.91
9	2376	2389	0.99	5.24
18	6060	6075	0.99	12.04
20	3518	3518	1	0
21	7267	8748	0.99	13.41
22	4683	4639	0.99	14.79
24	1640	4610	1	0
25	2081	2069	0.99	17.11
26	2579	2595	0.98	25.12

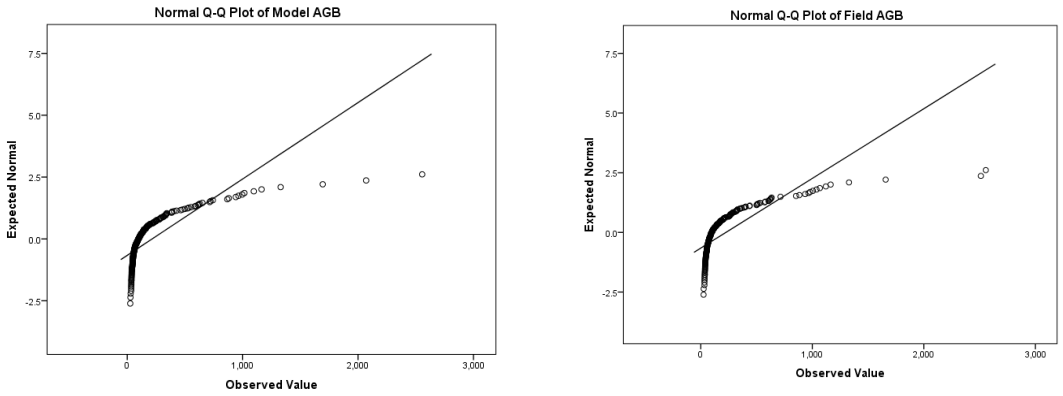

Figure 45. QQ plots of the modelled and field AGB.

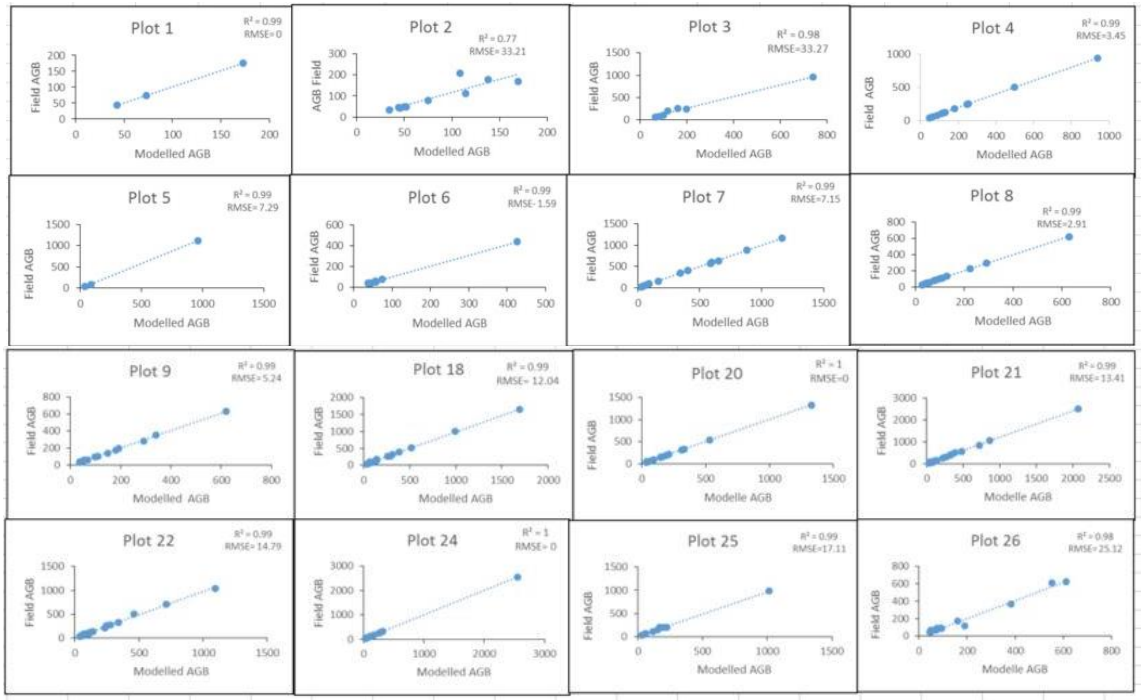

Figure 46. Plot comparison between the modelled and field AGB of the lower canopy.

4.11. Summation of modelled AGB from upper and lower canopies

The overall modelled AGB was quantified by combining the validated values from both upper and lower canopies. The combined values are presented in Table 34.

Table 34. Summation of modelled AGB from upper and lower canopies.

Plot No.	AGB (Upper) (kg/ plot)	AGB (Lower) (kg/ plot)	Total Modelled AGB	Plot No.	AGB (Upper) (kg/plot)	AGB (Lower) (kg/plot)	Total Modelled AGB
1	4808	288	5096	9	7767	2376	10143
2	30214	831	31045	18	10553	6060	16613
3	15045	1469	16514	20	14955	3518	18473
4	9627	2666	12293	21	7944	7267	15211
5	15822	1093	16915	22	9235	4683	13918
6	6876	800	7676	24	11295	1640	12935
7	2883	5192	8075	25	11084	2081	13165
8	2153	1894	4047	26	6372	2579	8951

4.12. Summation of field AGB from upper and lower canopies

Likewise the overall field AGB from both upper and lower canopies were also combined. The combined values are presented in Table 35.

Table 35. Summation of field AGB from upper and lower canopies

Plot No.	AGB (Upper) (kg /plot)	AGB (Lower) (kg /plot)	Total Field AGB	Plot No.	AGB (Upper) (kg /plot)	AGB Field (Lower) (kg /plot)	Total Field AGB
1	3991	294	4285	9	7928	2389	10317
2	20827	966	21793	18	10609	6075	16684
3	15348	1918	17266	20	15131	3518	18649
4	9855	2683	12538	21	10332	8748	19080
5	16396	1251	17647	22	9365	4639	14004
6	7075	818	7893	24	11597	4610	16207
7	2920	5188	8108	25	11987	2069	14056
8	2192	1907	4099	26	6401	2595	8996

4.13. Accuracy assessment of the total modelled AGB

The accuracy of the combined modelled AGB was assessed by calculating the R^2 and RMSE. The graphical presentation of the accuracy of the combined upper and lower AGB is presented in Figure 47. The tabulated accuracy result for the upper and lower canopies are presented in Table 36. The accuracy of the combined upper and lower canopies is presented in Table 37. Figure 48 show the QQ plot distribution of the modelled and field measured AGB.

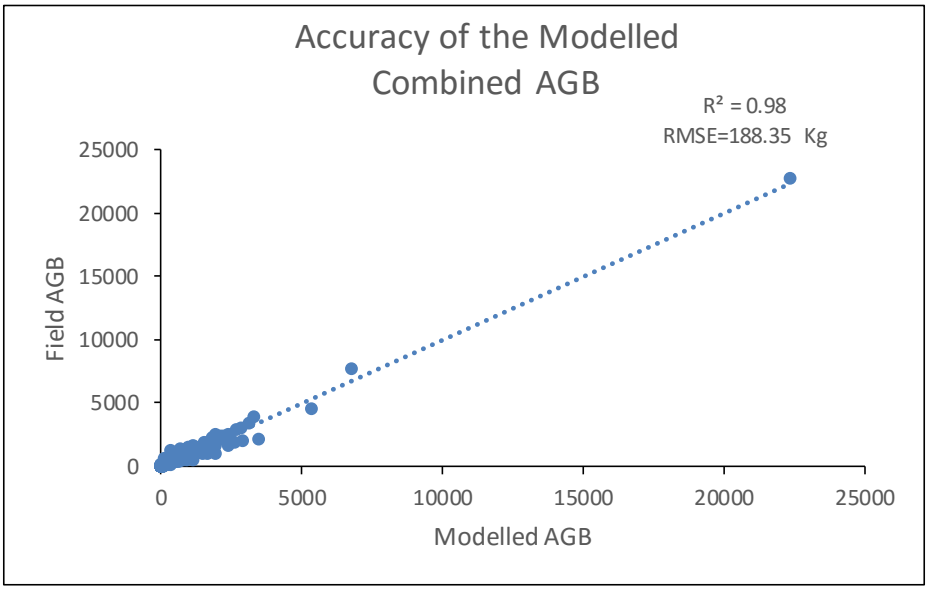

Figure 47. Accuracy of the combined upper and lower canopy modelled AGB.

Table 36. Accuracy of the modelled upper and lower AGB.

Plot No.	Total Modelled AGB(Kg/plot)	R^2 Upper Canopy	R^2 Lower Canopy	RMSE Upper Canopy(Kg)	RMSE Lower Canopy(Kg)
1	5096	0.95	1	68.67	2.00
2	31045	0.99	0.77	171.90	33.21
3	16514	0.95	0.99	200.20	33.27
4	12293	0.75	0.99	309.73	3.45
5	16915	0.84	0.99	451.30	7.29
6	7676	0.77	0.99	175.49	1.59
7	8075	0.91	0.99	68.95	7.15
8	4047	0.94	0.99	65.21	2.91
9	10143	0.95	0.99	147.07	5.24
18	16613	0.95	0.99	249.05	12.04
20	18473	0.96	1	425.53	0.00
21	15211	0.93	0.99	221.29	13.41
22	13918	0.88	0.99	250.34	14.79
24	12935	0.72	1	454.81	0.00
25	13165	0.95	0.99	334.71	17.11
26	8951	0.74	0.98	366.95	25.12

Table 37. Accuracy of the combined modelled AGB

Plot no	Total Modelled AGB (Kg/plot)	R^2	RMSE Kg
1	5096.03	0.96	60.67
2	31045.28	1.00	130.39
3	12293.66	0.95	175.96
4	16915.45	0.84	219.15
5	7676.42	0.85	415.12
6	8074.89	0.84	140.02
7	4046.81	0.98	43.36
8	10142.22	0.96	41.87
9	10142.22	0.96	96.94
18	16613.15	0.97	126.53
20	18473.23	0.97	261.82
21	15211.01	0.97	117.41
22	13917.83	0.93	141.36
24	15905.61	0.88	280.63
25	13165.34	0.96	250.91
26	8950.68	0.79	234.30

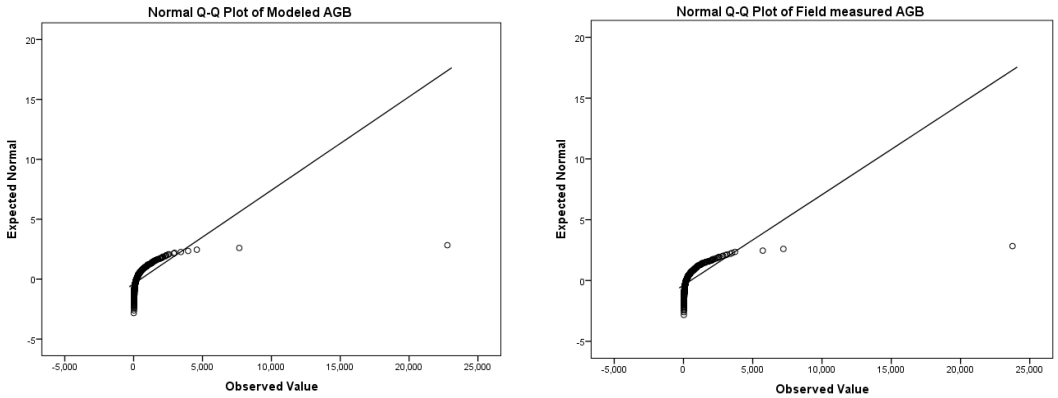

Figure 48. QQ plot distribution of the total modelled and field measured AGB.

4.14. AGB/Carbon estimation of the study area

Average total AGB per plot from the respective modelled and field measured was calculated (Table 38). Using the average per plot values AGB was estimated based on the plot area which is 500 m². The calculation of the respective AGB and carbon are shown below Table 39.

Table 38. Calculated total mean AGB for the 16 plots.

Plot No.	Total Modelled AGB Model (Kg)	Total Field AGB (Kg)
1	5096	4285
2	31045	21793
3	16514	17266
4	12293	12538
5	16915	17647
6	7676	7893
7	8075	8108
8	4047	4099
9	10143	10317
18	16613	16684
20	18473	18649
21	15211	19080
22	13918	14004
24	12935	16207
25	13165	14056
26	8951	8996
Average AGB per plot	**13191.875**	**13226.375**

Table 39. Calculation for modelled and field measured AGB.

Modelled AGB / Carbon Calculation			**Field Measured AGB/Carbon Calculation**	
Average AGB/plot		13191.875 kg/500 m^2		13226.375 kg/500 m^2
Conversion to Ton/ m^2	13191.875/1000	13.18 T/500 m^2	13191.875/1000	13.23 T/500 m^2
Conversion to Ton/ Ha	13.18 T/500 m^2 /0.05	263.84 T/Ha	13.18 T/500 m^2 /0.05	264.53 T/Ha
	Area of AHFR	1248 Ha	**Area of AHFR**	1248 Ha
	AGB of AHFR	(263.84 T/Ha) (1248 Ha)	**AGB of AHFR**	(264.53 T/Ha) (1248 Ha)
		329,272 T		**330,133 T**
	Carbon Stock Of AHFR	(329,272 T) (0.5)	**Carbon Stock Of AHFR**	(330,133 T) (0.5)
		164,636 T		**165,066 T**

5. DISCUSSION

5.1. Data Distribution

Assessment of data normality needs to be checked for subsequent statistical procedures such as correlation, regression, t tests and ANOVA and other parametric tests to determine data validity (Ghasemi & Zahediasl, 2012). The normality distribution of the field measured and sensor derived parameters were assessed because these parameters were of primary importance for the subsequent regression analysis to derive AGB and carbon estimation. One of the ways to visually display normality distribution is through a histogram by representing the skewness of the data distribution as shown in Figure 49 (Doane & Seward, 2011). Further the probability distribution can be positively skewed if the long tail is skewed to the right and negatively skewed if the long tail is skewed to left.

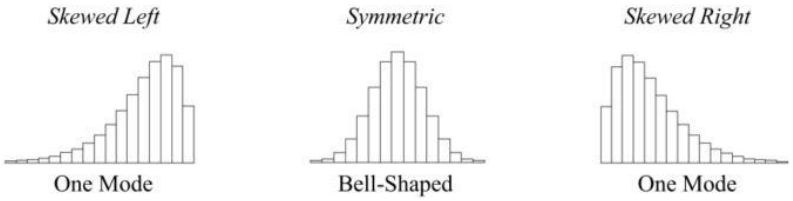

Figure 49. Histogram illustration of skewness ((Doane & Seward, 2011).

The distribution of the field measured DBH as showed in the result indicated a positive distribution to the right as well as the measured tree crown. This is because when field measurement was done trees with DBH of more than 10 cm DBH were selected for measurement. Since the objective is for AGB estimation DBH less than 10 cm were excluded for they do not contribute much biomass. For the crown measurement there is a similarity on the positive skewness direction. This is because crown structure have direct relationship to DBH in terms of diameter growth as revealed by the study of King, et al., (2005). The study was conducted in a mixed dipterocarp forest in Sarawak Malaysia where a light interception index was established using crown area and crown illumination as factors to correlate with DBH. The study revealed that the two parameters are linearly correlated.

For the derived image parameter the distribution was symmetrical for the CHM and positively skewed to the right for the CPA. This symmetrical distribution of the CHM could be attributed to the identified trees from the image that are of taller heights except from the reforested area where trees of lower heights could be detected. In addition, taller trees have a greater chance of detection in airborne LiDAR because it has been proven to provide highly accurate height measurements due to higher point cloud densities near the sensor (Van Leeuwen et al., 2011). For the CPA it assumes a similar distribution pattern to the field measured crown which is positively skewed. This also implies that it has a similar distribution as the field measured DBH. As the result of King et al., (2005) who showed these parameters having a direct relationship therefore the CPA has shown similar variability as the field measured crown and DBH.

To test validity of the modelled and field DBH for subsequent AGB modelling the distribution was also tested. The distribution showed that it is positively skewed due to the one measurement which was extremely

high. In this case it was included because the study is accounting for the accurate biomass on a plot basis. Excluding the tree would not reflect the substantial amount of biomass it has stored.

Testing the normality of TLS and field DBH distribution showed a positive skewness. This is because trees extracted from TLS reflect the same trees measured in the field. Thus similarity in the pattern of distribution can be observed because trees above 10cm DBH were the ones measured. TLS height showed positive skewness because the trees extracted from the sensor are mostly of lower heights except for two trees which is way above the mean. As mentioned earlier for DBH extreme values were not excluded because estimation was based per plot and the substantial biomass stored of these trees must be accounted for.

5.2. Upper Canopy Layer

Calculating for the AGB of the upper canopy layer requires the generation of CHM from airborne LiDAR and CPA from the Orthophoto. DBH is one of the primary parameter required to calculate for the AGB. Further, the accuracy of the modelled DBH is validated by the field measured DBH and the accuracy of the modelled AGB was validated by the field AGB. The succeeding sections discusses the obtained results and its importance to meet the objectives of this study.

5.2.1. Pit-free CHM

Tree canopy height is one of the basic measurements in forest inventory (Wang & Glenn, 2008). The use of LiDAR technology utilizes its capacity to provide 3D point clouds to obtain forest structure in 3D (Chen et al., 2005). CHMs are derived from airborne LiDAR for forest inventory to obtain height information. However, generating CHMs from airborne LiDAR poses certain irregularities in canopy surface or termed as "data pits" have a disruptive effect on the generated CHM. The presence of these pits will reduce tree detection accuracy and subsequent biophysical measurements (Ben-Arie et al., 2009).

Generating pit-free CHM based on the study of Khosravipour et al., (2014) is a method of constructing CHMs directly from LiDAR data. The study revealed that even if the point cloud data is thinned out the accuracy index is still 67.7%. Although the study is mainly tested on temperate species of trees it is of importance to the application of this study. This is because LiDAR point cloud density used have lower density which is 5-6 points per m^2. According to Hyyppä, and Inkinen, (1999) successful modelling of airborne LiDAR point cloud densities must approximately have 10 points or greater per m^2. Moreover as recommended by Khosravipour et al., (2014) using the method and algorithm for subsequent biomass assessment has yet to be tested. Therefore, applying the method also add to a novel way of measuring height using lower density point cloud for subsequent biomass estimation of a complex forest like AHFR.

Generating CHM of better accuracy for this study is an important factor that needs to be addressed because of the reliability of the field measured height. Due to the environmental condition of this type of forest it affected the use of the handheld laser instrument used in the field. The presence of thick undergrowth (Figure 50) causes occlusion upon tree height measurement. These occlusions causes error readings in the Laser distance meter. Further, when measurement is done underneath this type of forest with intermingling thick tree canopies, (Figure 51) determining the highest point of the tree is very difficult to identify and depends highly on the one handling the instrument. This alone would already cause bias on the measurement. Moreover, inappropriate determination of the highest point have a greater chance of overestimation. This also entailed repetitive measurement that is time consuming. Figure 52 illustrate how errors were incurred during field height measurement.

Figure 50. Presence of thick undergrowth inside the forest reserve.

Figure 51. Intermingling tree crowns.

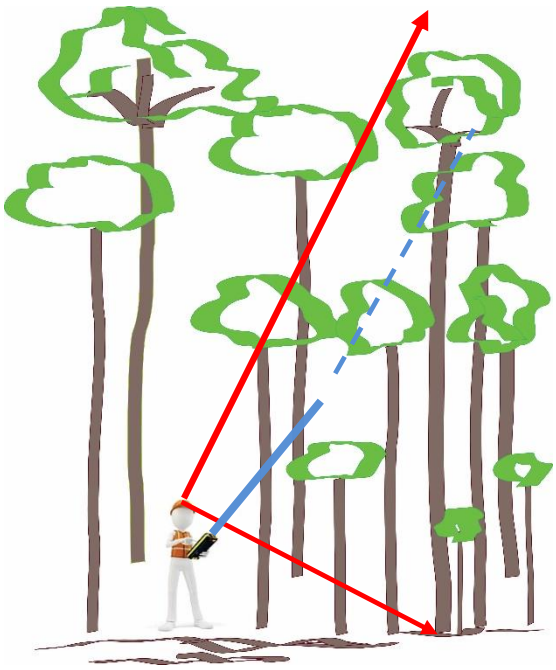

Figure 52. Error in field height measurement.

This observation is supported by the study done by O'Beirne, (2012) in closed stand urban temperate forest. The study showed that the use of laser range finder is extremely difficult and almost impossible to use in areas of closed stands where it is difficult to see top of tree. This was also cited by Andersen, et al., (2006) that in closed stands the use of such devices is impossible to implement due to issues on tree top visibility. The findings of Rönnholm et al., (2004) also shared similar result where error in field measurements consistently overestimate tree heights compared to LiDAR both for conifer and deciduous trees. Therefore, for the assessment of this forest it is more practical to use the LiDAR data to derive the height. Moreover, the study of O'Beirne, (2012) revealed that the random error and extensive labor to measure trees in the field created much error as compared to the results from LiDAR. As reviewed by Wulder et al., (2012) LiDAR sampling for large area forest characterization concluded that LiDAR can be treated as an independent measure to generate estimates of forest attributes for scientific studies. Such that the applicability of LiDAR based forest measurements to forest inventory and canopy structure modelling have been tested in the studies done by Lefsky et al., (2002); Popescu & Wynne, (2004). As well as deriving digital elevation models which is done by Hodgson & Bresnahan, (2004). Further, Lefsky et al., (2002) has proven that LiDAR sensors can provide accurate and non-asymptotic estimates of various forest indices. The superiority of airborne LiDAR in tropical forest application has been proven by Hou, et al., (2011) via a comparative study of using Airborne CIR (color infrared) image, ALOS AVNIR and airborne LiDAR. The use of airborne LiDAR provided the lowest RMSE of 36.92% for stem volume and 47.35% for basal area. As pointed out by Aardt & Wynne, (2006) LiDAR based approach to forest inventory could negate the need for ground-based small scale measurements of tree heights and or canopy.

5.2.2. Segmentation Accuracy

Accuracy assessment of the multi-resolution segmentation for the individual tree crown was assessed in two ways. The first one which was based on the overlap of the segmented and referenced was considered as 1:1 if the overlap is more than 50% (Zhan, et al., 2005). The result showed an accuracy of 77% which is slightly lower to the result of Asmare, (2013) who obtained an overall accuracy of 78.8% using the combination of airborne LiDAR derived CHM and Worldview 2 image for a subtropical forest in Nepal. The result however is slightly higher as compared to the result of Karna, (2012) with an overall accuracy of 75.13% with the use of WorldView and CHM from airborne LiDAR also for a forest in Nepal. It is also higher compared to the result of Wang, et. al., (2004) who obtained 75.6% using high spatial resolution aerial imagery for a coniferous forest. The result is much lower compared to the accuracy obtained by Chen et al., (2005) which is 88% who implemented a similar process of combining LiDAR data and high resolution images. However, the study is tested in an urban orchard of trees where trees are almost of the same height with less intermingling of tree crowns thus ease in tree detection and extraction and subsequent matching yield higher results. According to Sium, (2015) this is the challenge of applying image segmentation in a tropical rain forest with complex canopy structure and highly diverse species of trees. Tropical rainforests are naturally dense with intermingling of crown layers and differences in illumination within and between crowns are common as in the case of AHFR as shown in Figure 53. The factors that must be considered are the conditions where the study is conducted, the spatial and spectral resolution of image, species and forest type (Brandtberg & Walter, 1998). The application of multi-resolution in this study is considered appropriate method to use because it considers both spatial and spectral homogeneity of pixels in merging image objects in this case the tree crowns. Kim et al., (2010) tested the method of combining aerial photograph and LiDAR data using multi-resolution segmentation to segment heterogeneous forest and found the algorithm is the most appropriate one. Moreover, this is supported by the study of Lamonaca, et al., (2008) that the method have a very good potential of extracting meaningful information from high resolution imagery for heterogeneous type forests. Segmentation methods for tree crowns that only considers tree top as the brightest point of the tree crown (Culvenor, 2002; Gonzalez et al., 2010; Wang et al., 2004) is deemed inappropriate for this type of forest. This is because in coniferous type of forests the reflectance value on top would most likely represent a singular tree crown due its conical structure. Whereas for tropical forests

the tree structure have multiple branches and the crown does not assume a conical shape thus implementing the method is considered appropriate.

Figure 53. Multi-layered canopy structure of AHFR.

In implementing multi-resolution segmentation the scale parameter determines the size and homogeneity of the image objects (Definiens, 2012). Fine scale values according to Benz, et al., (2004) is the most suitable for segmenting small objects like trees, buildings and roads. In this study the most suitable value obtained using the ESP tool is 10. To verify the appropriateness of the scale, this was compared to the scale value used by Chen et al., (2005) that used the same scale of 10 using the method for aerial images and LiDAR data. The value is also considered fit based on visual interpretation of the image because at 13 cm spatial resolution (e.g. Orthophoto) finer details of the object can be detected. Since the objective is to segment tree crowns of the upper canopy layer this fine scale is found to be appropriate that produced an optimum fit of automated segments with the manually delineated reference objects of 0.09 over segmentation and 0.03 under segmentation. The obtained over segmentation value is higher compared to the under segmentation value indicating that the automated segments exceeded the area of the referenced polygons. This outcome is normal, especially for complex natural forests which have very high variability in terms of crown shape, multi-scale branching and tree clustering that result to over segmentation (Jing, et al., 2012). The final segmentation accuracy however is already reasonable in comparison to studies done by Karna, (2012) and Asmare, (2012) who obtained 75.13% and 78.8% respectively. Both studies used the combination of Worldview image and LiDAR data and suggests that the inclusion of the height information improved the segmentation process.

5.2.3. Accuracy of the modelled DBH

DBH is a reliable factor for biomass estimation (Popescu, 2007). Thus, deriving this parameter is the basic step for accurate AGB estimation. Modelling DBH of the upper tree canopy using multiple regression, adopted the method developed by Popescu, (2007). The study used LiDAR derived tree measurements of height and crown width as independent variables and field measured DBH to estimate DBH for 43 loblolly pines. Similar multivariate modelling concept was also developed by Repola, (2008) for biomass estimation for 24 birch stands using tree diameter and height.

The obtained R^2 value of the DBH for the 16 plots is 0.90 and RMSE of 0.02 cm. Figure 54 show the modelled DBH as compared to the field measured DBH for the 16 plots. The results revealed that the values are greater than the values obtained by Popescu, (2007) who obtained an R^2 of 0.87 and RMSE of 4.9 cm. The obtained results support the study of (Popescu, 2007) that there is indeed a strong relationship between height and CPA to model DBH. This further signifies that for the upper canopy layer DBH models can be accurately modelled from LiDAR derived height and CPA derived from Orthophoto and have the potential use for subsequent AGB estimation. The highly accurate values can be attributed to the fact the derived

parameters come from trees measured from the upper canopy layers only. For the height this will support to the contention of Van Leeuwen et al., (2011) that the bias of airborne LiDAR to accurately measure stand height is towards the upper layers because point cloud density is dependent on the last returns. When airborne LiDAR data is acquired this is on a top-down perspective and the resultant bias is towards the upper layers. As a consequence vegetation understory is underrepresented due to the infrequency of laser returns from mid and understory layers (Figure 55). Moreover, this has been proven in the study of Maltamo, et al., (2004) that height can be accurately estimated for open canopy temperate forests providing results of R^2 values ranging from 83 to 98%. For CPA, (Figure 56) the use of aerial photos or high resolution imagery would only yield better information of crown diameters for the upper canopy because it is impossible to directly observe tree crowns from the middle and lower layers of a multi-layered forest (Hirata et al., 2012). Further, related findings of Hou et al., (2011) of using optical sensors in combination with airborne LiDAR for tropical forest application revealed that optical sensors can record mainly the tree crown surface while the understory will remain undetected.

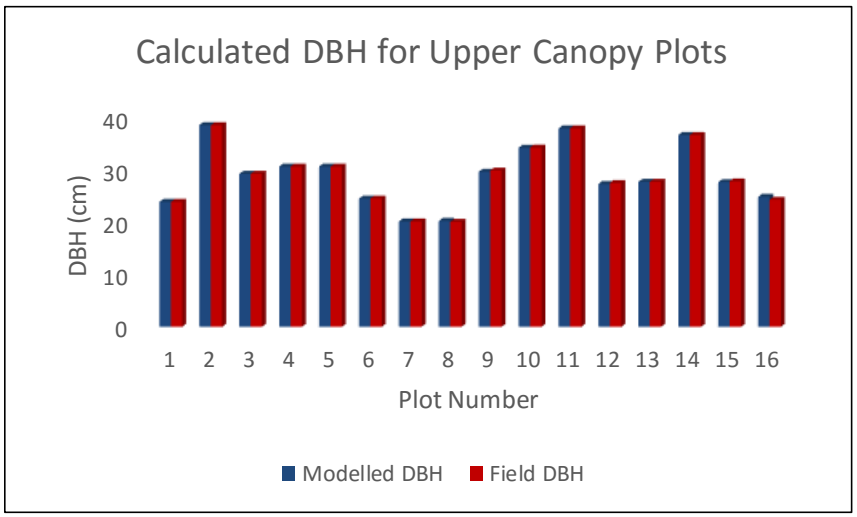

Figure 54. Comparison of the calculated average modelled and field measured DBH.

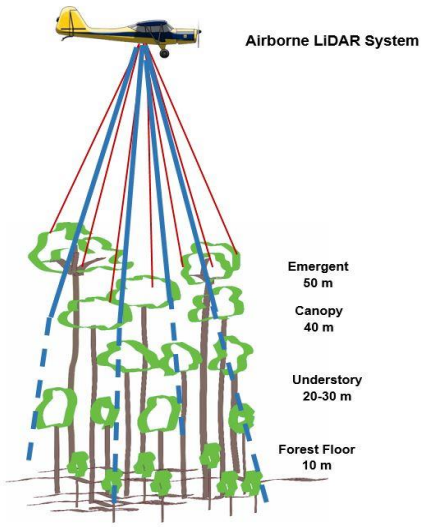

Figure 55. Point cloud distribution upon airborne LiDAR data acquisition.

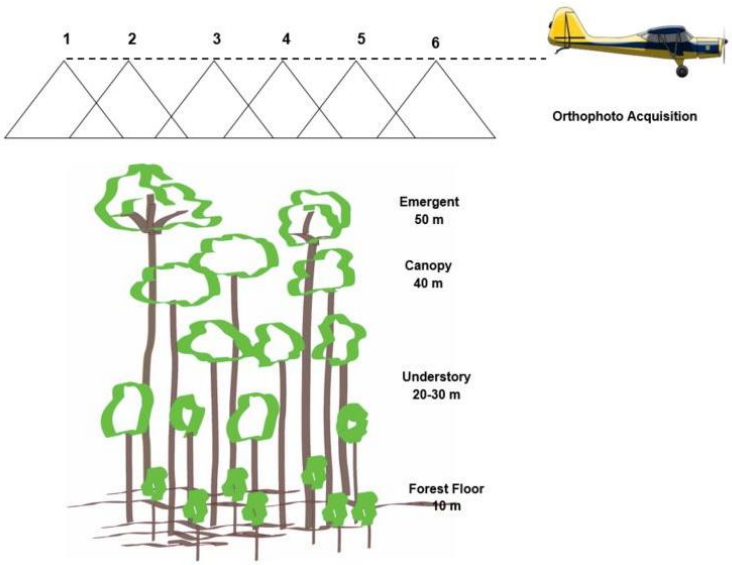

Figure 56. Acquisition of Orthophoto images.

5.2.3. Accuracy of the modelled AGB

AGB calculation for this study adopted the generic allometric equation of Chave et al., (2014) because using the local equation of Yamakura, et al., (1986) with DBH as the lone parameter to calculate AGB yield very low values. Moreover, as pointed out by Gibbs, et al., (2007) for highly diverse tropical forests using local or regional equations are not appropriate. The use of generic allometric equation is more suitable because these equations are developed based on larger number of trees (Gibbs et al., 2007; Chave et al., 2014). Hence, to calculate for AGB, height and DBH were the parameters used. In this case the LiDAR derived height is the only parameter used for all the calculations from AGB modelling and validation for the reasons discussed in section 5.2.1. Since the accuracy of airborne LiDAR has been extensively studied (Lefsky et al., 2002; Popescu & Wynne, 2004) and proven to provide superior results for tropical forests (Hou et al., 2011; Tokola & Hou, 2012) using the field data of low reliability for comparative purposes would be inappropriate. Further, it is not logical to compare data of known low reliability to the data which is proven to provide accurate results.

The calculated R^2 and RMSE for the 16 plots is 0.98 and 69.44 Kg respectively. Figure 57 show the comparison of the modelled and field measured AGB. The result is compared to related studies in calculating AGB through the combination of airborne LiDAR and the use of multispectral images conducted in the tropics because specific studies for upper canopy structure of tropical forest through fusion methods are not found as of this writing. There are studies, however, they apply the method for the overall estimation of a specific area of the forest (i.e., upper and lower canopies). To confirm if the result is of reasonable values, it was compared to some studies. The obtained result is relatively higher compared to calculated AGB results of Ediriweera, et al., (2014) who obtained an R^2 of 0.83 and 16.8 % RMSE. This was obtained by combining airborne LiDAR and multispectral data for estimating biomass for subtropical and eucalypts forest. The authors pointed out that combining the two image data sets has improved the AGB estimation than using the individual image data set. The result however is more comparable to the study of Karna et al., (2015) for reforested tropical forest in Nepal that obtained R^2 estimates ranging from 78-94% AGB estimations through the integration of WorldView 2 image and airborne LiDAR. The higher result obtained could be due to the use of the same height values to calculate both the modelled and field AGB compared

to the two studies that have used field measured data. Since in this study this is not possible what is being utilized is the height measured from airborne LiDAR as the truth or the standard height. The compared studies have shown that using the method provided robust results to attain their objective. Thus, for this study the high accuracy of the obtained results showed its relevance to meet the objective of the study which made use of the combined data to assess the AGB of the upper canopy. Moreover, the result signifies that the use of height from airborne LiDAR indeed can provide accurate result because its strength is towards the upper layers of the forest (Van Leeuwen et al., 2011) and as pointed out by Hirata et al., (2012) the strength of aerial and high resolution images is for the measurement of the upper crowns. Lastly, according to Lu, (2006) generally in AGB assessment high R^2 values and low RMSE indicates good fit between the developed model and the sample plot.

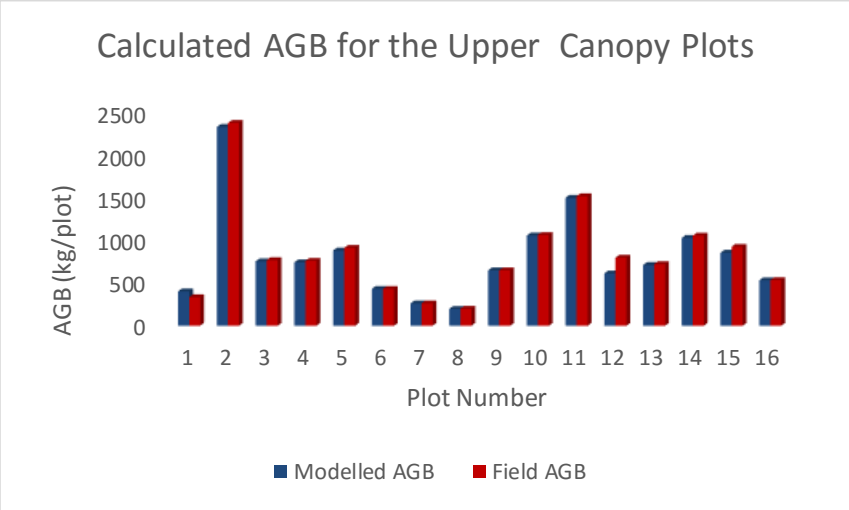

Figure 57. Comparison of the calculated average modelled and field measured AGB.

5.3. Lower Canopy Layer

Calculating the AGB for the lower canopy of the forest complement to what is calculated from the upper canopy layer. According to Hirata et al., (2012) estimating biomass using the crown diameter method with aerial or high resolution images is not possible for multi-layered forests because tree crowns in the middle and lower canopy cannot be observed. Moreover, the author stated that a method of estimating carbon stocks per unit area that would include the middle and lower layers is needed. This study tested the use of TLS to address this need. The trees extracted from the TLS were measured for the parameters required for AGB estimation of the lower canopy. The following sections discuss the results as well as the accuracy of the derived AGB.

5.3.1. Multiple Scanning

To derive tree parameters from TLS this employed multiple scanning of the trees. Implementing the method provided full coverage of the tree surface from the different scan positions from the centre and from the 3 outer positions. Registering the four scanned positions allow the alignment of the scanned positions to create a three dimensional perspective of the scene (Figure 58). The technique has been used for forestry applications in the studies of Huang et al., (2010); Hopkinson, et al., (2004). In the studies of Liang, (2013); and; Kankare et al., (2013) it showed that multiple scans can provide better scenes from merged point clouds that will consequently facilitate tree extraction.

Figure 58. Sample of the aligned and registered 3-D scene prepared for tree extraction.

5.3.2. Tree height measurement

Tree height is one of the main parameter measured from TLS to calculate the AGB for the lower canopy. Before measurements were done the trees were extracted from the registered scene. Using the RiSCAN interface trees were manually extracted from the 3-D registered scene through visual judgment and the shape of the point cloud distribution. The extracted trees were then stored as polygon shape that will be used for parametric measurement. Tree extraction was a challenging task because it is difficult to extract canopy structure in tropical forests where intermingling of tree crowns is a natural process. The presence of Lianas and undergrowth causes noise and occlusion added another challenge to define the canopy structure. Moreover, point cloud density decreases as the distance from sensor also increases (Maas et al., 2008). Thus adding the difficulty to define tree top structure for taller trees compared to trees of lower height. Figure 59 illustrate the difference in point cloud distribution between trees of higher and lower height. Since the focus of this part of study is the assessment of the lower canopy of trees, only the trees of lower height were subsequently retrieved and measured for height. Comparison with field measured heights was not done for reasons discussed in 5.2.1 and 5.2.3. Further, studies on the use of TLS in forestry applications emphasizes its potential use to substitute conventional field inventory (Lovell et al,. 2003; Bienert, et al., 2006 ; Lindberg, et al., 2012). Accuracy of the instrument could reach as high as 0.976 for correlations compared to manual measurements as studied by (Rosell et al., 2009) or R^2 of 0.99 for stand parameter (Strahler et al., 2008).

Figure 59. Illustration of the difference in point cloud densities between trees of higher and lower heights.

5.3.2. DBH measurement

Another parameter measured from TLS for AGB calculation is DBH. Determining the parameter from TLS used the extracted trees. The manual measurement in RiSCAN as described in section 3.4.5.5 is done so that measurement is in parallel to what was done in the field as discussed in 3.3.3.1. The correlation result between the TLS and field measured DBH for this study showed an R^2 value of 0.99 and an RMSE of 1.03 cm. The RMSE result is slightly higher compared to the obtained values of Bienert et al., (2006) and Kankare et al., (2013) who obtained an RMSE of 1.5 cm and 1.48 cm respectively. This indicate that the obtained values of the two parameters would provide robust values for the estimation of the AGB.

5.3.3. AGB Accuracy

The same allometric equation which was used to calculate the AGB for upper canopies is used to calculate AGB for the lower canopies. The calculated R^2 and RMSE for the 16 plots is 0.99 and 19.23 Kg respectively. The obtained R^2 value is slightly higher and RMSE lower compared to the study of Prasad, (2015) using TLS derived parameters to estimate biomass for a highland tropical forest in Malaysia. The values obtained were 0.93 and 42.4 for R^2 and RMSE respectively. This is because this study is estimating AGB of the lower canopies using TLS. While Prasad, (2015) used TLS to estimate AGB for both lower and higher canopies which may cause the lower $R^2$and higher RMSE. The R^2 value is also higher and RMSE is lower compared to a similar study done by Kankare et al., (2013) for Scots pine and Norway spruce forest, with R^2 of 0.90 and 0.91 and RMSE of 22.12 kg and 26 kg achieved at tree level. The relatively low RMSE could be attributed to the lesser variability of the measured height because the trees come from the same canopy layer. Prasad, (2015) pointed out that the high RMSE obtained of his study was due to differences in height. However, it is most likely because he assessed all upper and lower canopies. Assessing height of upper canopies was difficult and with some error in his case. Figure 60 show the comparative values of the modelled and field AGB. Therefore, the obtained high R^2 and low RMSE indicate good fit of the modelled AGB.

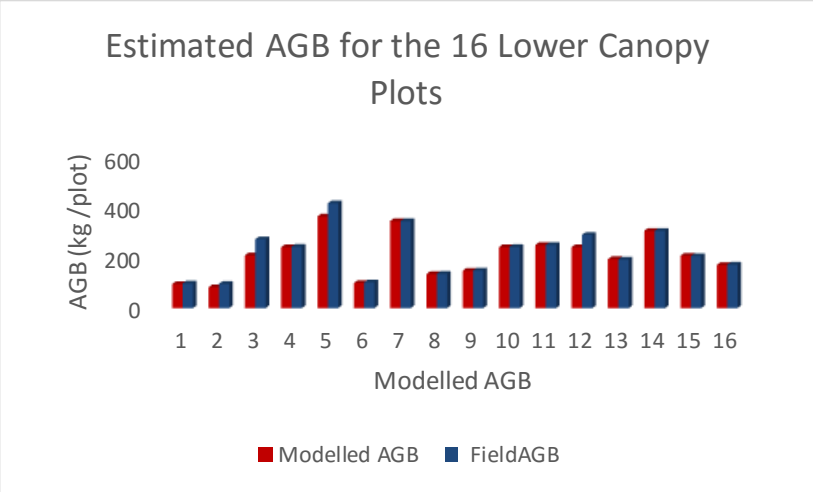

Figure 60. Comparison of the calculated average modelled and field measured AGB.

5.4. Accuracy of the overall modelled AGB

Combining the calculated AGB from the upper and lower canopy of the forest provided an overall estimation of the total AGB of the different canopy layers of the forest. Based on the calculated RMSEs for both the upper and lower modelled AGBs exhibited robust values. RMSEs according to Chai & Draxler, (2014) errors are unbiased and follow a normal distribution providing a complete picture of error distribution. Moreover, when there are more samples (eg. ≥100) reconstructing the error distribution using

RMSE is more reliable. In this study both upper and lower tree canopy have tree samples of more than 200 to support very strong reliability of the modelled outcome. This is a strong indication that both values can be complemented to attain a very accurate estimate of AGB for this study. The AGB values of the upper and lower canopy were then combined and subsequently R^2 and RMSE values were also combined. The achieved average R^2 and RMSE is 0.98 and 188.35 Kg respectively.

5.5. Overall AGB/Carbon of the study area

The total calculated AGB per hectare is 263.84 T/Ha for the modelled and 264.53 T/Ha for the field measurement. A review done by Majid & Nurudin, (2015) for AGB assessments for the study area from 1983 to 2007 revealed different trends of the calculated values per hectare. The pattern showed an increase and decrease of the obtained values. According to the authors this is due to lack of standard model for converting tree measurements to AGB estimation. Further, the estimation by Heng & Tsai, (1999) who implemented DBH measurement of trees above 10cm for calculating AGB estimated 223,568 T for the entire study area. To date, AGB assessment using the complementary use of airborne LiDAR and terrestrial laser scanning is the first time for the study area. In this study the total calculated AGB for the study area is 329,272 T for the modelled and 330,133 T for the field measurement. Compared to the result of Heng & Tsai, (1999), this would indicate that there is an increase of the AGB of the study area. The monetary value of the carbon stored in the area was estimated by Ismariah & Fadli, (2007). The estimated values range from RM2.06-25.96 million (€432,026-5,590,934). However, under the REDD+ program AGB stored for a forested area must be assessed based on remote sensing methods to accurately quantify its monetary values. Thus, the current result could then add a recent robust information for studies to quantify the value of the ecosystem service and monetary value of AGB/carbon stored in this forest since the time it was established as reserve. Robust information like these are much needed for the REDD+ program especially for a multi-layered tropical rainforest.

6. CONCLUSION

This study developed an approach of accurately assessing the AGB/carbon of a vertically complex structured tropical rain forest in Ayer Hitam Malaysia. A complementary method of utilizing the strengths of airborne LiDAR and terrestrial laser scanning system to accurately assess the AGB/carbon of the different canopy layers of the forest. Estimating the AGB of the upper canopy layer made use of airborne LiDAR derived height and CPA from Orthophoto to derive a robust model of DBH through multiple regression. The achieved R^2 value of the modelled DBH for the 16 plots is 0.90 and RMSE of 0.02 cm. The modelled DBH together with LiDAR derived height was subsequently applied to the generic allometric equation to calculate for the modelled AGB and validated using the field measured DBH and LiDAR derived height. The result for the 16 plots achieved a robust model with an R^2 of 0.98 and RMSE of 69.44 Kg. To complement the AGB from the upper canopy the AGB of the lower canopy of the forest was assessed through the use of the TLS extracted trees that were not identified in the upper canopy layer. Using the derived measured parameters from the extracted trees, AGB of the lower canopy was calculated. The correlation of the TLS and field measured DBH was established and revealed an R^2 value of 0.99 and RMSE of 1.03 cm. The TLS height and DBH was then applied to the allometric equation and was used to derive the AGB of the lower canopy. Then the model was validated using the field measured DBH and TLS derived height. The achieved result was a robust model with an R^2 value of 0.99 and RMSE of 19.23 Kg for the 16 plots. The modelled AGB for the upper and lower canopies were then combined and further assessed for accuracy using R^2 and RMSE. The R^2 value achieved is 0.98 and the average RMSE is 188.35. The overall result would show that using the method of complementing the strengths of the two sensors would indeed provide an accurate information to estimate AGB/carbon for a vertically complex tropical rainforest. Therefore, this study presented a novel method to address the need of the REDD+ program to provide accurate AGB/carbon assessment for a complex multi-layered tropical rain forest. Therefore, the research questions asked in the introduction chapter are now answered.

How accurate is the modelled DBH from airborne LiDAR derived CHM and segmented CPA from Orthophoto and field measured DBH?

The use of airborne LiDAR derived CHM and segmented CPA and subsequent application of multiple regression techniques with the field measured DBH to obtain a modelled DBH achieved a robust model having an R^2 of 0.90 and RMSE of 0.02 cm.

How accurate is the modelled AGB compared to the estimated AGB from field measured DBH and airborne LiDAR derived height of trees from higher canopy?

The accuracy of the modelled AGB (modelled DBH and LiDAR derived height) when compared with the field measured DBH and airborne LiDAR height also achieved a robust model of R^2 of 0.98 and RMSE of 69.44 Kg.

How accurate is the TLS modelled AGB compared to the field estimated AGB of trees from lower canopy?

The accuracy of the TLS modelled AGB upon comparing with the field estimated AGB achieved an R^2 value of 0.99 and RMSE and 19.23 Kg for the 16 plots.

How accurate is the estimated AGB combined from both TLS and airborne LIDAR based models to assess the stock of the study area?

The accuracy of the combined AGB models derived from TLS and airborne LIDAR achieved an R^2 of 0.98 and RMSE of 188.35

APPENDIXES

Appendix 1: Sample of data collection sheet

DATA COLLECTION|SHEET (AYER HITAM TROPICAL RAIN FOREST RESERVE, MALAYSIA

Name of recorder..... **Date**.....

Sample Plot No.		GPS Coordinates	X:	Grid cell No.	Slope (%)	Plot Radius	Undergrowth		Crown Cover (%)
			Y:				Y	N	

Tree No.	Species	DBH (cm)	Hgt 1 (Leica)	Hgt 2 (Haga)	Hgt 3 (TruPulse)	Crown diam.(m)	Tree No.	Species	DBH (cm)	Hgt 1 (Leica)	Hgt 2 (Haga)	Hgt 3 (TruPulse)	Crown diam.(m)
1							36						
2							37						
3							38						
4							39						
5							40						
6							41						
7							42						
8							43						
9							44						
10							45						
11							46						
12							47						
13							48						
14							49						
15							50						
16							51						
17							52						
18							53						
19							54						
20							55						
21							56						
22							57						
23							58						
24							59						
25							60						
26							61						
27							62						
28							63						
29							64						
30							65						
31							66						
32							67						
33							68						
34							69						
35							70						

Appendix 2: Slope correction table

Slope correction table

Plot size 500 m^2

Slope%	Radius(m)	Slope%	Radius(m)	Slope%	Radius(m)
0	12.62				
1	12.62	36	13.01	71	13.97
2	12.62	37	13.03	72	14.00
3	12.62	38	13.05	73	14.04
4	12.62	39	13.07	74	14.07
5	12.62	40	13.09	75	14.10
6	12.63	41	13.12	76	14.14
7	12.63	42	13.14	77	14.17
8	12.64	43	13.16	78	14.21
9	12.64	44	13.19	79	14.24
10	12.65	45	13.21	80	14.28
11	12.65	46	13.24	81	14.31
12	12.66	47	13.26	82	14.35
13	12.67	48	13.29	83	14.38
14	12.68	49	13.31	84	14.42
15	12.69	50	13.34	85	14.45
16	12.70	51	13.37	86	14.49
17	12.71	52	13.39	87	14.52
18	12.72	53	13.42	88	14.56
19	12.73	54	13.45	89	14.60
20	12.74	55	13.48	90	14.63
21	12.75	56	13.51	91	14.67
22	12.77	57	13.53	92	14.71
23	12.78	58	13.56	93	14.74
24	12.79	59	13.59	94	14.78
25	12.81	60	13.62	95	14.82
26	12.82	61	13.65	96	14.85
27	12.84	62	13.68	97	14.89
28	12.86	63	13.72	98	14.93
29	12.87	64	13.75	99	14.97
30	12.89	65	13.78	100	15.00
31	12.91	66	13.81	101	15.04
32	12.93	67	13.84	102	15.08
33	12.95	68	13.87	103	15.12
34	12.97	69	13.91	104	15.15
35	12.99	70	13.94	105	15.19

A. de Gier – 2000

Appendix 3: Orthophoto of AHFR

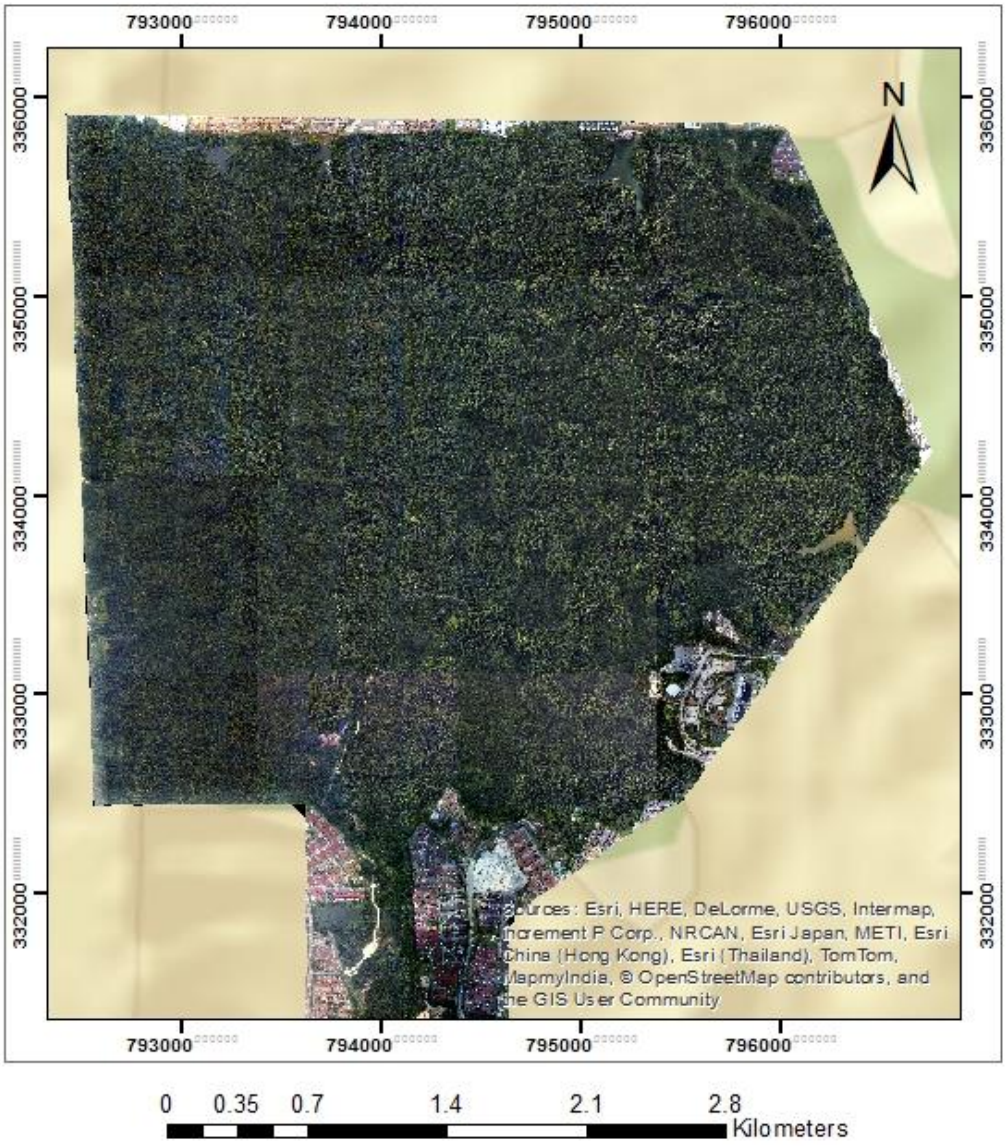

Appendix 4: WorldView 3 image of AHFR.

Appendix 5: Layout of the 26 sampled plots.

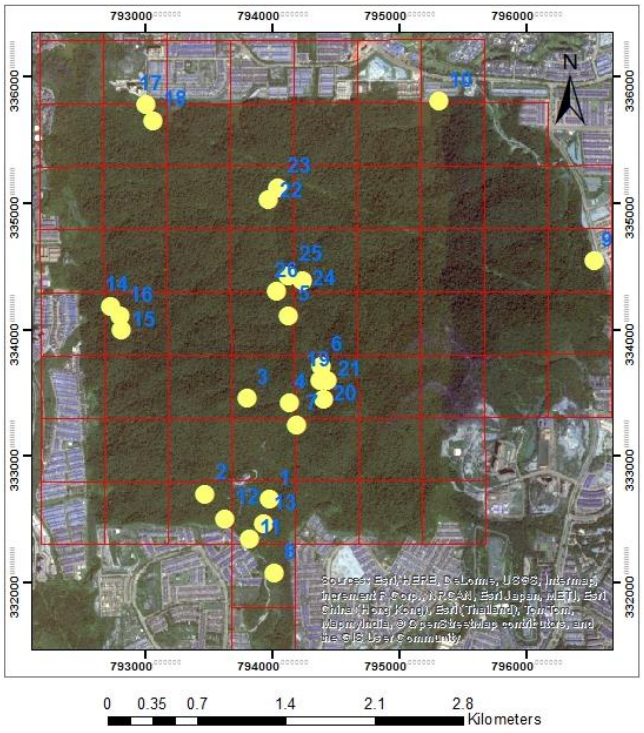

Appendix 6: Fieldwork pictures

LIST OF REFERENCES

Aardt, J. N. Van, Wynne, R. H., & Oderwald, R. G. (2004). A multi-resolution approach to forest segmentation as a precursor to estimation of volume and biomass by species. *Proceedings of the American Society for Photogrammetric Engineering and Remote Sensing Annual Conference*, 24–28. Retrieved from http://scholar.google.com/scholar?hl=en&btnG=Search&q=intitle:A+MULTI-RESOLUTION+APPROACH+TO+FOREST+SEGMENTATION+AS+A+PRECURSOR+TO+ESTIMATION+OF+VOLUME+AND+BIOMASS+BY+SPECIES#0

Aardt, J. Van, & Wynne, R. (2006). Segment-based forest volume-by-type modelling using small footprint LiDAR height distributions. *IUFRO International Precision Forestry*, 85–104. Retrieved from http://www.ecognition.com/sites/default/files/182_10.pdf

Andersen, H.-E., Reutebuch, S. E., & McGaughey, R. J. (2006). A rigorous assessment of tree height measurements obtained using airborne lidar and conventional field methods. *Canadian Journal of Remote Sensing*, *32*(5), 355–366. doi.org/10.5589/m06-030

Asmare, M. F. (2013). *Airborne LiDAR Data and VHR WorldView Satellite Imagery To Support Community Based Forest Certification in Chitwan, Nepal.* MSc Thesis, University of Twente, Faculty of Geo-Information Science and Earth Observation (ITC), Enschede,The Netherlands. Retrieved from https://www.itc.nl/library/papers_2013/msc/nrm/asmare.pdf

Baral, S. (2011). *Mapping Carbon Stock Using High Resolution Satellite Images In Sub-Tropical Forest Of Nepal.* Unpublished MSc Thesis University of Twente, Faculty of Geo-Information Science and Earth Observation (ITC), Enschede,The Netherlands. Retrieved from http://www.itc.nl/Pub/Home/library/Academic_output/AcademicOutput.html?p=11&y=11&l=20

Bautista, L. A. A. (2012). *Biomass Carbon Estimation and Mapping in the Subtropical Forest of Chitwan, Nepal : A Comparison between VHR, Geo-eye Satellite Images and Airborne LIDAR.* Unpublished MSc Thesis University of Twente, Faculty of Geo-Information Science and Earth Observation (ITC), Enschede,The Netherlands.Retrieved from http://www.itc.nl/library/papers_2012/msc/nrm/lopezbautista.pdf

Ben-Arie, J. R., Hay, G. J., Powers, R. P., Castilla, G., & St-Onge, B. (2009). Development of a pit filling algorithm for LiDAR canopy height models. *Computers and Geosciences*, *35*(9), 1940–1949. doi.org/10.1016/j.cageo.2009.02.003

Benz, U. C., Hofmann, P., Willhauck, G., Lingenfelder, I., & Heynen, M. (2004). Multi-resolution, object-oriented fuzzy analysis of remote sensing data for GIS-ready information. *ISPRS Journal of Photogrammetry and Remote Sensing*, *58*(3-4), 239–258. doi.org/10.1016/j.isprsjprs.2003.10.002

Bienert, A., Maas, H., & Scheller, S. (2006). Analysis of the information content of terrestrial laserscanner point clouds for the automatic determination of forest inventory parameters. Retrieved from http://www.riegl.com/uploads/tx_pxpriegldownloads/Bienert-Maas-2006.pdf

Bhattarai, T., Margaret, S., D. M. and Him, L. S. (2015). Carbon measurement : an overview of forest carbon estimation methods and the role of geographical informationsystem and remote sensing techniques for REDD + implementation. *Journal of Forest and Livelihood,13*(1).

Brandtberg, T., & Walter, F. (1998). Automated delineation of individual tree crowns in high spatial resolution aerial images by multiple-scale analysis. *Machine Vision and Applications*, *11*, 64–73. doi.org/10.1007/s001380050091

Bourgeron, P. S. (1983). Spatial Aspects of Vegetation Structure. In F. B. Golley (Ed.) *Ecosystems of the World. Tropical Rainforest Ecosystems Structure and Function* (pp. 29-43). Amsterdam, Oxford, New York: Elsevier Publishing.

Brown, S. (1999). *Estimating Biomass and Biomass Change of Tropical Forests: a Primer. (FAO Forestry Paper -134)* Retrieved September 16, 2015 from: http://www.fao.org/docrep/w4095e/w4095e00.HTM

Brown, S. (2002). Measuring carbon in forests: Current status and future challenges. *Environmental Pollution*, *116*(3), 363–372. doi.org/10.1016/S0269-7491(01)00212-3

Chai, T., & Draxler, R. R. (2014). Root mean square error (RMSE) or mean absolute error (MAE)? - Arguments against avoiding RMSE in the literature. *Geoscientific Model Development*, *7*(3), 1247–1250. doi.org/10.5194/gmd-7-1247-2014

Chambers, J. Q., Asner, G. P., Morton, D. C., Anderson, Anderson, L. O., Saatchi, S. S., Espírito-Santo, F. D. B., Palace, M., Souza, C. (2007). Regional ecosystem structure and function: ecological insights from remote sensing of tropical forests. *Trends in Ecology & Evolution*, *22*(8), 414–423. doi.org/10.1016/j.tree.2007.05.001

Chasmer, L., Hopkinson, C., & Treitz, P. (2006). Investigating laser pulse penetration through a conifer canopy by integrating airborne and terrestrial lidar. *Canadian Journal of Remote Sensing*, *32*(2), 116–125. doi.org/10.5589/m06-011

Chave, J., Andalo, C., Brown, S., Cairns, M. A., Chambers, J. Q., Eamus, D., Folster H., Fromard, F., Higuchi, N., Kira, T., Lescure J.P., Nelson, B. W., Ogawa, H., Puig, H., Riera, B., Yamakura, T. (2005). Tree allometry and improved estimation of carbon stocks and balance in tropical forests. *Oecologia*, *145*(1), 87–99. doi.org/10.1007/s00442-005-0100-x

Chave, J., Réjou-Méchain, M., Búrquez, A., Chidumayo, E., Colgan, M. S., Wellington, B. C., Delitti, A. D., Eid T., Fearnside, P. M., Goodman R. C., Henry, M., Martinez-Yrizar, A., Mugasha, W.A., Muller-Landau H. C., Mencucinni, M., Nelson, B. W., Ngomanda, A., Noguira, E. M., Ortiz-Malvassi, E., Pelissier R., Ploton, P., Ryan, C.M., Saldarriaga, J. G., Vieilledent, G. (2014). Improved allometric models to estimate the aboveground biomass of tropical trees. *Global Change Biology*, *20*(10), 3177–3190. doi.org/10.1111/gcb.12629

Chen, J. M., Liu, J., Leblanc, S. G., Lacaze, R., & Roujean, J. L. (2003). Multi-angular optical remote sensing for assessing vegetation structure and carbon absorption. *Remote Sensing of Environment*, *84*(4), 516–525. doi.org/10.1016/S0034-4257(02)00150-5

Chen, L., Chiang, T., & Teo, T. (2005). Fusion of LiDAR data and high resolution images for forest canopy modeling. *Asian Conference on Remote Sensing*, (1), 3–9.

Chen, Q. C. Q., Yang, X. Y. X., & Petriu, E. M. (2004). Watershed segmentation for binary images with different distance transforms. *Proceedings. Second International Conference on Creating, Connecting and Collaborating through Computing*, 111–116. doi.org/10.1109/HAVE.2004.1391891

Cheng, H. D., Jiang, X. H., Sun, Y., & Wang, J. (2001). Color image segmentation: Advances and prospects. *Pattern Recognition*, *34*(12), 2259–2281. doi.org/10.1016/S0031-3203(00)00149-7

Clinton, N., Holt, a, Scarborough, J., Yan, L., & Gong, P. (2010). Accuracy assessment measures for object-based image segmentation goodness. *Photogrammetric Engineering and Remote Sensing*, *76*(3), 289–299. doi.org/10.14358/PERS.76.3.289

Côté, J. F., Widlowski, J. L., Fournier, R. a., & Verstraete, M. M. (2009). The structural and radiative consistency of three-dimensional tree reconstructions from terrestrial lidar. *Remote Sensing of Environment*, *113*(5), 1067–1081. doi.org/10.1016/j.rse.2009.01.017

Corbera, E., & Schroeder, H. (2011). Governing and implementing REDD+. *Environmental Science and Policy*, *14*(2), 89–99. doi.org/10.1016/j.envsci.2010.11.002

Culvenor, D. S. (2002). TIDA: An algorithm for the delineation of tree crowns in high spatial resolution remotely sensed imagery. *Computers and Geosciences*, *28*(1), 33–44. doi.org/10.1016/S0098-3004(00)00110-2

Curtis, P.S. (2008). Estimating Aboveground Carbon in Live and Standing Dead Trees. In C. M. Hoover (Ed.) *Field Measurements for Forest Carbon Monitoring* (pp. 39-44). New York: Springer.

Dassot, M., Constant, T., & Fournier, M. (2011). The use of terrestrial LiDAR technology in forest science: application fields, benefits and challenges. *Annals of Forest Science*, *68*(5), 959–974. doi.org/10.1007/s13595-011-0102-2

Definiens. (2009). User Guide.

Definiens. (2012). Reference Book.

Derivaux, S., Forestier, G., Wemmert, C., & Lef, S. (2010). Supervised watershed segmentation using fuzzy classification and evolutionary computation. *Pattern Recognition Letters*, *31*(15), 2364–2374.

Doane, D. P., & Seward, L. E. (2011). Measuring skewness : A forgotten statistic? *Journal of Statistics Education*, *19*(2), 1–18. doi.org/10.1.1.362.5312

Drăguţ, L., Tiede, D., & Levick, S. R. (2010). ESP: a tool to estimate scale parameter for multiresolution image segmentation of remotely sensed data. *International Journal of Geographical Information Science*, *24*(6), 859–871. doi.org/10.1080/13658810903174803

Drake, J. B., Knox, R. G., Dubayah, R. O., Clark, D. B., Condit, R., Blair, J. B., & Hofton, M. (2003). Aboveground biomass estimation in closed canopy neotropical forests using lidar remote sensing: Factors affecting the generality of relationships. *Global Ecology and Biogeography*, *12*(2), 147–159. doi.org/DOI 10.1046/j.1466-822X.2003.00010.x

Ediriweera, S., Pathirana, S., Danaher, T., & Nichols, D. (2014). Estimating above-ground biomass by fusion of LiDAR and multispectral data in subtropical woody plant communities in topographically complex terrain in North-eastern Australia. *Journal of Forestry Research*. doi.org/10.1007/s11676-014-0485-7

Frohlich, C. & Mettenleiter, M. (2004) Terrestrial laser scanning – New perspectives in 3D surveying. *Proceedings of the ISPRS Working Group VIII/2: Laser-Scanners for Forest and Landscape Assessment*, 7–13. doi.org/10.1002/asi

Gao, H., Siu, W., & Hou, C. (2001). Improved techniques for automatic image segmentation. *IEEE Transactions on Circuits and Systems for Video Technology*, *11*(12), 1273–1280. doi.org/10.1109/76.974681

Gatziolis, D., & Andersen, H. E. (2008). A guide to LIDAR data acquisition and processing for the forests of the Pacific Northwest. *Forestry Sciences*, (July), 1–40. doi.org/Gen. Tech. Rep. PNW-GTR-768

Ghasemi, A., & Zahediasl, S. (2012). Normality tests for statistical analysis: A guide for non-statisticians. *International Journal of Endocrinology and Metabolism*, *10*(2), 486–489. doi.org/10.5812/ijem.3505

Gibbs, H. K., Brown, S., Niles, J. O., & Foley, J. A. (2007). Monitoring and estimating tropical forest carbon stocks: making REDD a reality. *Environmental Research Letters*, *2*(4), 045023. doi.org/10.1088/1748-9326/2/4/045023

Goetz, S., & Dubayah, R. (2011). Advances in remote sensing technology and implications for measuring and monitoring forest carbon stocks and change. *Carbon Management*, *2*(3), 231–244. doi.org/10.4155/cmt.11.18

Gonzalez, P., Asner, G. P., Battles, J. J., Lefsky, M. A., Waring, K. M., & Palace, M. (2010). Forest carbon densities and uncertainties from Lidar, QuickBird, and field measurements in California. *Remote Sensing of Environment*, *114*(7), 1561–1575. doi.org/10.1016/j.rse.2010.02.011

Gougeon, F. (1995). A crown-following approach to the automatic delineation of individual tree crowns in high spatial resolution aerial images. *Canadian Journal of Remote Sensing*, *21*(3), 274–284. doi.org/10.2307/302397

Gschwantner, T., Schadauer, K., Vidal, C., Lanz, A., Tomppo, E. O., Di Cosmo, L., Robert, N.,Duursma, D. E., and Lawrence, M. (2009). Common tree definitions for national forest inventories in Europe. *Silva Fennica*, *43*(2), 303–321. doi.org/10.14214/sf.463

Hay, G. J., Castilla, G., Wulder, M. A., & Ruiz, J. R. (2005). An automated object-based approach for the multiscale image segmentation of forest scenes. *International Journal of Applied Earth Observation and Geoinformation*, *7*(4), 339–359. doi.org/10.1016/j.jag.2005.06.005

Heng, R. K., & Tsai, L.M. (1999). An estimate of forest biomass in Ayer Hitam Forest Reserve. *Pertanika Journal Tropical Agriculture Science*, *22*(2), 117–123.

Hilker, T., van Leeuwen, M., Coops, N. C., Wulder, M. A., Newnham, G. J., Jupp, D. L. B., & Culvenor, D. S. (2010). Comparing canopy metrics derived from terrestrial and airborne laser scanning in a douglas-fir dominated forest stand. *Trees - Structure and Function*, *24*(5), 819–832. doi.org/10.1007/s00468-010-0452-7

Hirata et al. (2012). *REDD+ Cookbook*. Japan: Forestry and Forest Products Research Institute

Hodgson, M. E., & Bresnahan, P. (2004). Accuracy of airborne LiDAR-derived elevation : empirical assessment and error budget. *Photogrammetric Engineering and Remote Sensing*, *70*(3), 331–339

Hogan, C.(2011). *Lowland tropical forests*. Retrieved 2/7/2016 from http://www.eoearth.org/view/article/154309

Holopainen, M., & Talvitie, M. (2012). Forest inventory by means of tree-wise 3D-measurements of laser scanning data and digital aerial photographs. *Int. Arch. Photogramm. Remote Sensing& Spatial Information Sciences 36*(8)167–172.

Hoover, C. M. (2008). *Field Measurements for Forest Carbon Monitoring; A landscape-scale approach*. New York: Springer.

Hopkinson, C., Chasmer, L., Lim, K., Treitz, P., & Creed, I. (2006). Towards a universal lidar canopy height indicator. *Canadian Journal of Remote Sensing*, *32*(2), 139–152. doi.org/10.5589/m06-006

Hopkinson, C., Chasmer, L., Young-Pow, C., & Treitz, P. (2004). Assessing forest metrics with a ground-based scanning lidar. *Canadian Journal of Forest Research*, *34*(3), 573–583. doi.org/10.1139/x03-225

Hou, Z., Xu, Q., & Tokola, T. (2011). Use of ALS, Airborne CIR and ALOS AVNIR-2 data for estimating tropical forest attributes in Lao PDR. *ISPRS Journal of Photogrammetry and Remote Sensing*, *66*(6), 776–786. doi.org/10.1016/j.isprsjprs.2011.09.005

Houghton, J. T., Ding, Y., Griggs, D. J., Noguer, M., Linden, P. J. van der, Dai, X., Maskell, K. Johnson, C. A. (2001). Climate change 2001: The scientific basis. *Climate Change 2001: The Scientific Basis*, 881. doi.org/10.1256/004316502320517344

Huang, P., & Pretzsch, H. (2010). Using terrestrial laser scanner for estimating leaf areas of individual trees in a conifer forest. *Trees - Structure and Function*, *24*, 609–619. doi.org/10.1007/s00468-010-0431-z

Hudak, A. T., Lefsky, M. A, Cohen, W. B., & Berterretche, M. (2002). Integration of LiDAR and Landsat ETM+ data for estimating and mapping forest canopy height. *Remote Sensing of Environment*, *82*(2-3), 397–416. doi.org/10.1016/S0034-4257(02)00056-1

Hug, C., Ullrich, A, & Grimm, A. (2004). Litemapper-5600 – A waveform-digitizing LIDAR terrain and vegetation mapping system. *International Archives of Photogrammetry Remote Sensing and Spatial Information Sciences*, *36* PAR, 24–29. doi=10.1.1.151.1124&rep=rep1&type=pdf

Husch, B., Beers, T. W., & Kershaw, J. A., Jr. (2003). *Forest Mensuration* (4th ed.). New York, ON: John Wiley and Sons, Inc.

Hyyppä, J., Inkinen, M., 1999. Detecting and estimating attributes for single trees using laser scanner. *The Photogrammetric Journal of Finland, 16* (2), 27–42.

Ibrahim, F. (1999). Plant diversity and conservation value of Ayer Hitam Forest, Selangor, Peninsular Malaysia. *Pertanika Journal of Tropical Agricultural Science*, *22*(2), 73–83. Retrieved from http://psasir.upm.edu.my/3795/

Ismariah, A., & Ahmad Fadli, S. (2007). Valuation of carbon stock and carbon sequestration in Ayer Hitam forest reserve, Puchong. *Pertanika Journal of Tropical Agricultural Science*, *30*(2), 109–116.

Jennings, S. B., Brown, N. D., & Sheil, D. (1999). Assessing forest canopies and understorey illumination : canopy closure , canopy cover and other measures. *Forestry*, *72*(1), 59–73. doi.org/10.1093/forestry/72.1.59

Jing, L., Hu, B., Noland, T., & Li, J. (2012). An individual tree crown delineation method based on multi-scale segmentation of imagery. *ISPRS Journal of Photogrammetry and Remote Sensing*, *70*, 88–98. doi.org/10.1016/j.isprsjprs.2012.04.003

Jupp, D. L. B., Culvenor, D. S., Lovell, J. L., Newnham, G. J., Strahler, A. H., & Woodcock, C. E. (2008). Estimating forest LAI profiles and structural parameters using a ground-based laser called 'Echidna(R). *Tree Physiology*, *29*(2), 171–181. doi.org/10.1093/treephys/tpn022

Kankare, V., Holopainen, M., Vastaranta, M., Puttonen, E., Yu, X., Hyyppä, J., Vaaja M., Hyyppä H., Alho, P. (2013). Individual tree biomass estimation using terrestrial laser scanning. *ISPRS Journal of Photogrammetry and Remote Sensing*, *75*, 64–75. doi.org/10.1016/j.isprsjprs.2012.10.003

Karna, Y. K. (2012). *Mapping Above Ground Carbon Using WorldView Satellite Image And Lidar Data In Relationship With Tree Diversity Of Forests*. MSc Thesis, University of Twente, Faculty of Geo-Information Science and Earth Observation (ITC), Enschede,The Netherlands. Retrieved from: http://www.itc.nl/library/papers_2012/msc/nrm/karna.pdf

Karna, Y. K., Hussin, Y. A., Gilani, H., Bronsveld, M. C., Murthy, M. S. R., Qamer, F. M., Bhaskar S. K. Bhattarai, T., Xu, A., Chitra B. B. (2015). Integration of WorldView-2 and airborne LiDAR data for tree species level carbon stock mapping in Khayar Khola watershed, Nepal. *International Journal of Applied Earth Observation and Geoinformation, 38* 280–291. doi.org/10.1016/j.jag.2015.01.011

Ketterings, Q. M., Coe, R., Van Noordwijk, M., Ambagau', Y., & Palm, C. A. (2001). Reducing uncertainty in the use of allometric biomass equations for predicting above-ground tree biomass in mixed secondary forests. *Forest Ecology and Management*, *146*(1-3), 199–209. doi.org/10.1016/S0378-1127(00)00460-6

Khosravipour, A., Skidmore, A. K., Isenburg, M., Wang, T., & Hussin, Y. A. (2014). Generating pit-free canopy height models from airborne LiDAR. *Photogrammetric Engineering & Remote Sensing*, *80*(9), 863–872. doi.org/10.14358/PERS.80.9.863

Kim, M., Madden, M., & Warner, T. (2008). Estimation of optimal image object size for the segmentation of forest stands with multispectral IKONOS imagery. *Object-Based Image Analysis*, 291–307. doi.org/10.1007/978-3-540-77058-9_16

Kim, S.R., Kwak, D.A., Lee, W.K., Lee, W.K., Son, Y., Bae, S.W., Kim, C., Yoo, S. (2010). Estimation of carbon storage based on individual tree detection in Pinus densiflora stands using a fusion of aerial photography and LiDAR data. *Science China. Life Sciences*, *53*(7), 885–97. doi.org/10.1007/s11427-010-4017-1

King, D. A., Davies, S. J., Nur Supardi, M. N., & Tan, S. (2005). Tree growth is related to light interception and wood density in two mixed dipterocarp forests of Malaysia. *Functional Ecology*, *19*(3), 445–453. doi.org/10.1111/j.1365-2435.2005.00982.x

Koch, B. (2010). Status and future of laser scanning, synthetic aperture radar and hyperspectral remote sensing data for forest biomass assessment. *ISPRS Journal of Photogrammetry and Remote Sensing*, *65*(6), 581–590. doi.org/10.1016/j.isprsjprs.2010.09.001

Koch, B., Heyder, U., & Weinacker, H. (2006). Detection of individual tree crowns in airborne lidar data. *Photogrammetric Engineering & Remote Sensing*, *72*(4), 357. doi.org/10.1007/s10584-004-3566-3

Kuuluvainen, T. (1991). Relationships between crown projected area and components of above-ground biomass in Norway spruce trees in even-aged stands: empirical results and their interpretation. *Forest Ecology and Management*, *40*(3-4), 243–260. doi.org/10.1016/0378-1127(91)90043-U

Lamonaca, a., Corona, P., & Barbati, a. (2008). Exploring forest structural complexity by multi-scale segmentation of VHR imagery. *Remote Sensing of Environment*, *112*(6), 2839–2849. http://doi.org/10.1016/j.rse.2008.01.017

Lefsky, M., & Cohen, W B, P. G. . and H. D. J. (2002). LiDAR remote sensing for ecosystem studies. *Bioscience*, *52*(1), 19–30. doi.org/0006-3568-052-01-0019

Li, H., & Zhang, X. (2009). Segmentation of forest terrain laser scan data. *Science*, 47–54. doi.org/10.1145/1900179.1900188

Liang, X. (2013). *Feasibility of terrestrial laser scanning for plotwise forest inventories*: (Doctoral dissertation). Retrieved from *Publications of the Finnish Geodetic Institute*. (978-951-711-298-7).

Lim, K., Treitz, P., Wulder, M., & Flood, M. (2003). LiDAR remote sensing of forest structure, *Progress in Physical Geography 27*,(1), 88–106. doi.org/10.1191/0309133303pp360ra

Lindberg, E., Holmgren, J., Olofsson, K., & Olsson, H. (2012). Estimation of stem attributes using a combination of terrestrial and airborne laser scanning. *European Journal of Forest Research*, *131*, 1917–1931. doi.org/10.1007/s10342-012-0642-5

Lovell J.L. D.L.B.D.S. N.C. Coops Culvenor, A. (2003). Using airborne and ground-based ranging lidar to

measure canopy structure in Australian forests. *Canadian Journal of Remote Sensing*, *29*(5), 607–622. doi.org/10.5589/m03-026

Lu, D. (2006). The potential and challenge of remote sensing-based biomass estimation. *International Journal of Remote Sensing*, *27*(7), 1297–1328. doi.org/10.1080/01431160500486732

Maas, H. -G. H.-G., Bienert, a., Scheller, S., & Keane, E. (2008). Automatic forest inventory parameter determination from terrestrial laser scanner data. *International Journal of Remote Sensing*, *29*(5), 1579–1593. doi.org/10.1080/01431160701736406

Majid, S. A., & Nurudin, A. A. (2015). Aboveground biomass and carbon stock estimation in logged-over lowland tropical forest in malaysia. *International Journal of Agriculture, Forestry and Plantation*, *1*, 1–14.

Maltamo, M., Mustonen, K., Hyyppä, J., Pitkänen, J., & Yu, X. (2004). The accuracy of estimating individual tree variables with airborne laser scanning in a boreal nature reserve. *Canadian Journal of Forest Research*, *34*(9), 1791–1801. doi.org/10.1139/x04-055

Mbaabu, P. R., Hussin, Y. A., Weir, M., & Gilani, H. (2014). Quantification of carbon stock to understand two different forest management regimes in Kayar Khola watershed, Chitwan, Nepal. *Journal of the Indian Society of Remote Sensing*, *42*(4),745–754. doi.org/10.1007/s12524-014-0379-3

Möller, M., Lymburner, L., & Volk, M. (2007). The comparison index: A tool for assessing the accuracy of image segmentation. *International Journal of Applied Earth Observation and Geoinformation*, *9*(3), 311–321. doi.org/10.1016/j.jag.2006.10.002

Ni-Meister, W., Strahler, A. H., Woodcock, C. E., Schaaf, C. L., Jupp, D. L. B., Yao, T., Feng, Z., Yang, X. (2008). Modeling the hemispherical scanning, below-canopy lidar and vegetation structure characteristics with a geometric-optical and radiative-transfer model. *Canadian Journal of Remote Sensing*, *34*, (Suppl.2)S385–S397. doi.org/10.5589/m08-047

Nurul Shida, S., Faridah-Hanum, I., Wan Razali, W. M. and Kamziah, K, (2014). Community structure of trees in Ayer Hitma Forest Reserve, Puchong Selangor, Malaysia. *The Malaysian Forester, 77*(1)73-86.

O'Beirne, D. (2012). *Measuring the Urban Forest: Comparing Lidar Derived Tree Heights to Field Measurements.* MA Thesis, San Francisco State University, San Franciso California USA. Retrived from: http://geog.sfsu.edu/sites/sites7.sfsu.edu.geog/files/thesis/Thesis_Final_Dobeirne.pdf

Patenaude, G., Hill, R. a., Milne, R., Gaveau, D. L. a, Briggs, B. B. J., & Dawson, T. P. (2004). Quantifying forest above ground carbon content using LiDAR remote sensing. *Remote Sensing of Environment*, *93*(3), 368–380. doi.org/10.1016/j.rse.2004.07.016

Pfeifer, N., & Briese, C. (2007). Geometrical aspects of airborne laser scanning and terrestrial laser scanning. *International Archives of Photogrammetry and Remote Sensing*, *36*(3), 311–319. Retrieved from http://www.isprs.org/proceedings/XXXVI/3-W52/final_papers/Pfeifer_2007_keynote.pdf

Pistorius, T. (2012). From RED to REDD+: The evolution of a forest-based mitigation approach for developing countries. *Current Opinion in Environmental Sustainability*, *4*(6), 638–645. doi.org/10.1016/j.cosust.2012.07.002

Popescu, S. C. (2007). Estimating biomass of individual pine trees using airborne lidar. *Biomass and Bioenergy*, *31*(9), 646–655. doi.org/10.1016/j.biombioe.2007.06.022

Popescu, S. C., & Wynne, R. H. (2004). Seeing the trees in the forest: using lidar and multispectral data fusion with local filtering and variable window size for estimating tree height. *Photogrammetric Engineering & Remote Sensing, 70*(5), 589–604. Retrieved from

http://asprs.org/a/publications/pers/2004journal/may/2004_may_589-604.pdf

Prasad, O. M. P. (2015). *Derivation of Forest Plot Inventory Parameters From Terrestrial Lidar Data for Carbon Estimation*. MSc Thesis, University of Twente, Faculty of Geo-Information Science and Earth Observation (ITC), Enschede,The Netherlands.

Rahman R and Saha S. (2008). Multi-resolution Segmentation for object-based classification and accuracy assessment of land use / land cover classification using remotely sensed data. *Journal of Indian Society of Remote Sensing*, *36*:189–201. doi.org/10.1007/s12524-008-0020-4

Repola, J. (2008). Biomass equations for birch in Finland. *Silva Fennica*, *42*(4), 605–624.

Riggan, N. D., & Weih, R. C. (2009). A comparison of pixel-based versus object-based land use / land cover classification methodologies. *Journal of the Arkansas Academy of Science*, *63*, 145–152.

Rönnholm, P., Hyyppä, J., Hyyppä, H., Haggrén, H., Yu, X., & Kaartinen, H. (2004). Calibration of laser-derived tree height estimates by means of photogrammetric techniques. *Scandinavian Journal of Forest Research*, *19*(6), 524–528. doi.org/10.1080/02827580410019436

Rosell, J. R., Llorens, J., Sanz, R., Arnó, J., Ribes-Dasi, M., Masip, J., Escola`, A., Camp, F., Solanelles, F., Gracia, F., Gil, E., Val, L., Planas, S., Palacín, J. (2009). Obtaining the three-dimensional structure of tree orchards from remote 2D terrestrial LIDAR scanning. *Agricultural and Forest Meteorology*, *149*(9), 1505–1515. doi.org/10.1016/j.agrformet.2009.04.008

Sium, M. T. (2015). *Application of Very High Resolution Imagery and Terrestrial Laser Scanning for Estimating Carbon Stock in Tropical Rain Forest of Royal Belum Malaysia.* MSc Thesis, University of Twente, Faculty of Geo-Information Science and Earth Observation (ITC), Enschede,The Netherlands. Retrieved from: http://www.itc.nl/library/papers_2015/msc/nrm/sium.pdf

Smith, J. M. B. (2015). *Tropical rainforest*. Retrieved February 7, 2016 from
http://www.britannica.com/science/tropical-rainforest.

Strahler, A. H., Jupp, D. L. B., Woodcock, C. E., Schaaf, C. B., Yao, T., Zhao, F., Xiaoyuan, Y., Lovell, J. Culvenor, D., Newnham, G., Ni-Miester, W., Boykin-Morris, W. (2008). Retrieval of forest structural parameters using a ground-based lidar instrument (Echidna??). *Canadian Journal of Remote Sensing*, *34*(SUPPL. 2). doi.org/10.1007/s10342-010-0381-4

Suárez, J. C., Ontiveros, C., Smith, S., & Snape, S. (2005). Use of airborne LiDAR and aerial photography in the estimation of individual tree heights in forestry. *Computers and Geosciences*, *31*(2), 253–262. doi.org/10.1016/j.cageo.2004.09.015

Vashum, T. K. (2012). Methods to estimate above-ground biomass and carbon stock in natural forests - a review. *Journal of Ecosystem & Ecography*, *2*(4). doi.org/10.4172/2157-7625.1000116

Tokola, T., & Hou, Z. (2012). Alternative remote sensing materials and inventory strategies in tropical forest inventory - Case Lao PDR. *Revista Ambiência*, *8* 483–500. doi.org/10.5777/ambiencia.2012.04.04

Tonolli, S., Dalponte, M., Neteler, M., Rodeghiero, M., Vescovo, L., & Gianelle, D. (2011). Fusion of airborne LiDAR and satellite multispectral data for the estimation of timber volume in the Southern Alps. *Remote Sensing of Environment*, *115*(10), 2486–2498. doi.org/10.1016/j.rse.2011.05.009

UN-REDD programme. (2015). The UN-REDD programme strategy. Retrieved from http://www.unep.org/forests/Portals/142/docs/UN-REDD Programme Strategy.pdf

Van Leeuwen, M., Hilker, T., Coops, N. C., Frazer, G., Wulder, M. A., Newnham, G. J., & Culvenor, D. S. (2011). Assessment of standing wood and fiber quality using ground and airborne laser scanning: A review. *Forest Ecology and Management*, *261*(9), 1467–1478. doi.org/10.1016/j.foreco.2011.01.032

Wang, C., & Glenn, N. F. (2008). A linear regression method for tree canopy height estimation using airborne lidar data. *Canadian Journal of Remote Sensing*, *34*(Supplement 2), s217–s227. doi.org/10.5589/m08-043

Walter, H. (1974). *Ecology of tropical and subtropical vegetation*. Edinburg, ON: Oliver and Boyd.

Wang, L., Gong, P., & Biging, G. S. (2004). Individual tree-crown delineation and treetop detection in high-spatial-resolution aerial imagery. *Photogrammetric Engineering & Remote Sensing*, *70*(3), 351–357.

Watt, P. J., & Donoghue, D. N. M. (2005). Measuring forest structure with terrestrial laser scanning. *Int J Remote Sens*, *26*(7), 1437–1446. doi.org/10.1080/01431160512331337961

Wehr, A., & Lohr, U. (1999). Airborne laser scanning—an introduction and overview. *ISPRS Journal of Photogrammetry and Remote Sensing*, *54*(2-3), 68–82. doi.org/10.1016/S0924-2716(99)00011-8

Wile, B. C. (1964). Crown size and stem diameter in red spruce and balsam fir. *Department of Forestry Canada* (1056), 1–9. Retrieved from: http://cfs.nrcan.gc.ca/bookstore_pdfs/24587.pdf

Wulder, M. A., White, J. C., Nelson, R. F., Næsset, E., Ørka, H. O., Coops, N. C., Hilker, T., Gobakken, Bater, W. B. Gobakken, T. (2012). Lidar sampling for large-area forest characterization: A review. *Remote Sensing of Environment*, *121*, 196–209. doi.org/10.1016/j.rse.2012.02.001

Xie, Z., Xu, S., & Li, X. (2010). A high-accuracy method for fine registration of overlapping point clouds. *Image and Vision Computing*, *28*(4), 563–570. doi.org/10.1016/j.imavis.2009.09.006

Yamakura, T., Hagihara, A., Sukardjo, S., & Ogawa, H. (1986). Aboveground biomass of tropical rain forest stands in Indonesian Borneo. *Vegetatio*, *68*(2), 71–82. doi.org/10.1007/BF00045057

Zhan, Q., Molenaar, M., Tempfli, K., & Shi, W. (2005). Quality assessment for geo-spatial objects derived from remotely sensed data. *International Journal of Remote Sensing*, *26*(14), 2953–2974. doi.org/10.1080/01431160500057764

.